Exploring the Chemical Composition and Double Horizontal Branch of the Bulge Globular Cluster NGC 6569

Christian I. Johnson[1,2], R. Michael Rich[3], Nelson Caldwell[1], Mario Mateo[4], John I. Bailey, III[5], Edward W. Olszewski[6], and Matthew G. Walker[7]

ABSTRACT

Photometric and spectroscopic analyses have shown that the Galactic bulge cluster Terzan 5 hosts several populations with different metallicities and ages that manifest as a double red horizontal branch (HB). A recent investigation of the massive bulge cluster NGC 6569 revealed a similar, though less extended, HB luminosity split, but little is known about the cluster's detailed chemical composition. Therefore, we have used high resolution spectra from the Magellan–M2FS and VLT–FLAMES spectrographs to investigate the chemical compositions and radial velocity distributions of red giant branch and HB stars in NGC 6569. We found the cluster to have a mean heliocentric radial velocity of –48.8 km s^{-1} (σ = 5.3 km s^{-1}; 148 stars) and $\langle$[Fe/H]$\rangle$ = –0.87 dex (19 stars), but the cluster's 0.05 dex [Fe/H] dispersion precludes a significant metallicity spread. NGC 6569 exhibits light and heavy element distributions that are common among old bulge/inner Galaxy globular clusters, including clear (anti–)correlations between [O/Fe], [Na/Fe], and [Al/Fe]. The light element data suggest NGC 6569 may be composed of at least two distinct populations, and the cluster's low $\langle$[La/Eu]$\rangle$ = –0.11 dex indicates significant pollution with r–process material. We confirm

[1]Harvard–Smithsonian Center for Astrophysics, 60 Garden Street, MS–15, Cambridge, MA 02138, USA; cjohnson@cfa.harvard.edu; ncaldwell@cfa.harvard.edu

[2]Clay Fellow

[3]Department of Physics and Astronomy, UCLA, 430 Portola Plaza, Box 951547, Los Angeles, CA 90095-1547, USA; rmr@astro.ucla.edu

[4]Department of Astronomy, University of Michigan, Ann Arbor, MI 48109, USA; mmateo@umich.edu

[5]Leiden Observatory, Leiden University, P. O. Box 9513, 2300RA Leiden, The Netherlands; baileyji@strw.leidenuniv.nl

[6]Steward Observatory, The University of Arizona, 933 N. Cherry Avenue, Tucson, AZ 85721, USA; eolszewski@as.arizona.edu

[7]McWilliams Center for Cosmology, Department of Physics, Carnegie Mellon University, 5000 Forbes Avenue, Pittsburgh, PA 15213, USA; mgwalker@andrew.cmu.edu

that both HBs contain cluster members, but metallicity and light element variations are largely ruled out as sources for the luminosity difference. However, He mass fraction differences as small as $\Delta Y \sim 0.02$ cannot be ruled out and may be sufficient to reproduce the double HB.

Subject headings: stars: abundances, globular clusters: general, globular clusters: individual (NGC 6569)

1. INTRODUCTION

Correlated star–to–star abundance variations involving elements ranging from at least carbon to aluminum are common within nearly all old globular clusters (see reviews by Kraft 1994; Gratton et al. 2004, 2012), and are driven by both evolutionary processes (e.g., first dredge–up and extra mixing; Charbonnel 1995; Denissenkov & VandenBerg 2003; D'Antona & Ventura 2007) and pollution from previous generations of more massive stars (e.g., Decressin et al. 2007; de Mink et al. 2009; Bastian et al. 2013; Ventura et al. 2013; Denissenkov & Hartwick 2014). Although the light element abundances can vary by more than a factor of 10 within a single cluster, for most systems the heavier α and Fe–peak element abundance dispersions are generally $\lesssim 0.05$ dex (e.g., Sneden 2004; Carretta et al. 2009a, 2010a). For the neutron–capture elements, a small number of clusters exhibit significant ($\gtrsim 0.3$ dex) abundance dispersions that may be attributed to primordial enrichment via the rapid neutron–capture process (r–process; Roederer 2011), but in most cases the intrinsic heavy element [X/Fe][1] variations do not exceed ∼0.2 dex (e.g., D'Orazi et al. 2010). Furthermore, a majority of clusters have [Ba/Eu] and [La/Eu] ratios that are consistent with an r–process dominated composition (e.g., Gratton et al. 2004). Taken together, the mean composition characteristics outlined above suggest that old globular clusters formed rapidly ($\lesssim 100$ Myr), self–enriched with the products of proton–capture nucleosynthesis, did not generally retain the ejecta of core collapse supernovae, and ceased star formation before the winds of $\lesssim 4$ $M_\odot$ asymptotic giant branch (AGB) stars could pollute cluster interstellar mediums with the products of slow neutron–capture process (s–process) nucleosynthesis.

However, new evidence indicates that several of the most massive Galactic globular clusters contain stellar populations with different light *and* heavy element abundances. These "iron–complex" clusters exhibit significant [Fe/H] dispersions and share a common trait that metallicity and s–process enhancements are strongly correlated (e.g., Norris & Da Costa

[1] $[A/B] \equiv \log(N_A/N_B)_{star} - \log(N_A/N_B)_\odot$ and $\log \epsilon(A) \equiv \log(N_A/N_H) + 12.0$ for elements A and B.

1995; Smith et al. 2000; Johnson & Pilachowski 2010; Marino et al. 2011a,b; Yong et al. 2014; Johnson et al. 2015a; Marino et al. 2015; Da Costa 2016a; Johnson et al. 2017a)[2]. Since second peak s–process elements are thought to be produced during the late stage evolution of low and intermediate mass AGB stars (e.g., Busso et al. 1999), the correlation between [Ba,La/Fe] and [Fe/H] is consistent with the idea that iron–complex clusters experienced prolonged star formation and chemical enrichment compared to monometallic systems. Although the origin of iron–complex clusters is not yet clear, the strong retrograde orbit exhibited by ω Cen (Dinescu et al. 1999; Tsuchiya et al. 2003) combined with M 54's likely origin in the Sagittarius dwarf spheroidal galaxy (e.g., Bellazzini et al. 2008) makes plausible the idea that at least some iron–complex clusters may have been accreted by the Milky Way (Bekki & Tsujimoto 2016; Da Costa 2016a). In such a scenario, iron–complex clusters would represent the remnants of minor merger events with the Galaxy, and together with their progenitor systems would have contributed as "building blocks" to the formation of the halo, disk, and bulge.

In this context, the Galactic bulge globular cluster Terzan 5 is particularly interesting. Similar to more conventional iron–complex clusters, Terzan 5 exhibits a large metallicity spread with distinct populations near [Fe/H] $\approx$ –0.8, –0.25, and +0.3 dex (Ferraro et al. 2009; Origlia et al. 2011, 2013; Massari et al. 2014)[3]. On the other hand, Terzan 5 may be an entirely different class of object. For example, Massari et al. (2015) have ruled out an accretion origin for Terzan 5 based on proper motion measurements, and the cluster's metallicity dispersion appears to be correlated with an approximately 7.5 Gyr age spread (Ferraro et al. 2016). A comparison of the cluster's [Fe/H], age, [α/Fe], and light element abundance distributions with those of bulge field stars shows remarkable similarities, and raises the possibility that Terzan 5 may be a remnant primordial building block of the bulge rather than a genuine globular cluster (Ferraro et al. 2009; Origlia et al. 2011; Ferraro et al. 2016). However, a recent analysis by Schiavon et al. (2017a) found some evidence of (anti–)correlations between C, N, Na, and Al in a small sample of stars so the possibility remains that Terzan 5 may be an iron–complex cluster.

---

[2]Although the s–process abundance variations are generally reproduced by all analyses, the extent of the [Fe/H] variations have been questioned for several potential iron–complex clusters, including M 22 (Mucciarelli et al. 2015, but see also Lee et al. 2015), M 2 (Lardo et al. 2016), and NGC 1851 (Villanova et al. 2010). Additionally, the two most massive iron–complex clusters ω Cen and M 54 share similar metallicity and light element distributions (Carretta et al. 2010b), but M 54's s–process abundances have not been extensively explored.

[3]A confirmation of similar s–process element abundance variations is not yet available because the cluster is obscured by high foreground reddening (E(B–V) > 2; Massari et al. 2012).

One of the interesting aspects about Terzan 5 is that it was designated for spectroscopic follow–up because Ferraro et al. (2009) discovered the presence of two red horizontal branches (HBs) separated in the K–band by 0.3 magnitudes. The double HB feature in Terzan 5 has been linked to the cluster's metallicity and age spread (Ferraro et al. 2009, 2016). A similar analysis by Mauro et al. (2012) discovered that the two metal–rich bulge clusters NGC 6440 and NGC 6569 also exhibit double red HBs. However, in both of those cases the HBs were separated by only ∼0.1 mag in K_S, and the authors were not able to determine the cause of the HB luminosity differences. Recently, Muñoz et al. (2017) examined the chemical composition of RGB stars in NGC 6440, but did not find evidence of an internal [Fe/H] spread nor any peculiar light element abundances that would explain the double HB feature. Muñoz et al. (2017) did find that NGC 6440 exhibits large ranges in [Na/Fe] and [Al/Fe], but curiously did not find a significant O–Na anti–correlation.

From a chemical perspective, little is known about NGC 6569, which is an old bulge/inner Galaxy (l,b) = (+0.48°, –6.68°) globular cluster that resides approximately 3 kpc from the Galactic center (Harris 1996, 2010 version). Valenti et al. (2011) represents the only high resolution spectroscopic analysis of the cluster, and did not find any evidence supporting an intrinsic metallicity spread nor extreme light element abundance variations. However, their sample size was only 6 stars and did not include any heavy s–process elements that would have helped identify NGC 6569 as a possible iron–complex cluster. Therefore, we provide here a detailed analysis of the cluster's chemical composition, including an examination of the "bright" and "faint" HB stars, in order to gain insight into both the cluster's chemical enrichment history and any possible explanations for its HB morphology.

2. OBSERVATIONS AND DATA REDUCTION

2.1. Magellan Spectroscopic Sample

The primary data obtained for this project were acquired on 2014 June 03 for the RGB sample and between 2016 June 28 and 2016 July 01 for the HB sample (see Table 1). All observations utilized the Magellan–Clay 6.5m telescope at Las Campanas Observatory instrumented with the Michigan–Magellan Fiber System (M2FS; Mateo et al. 2012) and MSpec spectrograph. Although the RGB stars were observed during excellent observing conditions (seeing $< 1''$), the HB observations were obtained in generally poor sky conditions with seeing $> 1.5''$.

Target coordinates and photometry for the RGB sample were taken from the Two Micron All Sky Survey (2MASS; Skrutskie et al. 2006). A selection function was generated

by identifying the fiducial RGB sequence in a K_S versus J–K_S color–magnitude diagram that included only stars within $1'$ of the cluster center. The selection box was then extended to include stars out to $\sim 5'$ from the cluster center, but only isolated (i.e., not blended in 2MASS J–band images) stars within $\sim$2 magnitudes of the RGB–tip were drilled into the M2FS plate as potential targets. Stars closer to the cluster core were also given a higher priority ranking in an effort to mitigate bulge field star contamination. The sky coordinates and photometry of all 42 RGB targets observed with M2FS are shown in Figure 1 and are also provided in Table 2.

For the M2FS HB sample, the target coordinates and photometry were obtained from the VISTA variables in the Vía Láctea (VVV; Saito et al. 2012) survey DR1 catalog. We used the selection boxes provided by Figure 3 of Mauro et al. (2012) to identify targets in the "bright" (HB–A) and "faint" (HB–B) HB populations. The observed sample shown in Figure 1 and listed in Table 2 includes 9 HB–A stars, 17 HB–B stars, and 17 additional stars that are near, but just outside, the HB–A and HB–B photometric boundaries of Mauro et al. (2012). Similar to the RGB sample, HB targets located closer to the cluster center were given a higher priority during the plate design process, but $\sim$15% of our sample fell between 5–$10'$ from the cluster core. A full list of the 2MASS and VVV star names, coordinates, and photometry for the HB targets is provided in Table 2.

The RGB and HB samples both utilized the same "Bulge_GC1" spectrograph configuration described in Johnson et al. (2015b) that provides continuous wavelength coverage from $\sim$6140–6720 Å for up to 48 targets. Additionally, all M2FS observations were obtained with 1 × 2 (dispersion × spatial) CCD binning, a four amplifier slow readout mode, and the 125μm slits. Combined with the $1.2''$ fibers and echelle gratings, we achieved a typical resolving power $R \equiv \lambda/\Delta\lambda \approx 27{,}000$ for all observations.

Data reduction for the RGB and HB data sets was carried out following the methods outlined in Johnson et al. (2015b). Specifically, we used standard IRAF[4] routines to subtract the overscan and bias levels, trim the overscan regions, and correct for dark current effects on each individual amplifier image. The *imtranspose* and *imjoin* IRAF tasks were then used to rotate, align, and join the individual amplifier images into single full CCD images. Additional data reduction tasks, including aperture tracing, flat–field normalization, scattered light removal, ThAr wavelength calibration, cosmic ray removal, fiber–to–fiber throughput correction, and spectrum extraction, were completed using the IRAF *dohydra* routine. The

[4]IRAF is distributed by the National Optical Astronomy Observatory, which is operated by the Association of Universities for Research in Astronomy, Inc., under cooperative agreement with the National Science Foundation.

sky fibers were extracted separately and used to create master (combined) sky spectra that were then subtracted from each exposure. For the high signal–to–noise (S/N) ratio RGB data (S/N > 50 per reduced pixel), the individual exposures were continuum normalized and then median combined; however, the HB data only had S/N ∼ 5–10 per reduced pixel per exposure so the extracted spectra were co–added before continuum normalization. The final combined RGB and HB spectra had typical S/N ratios of ∼100 and 20 per reduced pixel, respectively.

2.2. Very Large Telescope Spectroscopic Sample

Given the possibility that the double HB discovered by Mauro et al. (2012) could be driven by metallicity and/or light element abundance variations, we extended our sample by downloading FLAMES–GIRAFFE data from the ESO archive[5]. The archival data included observations for a combination of RGB and HB stars with the HR13 and HR21 configurations, respectively. As is summarized in Table 1, the HR13 VLT–FLAMES data were obtained between 2014 July 03 and 2014 August 01 and the HR21 data were obtained between 2015 June 22 and 2015 July 26. Both data sets were binned 1 × 1 with the HR13 and HR21 spanning 6115–6395 Å and 8482–8982 Å at R ∼ 26,400 and 18,000, respectively.

Figure 2 shows that the FLAMES observations span a luminosity range that is similar to the M2FS data, but include additional stars between the upper RGB and HB. When combined, the two FLAMES archival data sets provided spectra for ∼800 unique RGB and HB stars ranging from ∼0.05′ to 12.5′ from the cluster center (see Figure 2). However, only ∼115 stars were observed in the HR13 setup because the two observing runs targeted the same stars. Since the star names and coordinates provided in the FLAMES image headers did not exactly match 2MASS nor VVV, we selected the closest match within a radius of 2″ from each survey for each observed target. In cases where a clear match could not be found, we retained the objects for radial velocity measurements but did not measure the chemical compositions of these stars. A summary of the star identifiers, coordinates, and photometry for the FLAMES data sets is provided in Table 3.

A majority of the FLAMES data reduction was carried out using the GIRAFFE Base–Line Data Reduction Software (girBLDRS) package[6]. Similar to the IRAF reduction of our M2FS data, we used girBLDRS to overscan and bias correct the images, trim the overscan

[5]Based on data obtained from the ESO Science Archive Facility under request number 281576. The original data were taken as a part of programs 093.D–0286(A) and 193.D–0232(F).

[6]The girBLDRS software can be downloaded at: http://girbldrs.sourceforge.net/.

regions, fit and trace the apertures, subtract scattered light, apply the flat–field corrections, fit and apply the ThAr wavelength calibrations, and extract the object and sky spectra. Additional data reduction procedures, including sky subtraction, spectrum combining, continuum normalization, and telluric removal, were performed using standard IRAF routines.

Since the HR13 observations targeted the same stars twice, we co–added their spectra to achieve S/N ratios of ∼70–100 per reduced pixel for the brightest stars and ∼30 for the HB stars. However, since the S/N, spectral coverage, and membership fractions (see Section 3) are considerably smaller in the FLAMES sample compared to the M2FS sample, we did not perform detailed chemical composition analyses on the HR13 data. For the HR21 observations, the S/N ratios from individual exposures generally exceeded 100 per reduced pixel. As a consequence of the high S/N and resolution, we were able to perform radial velocity and Calcium Triplet (CaT) metallicity measurements on individual exposures. We note that two of the HR21 observation sets also targeted the same stars, but rather than combine the spectra we analyzed each set separately in order to estimate the measurement errors.

3. RADIAL VELOCITIES AND CLUSTER MEMBERSHIP

Radial velocities for all stars were measured using the XCSAO cross correlation code (Kurtz & Mink 1998). Since the M2FS and FLAMES data sets contain a combination of RGB and HB stars, we generated synthetic spectra representative of the parameter space spanned by the observations to serve as cross correlation templates. The fitting template returning the highest cross correlation coefficient was then used to calculate the final velocity for each star.

For the M2FS data, we independently measured radial velocities for each order of each exposure per star, and the mean velocities calculated with this method are listed in Table 2. In all cases, a heliocentric correction was determined for each exposure using the IRAF *rvcor* routine, and the correction was applied before averaging the individual measurements. Similarly, the standard deviations of all heliocentric corrected velocity measurements for each star are provided as the velocity error column in Table 2. For the FLAMES data, the HR13 observations and 2/7 HR21 observations targeted the same stars on two separate nights, and for those cases the velocity and error columns of Table 3 represent the mean velocities and standard deviations over the two nights. For the remaining HR21 fields that were only observed once, the velocity and error columns represent the values returned by the XCSAO code. The heliocentric corrections for all FLAMES data were obtained from the image headers.

In addition to stars being observed twice in the HR13 configuration and 2/7 HR21 setups, a small number of stars were also observed more than once in combinations of the M2FS, HR13, and HR21 fields. The M2FS/HR13, M2FS/HR21, and HR13/HR21 setups have 3, 21, and 4 stars in common and exhibit mean velocity differences of 0.0 km s^{-1} (σ = 0.6 km s^{-1}), 0.7 km s^{-1} (σ = 1.0 km s^{-1}), and 0.8 km s^{-1} (σ = 0.8 km s^{-1}), respectively. The mean velocity differences between setups are comparable to the mean M2FS, HR13, and HR21 measurement errors for individual stars of 0.4 km s^{-1}, 0.4 km s^{-1}, and 0.8 km s^{-1}, respectively.

Although Valenti et al. (2011) found NGC 6569 to have a velocity dispersion of ∼8 km s^{-1}, Figure 3 shows that cluster membership cannot be definitively determined based on radial velocity alone. The contamination rate appears to be very small for the M2FS observations, but may be substantial for the FLAMES data set. The cluster's mean velocity is clear in Figure 3 near –50 km s^{-1}, but the local Galactic bulge velocity dispersion is at least 50–100 km s^{-1} (e.g., Kunder et al. 2012; Ness et al. 2013; Zoccali et al. 2014) and overlaps significantly with the cluster distribution. Therefore, the FLAMES target stars were only identified as cluster members if their heliocentric radial velocities were between –63 and –30 km s^{-1} (∼3σ) *and* their [Fe/H] values were within ∼0.3 dex of the cluster's mean [Fe/H] ∼ –0.85 dex (see Section 5.1)[7]. Stars that fell in the correct velocity range but did not have [Fe/H] determinations were labeled as possible members, and those with velocity and/or [Fe/H] measurements that were inconsistent with cluster membership were labeled non–members.

For the M2FS RGB stars, we used the same membership criteria as for the FLAMES sample. However, since we were unable to measure [Fe/H] for the HB stars, and also for a few RGB stars, only the velocity values were used to assign membership in those cases. The low contamination fraction shown in Figure 3 for the M2FS observations indicates that the false–positive membership rate should be low for the HB stars. For the small number of stars observed in both the M2FS and FLAMES setups, and for cases where [Fe/H] measurements were unavailable, we used the M2FS velocity data to assign membership status.

Using the criteria outlined above and including only member stars, we found mean cluster velocities and dispersions of –49.0 km s^{-1} (σ = 5.0 km s^{-1}), –48.7 km s^{-1} (σ = 5.6 km s^{-1}), and –48.8 km s^{-1} (σ = 5.3 km s^{-1}) for the M2FS, FLAMES, and combined data sets, respectively. These values are in good agreement with Valenti et al. (2011), which measured a mean velocity of –47 ± 4 km s^{-1}. Cluster members were found as far out as 9.9′ from NGC 6569's core, but 96% of the combined M2FS and FLAMES members were located

[7]Most bulge field stars along NGC 6569's line–of–sight have [Fe/H] $\gtrsim$ –0.8 dex (Zoccali et al. 2008).

inside the 6.9′ tidal radius (Ortolani et al. 2001). For the M2FS sample, the percentages of member, possible member, and non–member stars relative to the total sample were 64%, 2%, and 34%, respectively. However, only 14% and 16% of the FLAMES sample included member and possible member stars while the remaining 70% were non–members.

4. DATA ANALYSIS

4.1. Model Atmosphere Parameters: M2FS RGB Stars

The model atmosphere parameters effective temperature ($T_{\rm eff}$), surface gravity (log(g)), metallicity ([Fe/H])[8], and microturbulence ($\xi_{\rm mic.}$) were determined via spectroscopic methods for all RGB cluster members in the M2FS sample. Since the M2FS HB and FLAMES HR13 data had lower S/N, resolution, and/or covered a much smaller wavelength region than the M2FS RGB data, we did not include a comprehensive composition analysis for those stars. For the M2FS RGB sample, $T_{\rm eff}$ values were derived by removing trends in plots of log ϵ(Fe I) versus lower excitation potential, and log(g) was estimated by enforcing ionization equilibrium between log ϵ(Fe I) and log ϵ(Fe II). The microturbulence value for each star was set by removing trends in plots of log ϵ(Fe I) versus line strength, and model atmosphere metallicities were set to the mean of [Fe I/H] and [Fe II/H]. On average, the log ϵ(Fe I) and log ϵ(Fe II) abundances were based on measurements of 40 and 5 lines, respectively.

For all M2FS RGB stars, we assumed initial $T_{\rm eff}$, log(g), [Fe/H], and $\xi_{\rm mic.}$ values of 4200 K, 1.40 cgs, –0.80 dex, and 2.0 km s^{-1} and modified all four parameters simultaneously until a solution was found. Since the ATLAS9 (Castelli & Kurucz 2004) model atmosphere database is only available in increments of 250 K, 0.5 cgs, and 0.5 dex for $T_{\rm eff}$, log(g), and [Fe/H], we interpolated within the available grid[9] in order to derive the values given in Table 4. In principle, near–infrared colors from 2MASS and VVV could be used to provide additional $T_{\rm eff}$ constraints. However, we did not employ this method for NGC 6569 because the J–K_S values for the RGB stars analyzed here (see Table 2) are ∼0.1–0.2 magnitudes redder than the calibration range of most color–temperature relations (e.g., Alonso et al. 1999; González Hernández & Bonifacio 2009). Additionally, the line–of–sight reddening is moderately large for NGC 6569 with E(B–V) > 0.55 magnitudes (Zinn 1980; Bica & Pastoriza 1983; Dutra & Bica 2000; Ortolani et al. 2001; Valenti et al. 2005), and the VVV differential reddening map (Gonzalez et al. 2012) resolution is too coarse (2′) to

[8]We used α–enhanced model atmospheres in order to account for differences between [M/H] and [Fe/H].

[9]The ATLAS9 model atmosphere grids can be accessed at: http://wwwuser.oats.inaf.it/castelli/grids.html.

provide dereddened magnitudes on a star–by–star basis.

Figure 4 compares our spectroscopic T_{eff} and log(g) values against those predicted by a Dartmouth α–enhanced isochrone (Dotter et al. 2008) assuming [Fe/H] = –0.85 (see Section 5.1) and an age of 10.9 Gyr (Santos & Piatti 2004), and shows that our adopted model atmosphere parameters are in good agreement with the isochrone predictions. Specifically, for a given measured T_{eff} value our log(g) determinations agree with the isochrone to within 0.02 cgs on average with a dispersion of 0.15 cgs. Similarly, for a given measured log(g) value our T_{eff} estimates agree with the isochrone to within 3 K on average with a dispersion of 80 K. Note that a small number of stars with log(g) noticeably lower than the isochrone may belong to the AGB sequence.

4.2. Equivalent Width and Spectrum Synthesis Analyses: M2FS RGB Stars

Abundances of Fe I, Fe II, Si I, Ca I, Cr I, and Ni I were determined using the line list from Johnson et al. (2015a, see their Table 2), the model stellar atmosphere parameters given in Table 4, equivalent widths measured with a Gaussian profile deblending routine, and the *abfind* driver of the local thermodynamic equilibrium (LTE) line analysis code MOOG (Sneden 1973). Although the abundances of Fe and other elements may be susceptible to errors introduced by departures from LTE, 1D versus 3D effects, and/or plane parallel versus spherical model atmosphere structure variations (e.g., Lind et al. 2011; Bergemann et al. 2012; Dobrovolskas et al. 2015), we did not include any explicit corrections for these issues. Instead, all abundances were measured relative to the cool, metal–poor giant Arcturus under the assumption that a differential analysis will cancel out most model atmosphere deficiencies. A list of the adopted Arcturus and solar log ϵ(X) abundances is provided in Table 2 of Johnson et al. (2015a). The final [Fe I/H], [Fe II/H], [Si I/Fe], [Ca I/Fe], [Cr I/Fe], and [Ni I/Fe] abundances for the M2FS RGB sample are provided in Tables 5–6.

The abundances of O I, Na I, Mg I, Al I, La II, and Eu II were determined using the *synth* driver in MOOG. Spectrum synthesis was required for these elements because their line profiles were affected by: nearby absorption lines, molecular equilibrium calculations, autoionization lines, isotopic broadening, and/or hyperfine broadening. Given the interplay between the C, N, and O abundances in cool stars and the ubiquity of CN lines in the 6140–6720 Å region analyzed here, we measured log ϵ(O) first for all stars. In particular, we set [C/Fe] = –0.3 dex and $^{12}C/^{13}C = 5$ following Valenti et al. (2011), and iteratively adjusted the log ϵ(O) and log ϵ(N) abundances until a satisfactory fit was obtained for both the 6300.3 Å [O I] line and nearby CN features. For oxygen and all other elements measured via spectrum synthesis, nearby atomic line log(gf) values were set via an inverse Arcturus

analysis assuming the abundances given in Ramírez & Allende Prieto (2011); however, the CN line lists were adopted from Sneden et al. (2014).

Following a satisfactory determination of the oxygen abundance, and by extension the C + N abundance, the 6154/6160 Å and 6696/6698 Å Na I and Al I doublets were fit for each star. In cases where we could not measure log ϵ(O), CN line strengths were approximated using molecular line features near the Na and Al lines. Mg abundances were derived from the 6319 Å triplet, and contributions from the overlapping Ca autoionization line were estimated by examining the amount of continuum suppression present between ∼6316–6320 Å. The Ca autoionization line strength was modified by altering the log ϵ(Ca) abundance.

Since many La lines in the 6140–6720 Å window analyzed here exhibit signs of significant hyperfine broadening, we fit the 6262 and 6390 Å La II lines using the hyperfine structure line lists from Lawler et al. (2001a). Similarly, we fit the 6437 and 6645 Å Eu II lines using the line lists from Lawler et al. (2001b), and assumed a solar isotope mixture of 47.8% and 52.2% for ^{151}Eu and ^{153}Eu, respectively. However, we did not include additional broadening effects due to isotope variations for La because each star's La abundance is expected to be dominated by ^{139}La. The adopted atomic parameters and reference Arcturus and solar abundances can be found in Johnson et al. (2015a), and a summary of the final [X/Fe] ratios for all elements measured via spectrum synthesis is provided in Tables 5–6.

4.3. Calcium Triplet [Fe/H] Determinations

Although we did not measure detailed chemical abundances for the FLAMES HR13 data, we did derive [Fe/H] values from the 8542 and 8662 Å Calcium Triplet lines of the HR21 spectra. As noted by numerous previous authors (e.g., Armandroff & Da Costa 1991; Olszewski et al. 1991; Idiart et al. 1997; Rutledge et al. 1997; Battaglia et al. 2008), the near–infrared CaT lines are reliable tracers of a star's metallicity and are relatively insensitive to age and [Ca/Fe] abundance variations (e.g., Cole et al. 2004; Carrera et al. 2007; Da Costa 2016b). Following the methods outlined in Yong et al. (2016) and Johnson et al. (2017a), we employed the calibration described in Mauro et al. (2014) to convert the measured CaT EWs into [Fe/H] abundances. A key advantage of the Mauro et al. (2014) CaT–[Fe/H] calibration is that a star's luminosity parameter is defined as the difference between its K_S–band magnitude and that of the HB. For NGC 6569, which has E(B–V) > 0.55 (see Section 4.1), a near–infrared calibration is preferred over those using V–band magnitudes (e.g., Starkenburg et al. 2010; Saviane et al. 2012; Carrera et al. 2013) because the K_S–band is less sensitive to reddening. As mentioned in Section 4.1, we do not have a high resolution differential reddening map for NGC 6569 and have assumed a uniform reddening distribution.

In order to obtain [Fe/H] abundances from the CaT data, we first fit the 8542 and 8662 Å features using a function that represents the sum of a Gaussian and Lorentzian profile. A summed EW (ΣEW) parameter is then defined as:

$$\Sigma EW = EW_{8542} + EW_{8662}, \tag{1}$$

and combined with Equation (3) in Mauro et al. (2014) to give:

$$W' = \Sigma EW - 0.385[K_S(HB) - K_S], \tag{2}$$

where W′ represents the reduced EW and K_S(HB) is the mean magnitude of the red HB. Since Mauro et al. (2012) found evidence supporting red HBs at K_S = 14.26 and 14.35, we have adopted K_S = 14.30 as the mean cluster HB magnitude. The final [Fe/H] abundances were determined using Equation (2) here and Equation (4) from Mauro et al. (2014) to give:

$$[Fe/H] = -4.61 + 1.842\langle W'\rangle - 0.4428\langle W'\rangle^2 + 0.04517\langle W'\rangle^3. \tag{3}$$

For cases in which both VVV and 2MASS K_S magnitudes were available, the VVV photometry was preferred. Stars lacking both VVV and 2MASS photometry were omitted from the CaT [Fe/H] analysis. Table 7 provides a summary of the individual CaT EWs, summed EWs, reduced EWs, and [Fe/H] determinations for all cluster member stars.

4.4. Abundance Uncertainties

4.4.1. M2FS RGB Stars

Given the moderately high resolution and S/N of our data, the internal abundance uncertainties are dominated by errors in model atmosphere parameter determinations. For T_{eff}, we have adopted an uncertainty value of 100 K based on the log ϵ(Fe I) versus lower excitation potential plots, previous comparisons of spectroscopic and photometric temperatures using low reddening clusters (e.g., Johnson et al. 2015b, 2017b), and the scatter present in a plot of J–K_S versus spectroscopic temperature for the current data set. Similarly, we have adopted a conservative log(g) uncertainty of 0.15 cgs for all stars based on an examination of the scatter present when binning the data into groups spanning ∼100 K each (see also Section 4.1 and Figure 4). The mean line–to–line dispersion in [Fe/H] is 0.12 dex for Fe I and 0.09 dex for Fe II, and we have adopted a typical uncertainty of 0.10 dex for the model [M/H]

value. Finally, the $\xi_{\rm mic.}$ uncertainty was set at 0.10 km s^{-1} based on both an examination of the scatter present in plots of log ϵ(Fe I) versus log(EW/λ) and the star–to–star dispersion in $\xi_{\rm mic.}$ for stars binned into 100 K groups.

The uncertainties in log ϵ(X) were determined by varying each model atmosphere parameter independently and measuring the difference in abundance with the "best–fit" value. For species other than Fe I and Fe II, the [X/Fe] ratio uncertainties listed in Tables 5–6 take into account the correlated variations in Fe I and Fe II. In cases where more than one line was used, a measurement uncertainty parameter defined as the standard deviation in log ϵ(X) divided by the square root of the number of lines was included in the final uncertainty estimate. For cases where only one line could be measured, a standard measurement uncertainty of 0.05 dex was included. The abundance uncertainties listed in Tables 5–6 represent the error sources listed above added in quadrature for each star.

4.4.2. HR21 CaT Data

For the HR21 data, the greatest source of uncertainty in the [Fe/H] determinations is the individual CaT EW measurements. Following (Johnson et al. 2017a), we estimated the profile fitting uncertainty by taking advantage of the strong correlation in EW between the 8542 and 8662 Å lines, and used the EW of each line to predict the expected EW of the other line. The new ΣEW values were then propagated through Equations 2–3 in Section 4.3 to produce the predicted [Fe/H] abundances. The mean difference in [Fe/H] between the predicted abundances and the value given in Table 7 was then adopted as the CaT metallicity uncertainty for each star. We found a mean uncertainty of 0.15 dex (σ = 0.11 dex), which is comparable to the fitting uncertainty of the (Mauro et al. 2014) calibration function.

Since one HR21 configuration was observed twice on nights separated by $\sim$1 month, we were able to perform an independent check of the CaT [Fe/H] uncertainty. For the EWs, we found that the ΣEW values agreed between the two nights to within 4%. Additionally, we found a mean difference in [Fe/H] between the two observation sets to be 0.15 dex (σ = 0.20 dex), which is compatible with our theoretical estimate.

Two remaining sources of uncertainty we did not account for are the cluster's HB K_S magnitude and the K_S measurement errors for individual stars. For most stars, the VVV and/or 2MASS data have K_S measurement errors $\lesssim$ 0.1 magnitudes and thus do not significantly affect the calibrated metallicities. In a similar sense, the $\sim$0.05 magnitude offset between our adopted reference K_S(HB) value and those of the HB–A and HB–B populations are unlikely to affect the [Fe/H] determinations at more than the 0.03 dex level. Differential

reddening can also affect the K_S(HB) – K_S parameter in the metallicity calibration, but unless the reddening varies by more than a few tenths of a magnitude we can safely ignore this effect.

5. RESULTS AND DISCUSSION

5.1. Metallicity Distribution Function

As mention in Section 1, the discovery of a bimodal HB in Terzan 5 has been linked to a trimodal metallicity distribution that spans at least a factor of 10 in [Fe/H]. Although the K_S–band HB spread in NGC 6569 noted by Mauro et al. (2012) is 0.2 magnitudes smaller than in Terzan 5, a possible cause of the cluster's double HB is that NGC 6569 may also host stars spanning a wide range in [Fe/H]. However, we note that Muñoz et al. (2017) examined the composition of NGC 6440, which also showed evidence of a bimodal red HB, and did not find evidence of a metallicity spread.

Figure 5 shows the results of our [Fe/H] measurements using both the M2FS RGB data and the FLAMES CaT observations. Although the [Fe/H] dispersion is 0.15 dex for the CaT data, this value is equivalent to the mean measurement uncertainty determined in Section 4.4.2 for individual stars and is consistent with no intrinsic metallicity spread. Similarly, the [Fe/H] dispersion determined from the M2FS RGB data is only 0.05 dex and is consistent with the [Fe/H] scatter found in other monometallic clusters (e.g., Carretta et al. 2009a). Neither data set provides evidence supporting the existence of a significant metallicity spread, and we conclude that NGC 6569 is a monometallic cluster.

For the M2FS RGB data and FLAMES CaT observations we find mean [Fe/H] abundances of –0.87 dex and –0.83 dex, respectively. These values are consistent with previous spectroscopic and photometric estimates that ranged from [Fe/H] $\sim$ –0.75 to –0.90 dex (Zinn 1980; Bica & Pastoriza 1983; Ortolani et al. 2001; Valenti et al. 2005, 2011; Dias et al. 2016), and indicate that NGC 6569 is a relatively metal–rich globular cluster.

5.2. Light Element Abundances

Valenti et al. (2011) represents the only high resolution spectroscopic analysis of RGB stars in NGC 6569 and found moderate enhancements in [O/Fe] and [Al/Fe]. However, the small sample size (6 stars) of Valenti et al. (2011) prevented a more detailed analysis, and they were not able to confirm whether the cluster exhibits the usual light element abundance

correlations. The general composition trends of the present analysis, based on 19 stars for most elements, are summarized in the box plot of Figure 6, and indicate in agreement with Valenti et al. (2011) that at least [O/Fe] and [Al/Fe] are moderately enhanced with $\langle$[O/Fe]$\rangle$ = +0.44 dex (σ = 0.29 dex) and $\langle$[Al/Fe]$\rangle$ = +0.52 dex (σ = 0.14 dex). We also find that most stars are Na–enhanced with $\langle$[Na/Fe]$\rangle$ = +0.13 dex (σ = 0.21 dex), and that O, Na, and Al exhibit the largest abundance ranges (0.6–0.8 dex) of all elements analyzed here.

Figure 7 indicates that NGC 6569 exhibits the classical light element abundance variations involving O, Na, and Al, such as the O–Na anti–correlation and Na–Al correlation, that are ubiquitous among old globular clusters (e.g., Carretta et al. 2009b,c). However, Figure 7 also shows that NGC 6569 does not exhibit any correlation between [Mg/Fe] and [Al/Fe]. Additionally, the full abundance range in [Mg/Fe] is more than a factor of two smaller than for [O/Fe] and the light odd–Z elements, and with $\langle$[Mg/Fe]$\rangle$ = +0.41 dex (σ = 0.09 dex) Mg follows a pattern reminiscent of heavier α–elements, such as Ca (see Section 5.3).

Assuming the light element abundance variations in NGC 6569 are a result of "pristine" material mixing with gas that experienced high temperature proton–capture burning in a previous generation of more massive stars, the presence of clear O–Na and Na–Al (anti–)correlations coincident without a Mg–Al anti–correlation indicates that the burning temperatures were likely in the range of ∼45–75 MK. Temperatures lower than ∼45 MK would not have been able to produce Na and Al while those exceeding ∼75–100 MK would have lead to significant ^{24}Mg depletion (e.g., Prantzos et al. 2007; D'Antona et al. 2016).

In general, clusters with higher masses and more extended blue HBs tend to exhibit signatures associated with more extreme light element processing (e.g., He enrichment; large O and Mg depletions; some Si production) and higher burning temperatures (e.g., Carretta et al. 2007b; Yoon et al. 2008; Milone et al. 2014). However, less advanced nuclear processing is expected as a cluster's metallicity increases due to effects such as: a general decline in the temperatures required to maintain hydrostatic equilibrium, enhanced mass loss, and an overall reduction in the range of light element yields from polluting stars (e.g., Ventura & D'Antona 2009; Ventura et al. 2013). Therefore, NGC 6569 follows a common trend among Galactic globular clusters with [Fe/H] $\gtrsim$ –1 where a strong Mg–Al anti–correlation is only observed in the most massive clusters that also contain significant populations of blue HB stars, such as NGC 6388 and NGC 6441 (e.g., Carretta et al. 2009c).

Figures 7 also shows evidence that NGC 6569 may host at least two stellar populations with distinct light element compositions. Although we were only able to measure [O/Fe] for 8 stars, the O–Na panel of Figure 7 suggests a possible gap in the distribution near [O/Fe] $\sim$ +0.5 dex and [Na/Fe] $\sim$ +0.1 dex. Similarly, Figure 8 plots [O/Na] as a function of [Al/H], which was shown by Johnson et al. (2017c) to assist in identifying discrete popula-

tions in globular clusters, and the data further reveal the possible presence of at least two populations. For example, the gap in [O/Na] between stars with [Al/H] $\sim$ –0.45 dex and those with [Al/H] $\sim$ –0.30 dex is at least a factor of 5, which is significantly larger than the measurement uncertainties. However, additional observations are required to determine how many chemically distinct populations exist in NGC 6569, and also to rule out the presence of stars with [O/Na] ratios between about +0.1 and +0.6 dex.

5.3. α, Fe–Peak, and Neutron–Capture Abundances

As is shown in Figure 6, we find that the heavier α–elements are enhanced in NGC 6569 with $\langle$[Si/Fe]$\rangle$ = +0.34 dex (σ = 0.09 dex) and $\langle$[Ca/Fe]$\rangle$ = +0.21 dex (σ = 0.10 dex). The results presented here are in general agreement with those of Valenti et al. (2011), but we derive mean [Si/Fe] and [Ca/Fe] ratios that are lower by 0.15 dex and 0.10 dex, respectively. However, the mean [Si/Ca] ratios of the present work and Valenti et al. (2011) agree to within 0.05 dex. For the Fe–peak elements, we find approximately solar abundance ratios with $\langle$[Cr/Fe]$\rangle$ = +0.02 dex (σ = 0.16 dex) and $\langle$[Cr/Fe]$\rangle$ = –0.08 dex (σ = 0.05 dex). Although the star–to–star dispersion in [Cr/Fe] is noticeably larger than for [Ni/Fe] (see Figure 6), we suspect that this is driven by larger measurement uncertainties rather than an astrophysical mechanism.

Figure 6 also shows that the neutron–capture elements are enhanced in NGC 6569 with $\langle$[La/Fe]$\rangle$ = +0.38 dex (σ = 0.14 dex) and $\langle$[Eu/Fe]$\rangle$ = +0.49 dex (σ = 0.12 dex). Similar to the case of Cr, the [La/Fe] and [Eu/Fe] dispersions are marginally larger than those for elements such as Si, Ca, and Ni, but the interquartile ranges (IQRs) of [La/Fe] and [Eu/Fe] are both smaller than for [Cr/Fe]. Additionally, an examination of the cluster's mean [La/Eu] composition, which is largely insensitive to surface gravity errors, indicates that NGC 6569 has a [La/Eu] dispersion of 0.11 dex. Since the star–to–star scatter in [La/Eu] is smaller than those of [La/Fe] and [Eu/Fe] individually, we conclude that the cluster's intrinsic heavy element spread does not exceed the $\sim$0.1 dex level. NGC 6569 also has $\langle$[La/Eu]$\rangle$ = –0.11 dex, which suggests that the cluster's primordial composition was dominated by the r–process. However, a mean [La/Eu] = –0.11 dex is a factor of 2–3 higher than the lowest [La/Eu] values found in more metal–poor systems, and suggests that the gas from which NGC 6569 formed may have also experienced some s–process enrichment (but see also Section 5.5 for an alternative interpretation).

5.4. Comparing NGC 6569 with Other Galactic Bulge Globular Clusters

The right panels of Figure 7 compare the [O/Fe], [Na/Fe], [Mg/Fe], and [Al/Fe] abundances of individual stars in NGC 6569 against those in several bulge/inner Galaxy clusters[10] with similar metallicities. The data indicate that O–Na anti-correlations and Na–Al correlations are common among bulge clusters with [Fe/H] $\gtrsim$ –1, with only a few exceptions such as HP–1 (Barbuy et al. 2006, 2016) and NGC 6440 (Muñoz et al. 2017) possibly lacking O–Na anti–correlations. Figure 7 also shows that except for the peculiar clusters NGC 6388 and NGC 6441, which contain extended blue HBs, none of the remaining bulge clusters within ∼0.3 dex of NGC 6569 exhibit Mg–Al anti–correlations. Therefore, NGC 6569 exhibits O–Na and Na–Al relations that are more extended than most metal–rich bulge clusters, but does not reach the most extreme levels of Na/Al–enhancement and O/Mg–depletion observed in NGC 6388 and NGC 6441.

Figures 9–10 compare the mean [X/Fe] ratios of NGC 6569 against those of several bulge/inner Galaxy globular clusters spanning a wide [Fe/H] range. Although the mean [O/Fe], [Na/Fe], and [Al/Fe] abundances of the bulge cluster population exhibit considerable scatter, NGC 6569 follows the bulk trend by having enhanced mean [X/Fe] ratios of all three elements. Figures 9–10 also show that NGC 6569 follows the well–defined α–element, Fe–peak, and neutron–capture element trends established by other bulge clusters. From a bulk chemical perspective, the mean composition properties of NGC 6569 are indistinguishable from those of other bulge clusters with similar metallicities.

5.5. Comparing the Composition Patterns of Galactic Bulge Globular Clusters and Field Stars

Several dedicated studies have established the overall chemical composition patterns of light, α, Fe–peak, and heavy elements in the Galactic bulge (e.g., McWilliam & Rich 1994; Fulbright et al. 2007; Meléndez et al. 2008; Alves-Brito et al. 2010; Ryde et al. 2010; Gonzalez et al. 2011; Hill et al. 2011; Rich et al. 2012; Bensby et al. 2013; Johnson et al. 2014; Van der Swaelmen et al. 2016; Jönsson et al. 2017). As is summarized in Figures 9–10, bulge field stars generally have: [Fe/H] $\gtrsim$ –1 dex, enhanced [α/Fe] and [Eu/Fe] for [Fe/H] $\lesssim$ –0.4 dex, [X/Fe] $\sim$ 0 dex for Fe–peak elements, enhanced [La/Fe] that declines with increasing metallicity, and [La/Eu] ratios between about –0.5 and –0.1 dex with a possible increase at super–solar metallicities. Furthermore, the bulge field stars exhibit [Na/Fe] abundances that

[10]In this context, bulge/inner Galaxy clusters are those with |l| $\lesssim$ 20°, |b| $\lesssim$ 20°, and $R_{GC} \lesssim$ 3 kpc.

either slowly increase with [Fe/H] or present a "zig–zag" pattern associated with competition between core–collapse and thermonuclear supernovae (McWilliam 2016), and [Al/Fe] traces the general trends of [α/Fe] and [Eu/Fe]. These observations indicate that a significant fraction of the bulge formed rapidly, experienced chemical enrichment dominated by massive stars, and likely had a star formation rate that was a few times higher than the local thick disk. However, the lowest metallicity ([Fe/H] $\lesssim$ –1.5 dex) bulge field stars exhibit chemical composition patterns that may be more similar to those found in metal–poor thick disk and halo stars (García Pérez et al. 2013; Howes et al. 2014, 2015).

Figures 9–10 compare the mean composition patterns of several bulge/inner Galaxy globular clusters against those of the bulge field stars. With the exception of [O/Fe], [Na/Fe], and [Al/Fe], Figures 9–10 indicate that the mean [α/Fe], Fe–peak, and heavy element compositions of the bulge globular cluster and field stars are similar, and perhaps indistinguishable for many elements, over a wide range in metallicity. A particularly interesting question is whether the bulge clusters remain α–enhanced to a higher metallicity than the field stars, but unfortunately the number of globular clusters studied at [Fe/H] $\gtrsim$ –0.3 dex is too small to draw any strong conclusions. For example, NGC 6528 is the most metal–rich cluster shown and exhibits mean [Mg/Fe] and possibly [Ca/Fe] abundances that are similar to the field, but the cluster may have a mean [Si/Fe] ratio that is $\sim$0.2 dex higher. However, the clusters that are only slightly more metal–poor than NGC 6528 have [α/Fe] ratios that are within the range observed for similar metallicity bulge field stars.

In a similar sense, Figure 10 shows some ambiguity regarding the [La/Fe] ratios for bulge field and cluster stars with [Fe/H] $\gtrsim$ –0.8 dex. Both Johnson et al. (2012) and Van der Swaelmen et al. (2016) noted a general decrease in [La/Fe] with increasing [Fe/H], and also found stars with [La/Fe] $\sim$ +0.2 dex at [Fe/H] $\gtrsim$ –0.6 dex; however, Johnson et al. (2012) found most stars with [Fe/H] between –0.8 and 0.0 dex to have [La/Fe] $<$ 0 dex while Van der Swaelmen et al. (2016) found most stars in that metallicity range to have [La/Fe] $>$ 0 dex. As a result, the data do not clearly differentiate between whether or not the bulge clusters near [Fe/H] $\sim$ –0.6 dex have elevated mean [La/Fe] ratios compared to the field stars or are within the normal range. The bulge clusters exhibit a similar decrease in [La/Fe] with increasing [Fe/H] observed in the field stars, but the metallicity at which the downturn occurs lies between the results of Johnson et al. (2012) and Van der Swaelmen et al. (2016).

Interestingly, the [Eu/Fe] trends in Figure 10 are nearly identical for the bulge cluster and field stars, and the two populations may share similar [La/Eu] distributions as well. The available [La/Eu] data indicate significant contributions by the r–process for both the cluster and field star compositions, but both populations have mean [La/Eu] ratios that are higher than the –0.6 dex pure r–process limit observed in some metal–poor halo and globular

cluster stars (e.g., Roederer et al. 2010). The enhanced [La/Eu] ratios in bulge cluster and field stars are likely a result of global s–process enrichment in the Galaxy driven by pollution from AGB stars (e.g., Gallino et al. 1998; Bisterzo et al. 2010) and/or massive "spinstars" (e.g., Frischknecht et al. 2016). In particular, previous data have shown that most Galactic cluster and field stars with [Fe/H] $\gtrsim$ –2 dex exhibit at least some evidence of s–process enrichment, such as [La/Eu] ratios that increase with metallicity (e.g., James et al. 2004; Simmerer et al. 2004; D'Orazi et al. 2010).

Alternatively, we note Roederer et al. (2010) found that pure r–process halo/disk cluster and field stars with [Fe/H] < –1.4 can have –0.6 $\lesssim$ [La/Eu] $\lesssim$ –0.05 dex, which suggests the moderately depleted [La/Eu] ratios in the bulge could still represent nearly pure r–process compositions, at least for [Fe/H] < 0 dex. This may be especially true for the bulge clusters shown in Figure 10, which have $\langle$[La/Eu]$\rangle$ = –0.14 dex (σ = 0.15 dex) and fail to exhibit any variations with metallicity. However, a predominantly r–process origin would require a high star formation rate in order to mitigate s–process pollution from $\lesssim$ 4 $M_{\odot}$ AGB stars.

While the bulge cluster and field stars may share similar mean [La/Eu] trends, Figure 9 shows that significant differences are found when examining the [O/Fe], [Na/Fe], and [Al/Fe] abundance trends. For example, the bulge clusters exhibit larger cluster–to–cluster variations in mean light element composition than are observed among field stars of similar [Fe/H]. Several clusters also contain large numbers of stars with lower [O/Fe] and higher [Na,Al/Fe] abundances than are found in the field, and most clusters exhibit clear O–Na anti–correlations and Na–Al correlations that reflect strong self–enrichment. Notably, the light element (anti–)correlations prevalent in globular clusters are not found in bulge field stars[11], which indicates that a large fraction of the bulge cannot have originated from dissolved globular clusters hosting the same chemical properties and population ratios as those in Figure 9. We note that a population of N/Al–rich stars has been found recently in the inner Galaxy (Schiavon et al. 2017b), but the metallicity distribution of these stars peaks near [Fe/H] $\sim$ –1 dex. As a result, their progenitor cluster systems are too metal–poor to have built–up the bulge field star population. However, self–enriched but now dissolved clusters could have contributed a small percentage of stars to the bulge's total mass.

[11]We note that [Na/Fe] and [Al/Fe] are correlated for intermediate metallicity bulge stars, but the [Na/Fe] and [Al/Fe] ranges are smaller than observed in globular clusters and are not accompanied by similar O–Na anti–correlations. The bulge Na–Al correlation is likely driven by the similar production mechanisms of Na and Al in massive stars, and does not reflect the same proton–capture nucleosynthesis processes that operate in cluster environments.

5.6. Insight into NGC 6569's Double Horizontal Branch

As mentioned in Section 1, NGC 6569 is particularly interesting because Mauro et al. (2012) found evidence that the cluster, along with NGC 6440, may host two red HBs separated in the K_S–band by ∼0.1 mag. An intriguing possibility raised by Mauro et al. (2012) is that split red HBs are common in massive, metal–rich bulge clusters, and that similar to Terzan 5 all bulge clusters with double HBs may host two or more stellar populations with different metallicities. However, RGB composition analyses have so far failed to detect intrinsic metallicity spreads in both NGC 6440 (Origlia et al. 2008; Muñoz et al. 2017) and NGC 6569 (Valenti et al. 2011, this paper).

In order to gain additional insight regarding the origin of the double HB in NGC 6569, we have derived radial velocities and CaT metallicities of stars in each HB group defined by Mauro et al. (2012). Additionally, we have combined the bluer but lower S/N M2FS and FLAMES spectra of individual stars in each HB population to create co–added spectra that will permit a search for mean light element variations between the two HBs. Although Mauro et al. (2012) found double red HBs in NGC 6440 and NGC 6569, similar observations of the metal–rich bulge clusters NGC 6380, NGC 6441, NGC 6528, and NGC 6553 did not reveal similarly complex red HBs. Therefore, it is prudent to confirm that the HB–A and HB–B populations both contain cluster members.

The HB targets analyzed in the present data set are shown in Figure 11, and indicate that both the HB–A and HB–B groups identified by Mauro et al. (2012) contain cluster members. If we restrict the examination to include only stars located within the selection boxes of Figure 11, then the data indicate that the mean heliocentric radial velocities of the HB–A and HB–B groups are identical within the errors. Specifically, the M2FS HB–A and HB–B populations have mean velocities of –49.5 km s^{-1} ± 1.2 km s^{-1} and –48.8 km s^{-1} ± 1.5 km s^{-1}, respectively, while the FLAMES HB–A and HB–B populations have mean velocities of –46.7 km s^{-1} ± 4.5 km s^{-1} and –45.9 km s^{-1} ± 2.5 km s^{-1}, respectively.

Having confirmed that the HB–A and HB–B groups contain cluster members, we can now investigate possible composition differences between the two populations. Using the FLAMES CaT data, and again restricting the observations to include only stars within the selection boxes of Figure 11, we find the HB–A group to have a mean [Fe/H] = –0.76 dex (σ = 0.07 dex) and the HB–B group to have a mean [Fe/H] = –0.89 dex (σ = 0.05 dex). Although the brighter K_S–band magnitude of the HB–A population is consistent with a higher mean metallicity and matches the pattern observed in Terzan 5, we suspect that the 0.13 dex difference in mean metallicity between the HB–A and HB–B groups is not significant. For example, the mean CaT measurement uncertainty is ∼0.15 dex (see Section 4.4.2 and Table 7) for individual stars, and the HB metallicity estimates are based

on only ∼5 stars in each group. Additionally, the metallicity distribution functions shown in Figure 5 are not bimodal, and the RGB line–by–line abundance analysis produced an [Fe/H] dispersion of only 0.05 dex, despite spanning the full color range of the RGB (see Figure 1). A comparison of the co–added HB–A and HB–B spectra in Figures 12–13 also reveals that their line strengths agree to within 1.8–3.4%, which leaves little room for significant composition differences. Therefore, we conclude that the double HB in NGC 6569 is not driven by an intrinsic metallicity spread.

Assuming the age dispersion within NGC 6569 is negligible, He enhancement is an additional parameter that can produce a luminosity dispersion on the HB (e.g., Valcarce et al. 2012). Although we cannot directly measure He abundances with the present data set, extreme He variations can be traced in globular clusters by searching for large light element abundance variations (e.g., Bragaglia et al. 2010a,b; Dupree et al. 2011). Mauro et al. (2012) noted that He enhancements of $Y > 0.30$ could be required to explain the HB luminosity variations in at least NGC 6440, and if this is the cause for the double HB feature in NGC 6569 too then we should be able to detect higher mean Na abundances in the He–enhanced HB stars.

Figure 7 indicates that if the HB–A and HB–B populations exhibit different light element abundances then the expected lower limit in Δ[Na/Fe] between the two groups should be ∼0.4 dex. For a typical red HB star with [Fe/H] ∼ –0.85 dex, a [Na/Fe] difference of 0.4 dex translates to a central line depth difference of ∼5–7% for the 6154/6160 Å Na I lines in R ∼ 27,000 spectra. However, comparisons of the co–added HB–A and HB–B M2FS and FLAMES spectra in Figures 12–13 show that, at least on average, the Na I lines vary by $\lesssim 2\%$ in depth. Therefore, the HB–A and HB–B populations likely have mean [Na/Fe] abundances that agree to within about 0.2–0.3 dex. Although a detailed analysis of individual stars should be carried out for confirmation, with the present co–added spectra we conclude that the HB–A and HB–B populations do not possess significantly different mean [Na/Fe] abundances. As a result, He mass fraction differences exceeding $\Delta Y = 0.05$–0.10 are unlikely.

We conclude by investigating the possibility that a small He abundance variation could both be present in NGC 6569 and be responsible for the double red HB feature. The top panel of Figure 14 illustrates the expected difference in K_S between two zero age HB (ZAHB) stars with similar ages, metallicities, and [α/Fe] abundances but with various differences in He mass fraction (ΔY)[12]. Under these assumptions, Figure 14 indicates that the HB–A and

[12]The isochrone models used in Figure 14 are from the Princeton–Goddard–PUC (PGPUC) database (Valcarce et al. 2012), which can be accessed at http://www2.astro.puc.cl/pgpuc/index.php. A significant limitation of the present investigation is that the comparison stars are assumed to reach the RGB–tip with

HB–B populations could exhibit 0.1 magnitude differences in K_S if the two groups differed in Y by ∼0.02–0.025. Is such a He difference compatible with the observations? Gratton et al. (2010) showed that a correlation exists between a cluster's [Al/Mg] IQR and ΔY, and the bottom panel of Figure 14 compares these data against similar IQR measurements for NGC 6569 RGB stars[13]. Figure 14 shows that NGC 6569's [Al/Mg] IQR of 0.20 ± 0.05 dex is compatible with a ΔY value of ∼ 0.015–0.03. Although the present data do not provide a clear explanation for the origin of the double red HB feature in NGC 6569, we can conclude that the light element abundance spreads in NGC 6569 are consistent with other clusters for which ΔY reaches the 0.02 threshold necessary to separate ZAHB stars by ∼ 0.1 magnitudes in the K_S–band.

6. SUMMARY

We utilized new and archival high resolution (R ∼ 27,000) spectra from the Magellan–M2FS and VLT–FLAMES spectrographs to investigate the radial velocities, light and heavy element abundances, and CaT metallicities of RGB and HB stars located near the Galactic bulge globular cluster NGC 6569. We derived a mean cluster heliocentric radial velocity of –48.8 km s^{-1} (σ = 5.3 km s^{-1}), but recommend using both velocity and metallicity measurements to establish membership because the cluster's systemic velocity overlaps significantly with the bulge field distribution. Fortunately, the cluster has a mean [Fe/H] ≈ –0.85 dex, which is more metal–poor than most bulge field stars. We note that the M2FS 6140–6720 Å data and FLAMES CaT data yielded [Fe/H] dispersions of only 0.05 and 0.15 dex, respectively, which are consistent with NGC 6569 being a monometallic cluster.

The light element abundance distributions of NGC 6569 follow the typical patterns observed in old globular clusters. For example, the [O/Fe], [Na/Fe], and [Al/Fe] abundances exhibit full ranges of ∼0.6–0.8 dex, and the cluster exhibits a clear O–Na anti–correlation and Na–Al correlation. However, [Mg/Fe] and [Si/Fe] exhibit dispersions of only 0.09 dex each, and neither abundance ratio is correlated with [O/Fe], [Na/Fe], or [Al/Fe]. The data are therefore consistent with a scenario in which second generation (O–poor; Na/Al–rich) stars formed from gas that was processed at temperatures of ∼45–75 MK. We also find some

---

the same mass (0.7 $M_\odot$; the PGPUC grid lower HB mass limit); however, He–rich stars are likely to evolve faster and have a lower ZAHB mass. Additional effects such as mass loss and rotation are also not considered.

[13]An important caveat in this analysis is that the [Al/Mg] IQR versus ΔY correlation shown in Figure 14 is primarily based on clusters with [Fe/H] < –1. Higher metallicity clusters tend to have smaller [Al/Fe] spreads (e.g., Carretta et al. 2009c, see their Figure 3) so the ΔY value estimated here for NGC 6569 may be a lower limit.

evidence that NGC 6569 may be decomposed into at least two distinct populations with different light element compositions.

The α, Fe–peak, and neutron–capture element abundances are generally consistent with rapid formation and chemical enrichment. The [X/Fe] ratios of Mg, Si, and Ca are all enhanced by about a factor of two relative to the Sun, and the star–to–star scatter is $\lesssim$ 0.1 dex for each element. Both [Cr/Fe] and [Ni/Fe] exhibit mean abundances that are approximately solar with dispersions of 0.16 and 0.05 dex, respectively. We suspect that the larger [Cr/Fe] dispersion is due to increased measurement uncertainties rather than intrinsic cosmic scatter. For the neutron–capture elements, we find $\langle$[La/Fe]$\rangle$ = +0.38 dex (σ = 0.14 dex) and $\langle$[Eu/Fe]$\rangle$ = +0.49 dex (σ = 0.12 dex), and the moderately depleted mean [La/Eu] ratio of –0.11 dex suggests significant pollution via the r–process. However, NGC 6569 does not reach the lowest [La/Eu] values found in some halo clusters, and as a result may have experienced some s–process enrichment.

The overall light and heavy element chemical composition patterns of NGC 6569 match the mean trends exhibited by other bulge/inner Galaxy globular clusters. However, the O–Na anti–correlation and Na–Al correlation in NGC 6569 extend to some of the lowest [O/Fe] and highest [Na,Al/Fe] values found in metal–rich ([Fe/H] $\gtrsim$ –1 dex) bulge clusters, but do not reach the most extreme values observed in clusters such as NGC 6388 and NGC 6441. As a population, the bulge clusters exhibit little change in their mean [La/Eu] abundances from at least [Fe/H] $\sim$ –2.2 to –0.15 dex, which suggests s–process enrichment has been minimal. In fact, the mean heavy element composition of $\langle$[La/Eu]$\rangle$ = –0.14 dex (σ = 0.15 dex) for the bulge clusters is within the pure r–process range observed in metal–poor ([Fe/H] < –1.4 dex) halo stars and clusters.

A comparison of mean compositions between bulge/inner Galaxy globular cluster and field stars revealed that both populations exhibit similar abundance trends for a wide range of elements. For [Fe/H] $\lesssim$ –0.4 dex, the [α/Fe], [Cr/Fe], [Ni/Fe], [Eu/Fe], and [La/Eu] distributions are nearly indistinguishable between the two groups. At [Fe/H] $\gtrsim$ –0.4 dex, more data are needed to determine if the clusters remain α–enhanced to higher [Fe/H] than the field stars, and also to determine if the two populations share similar [La/Fe] trends. Clear light element abundance differences are present between the bulge cluster and field stars for [O/Fe], [Na/Fe], and [Al/Fe] across a wide range in [Fe/H]. Specifically, the clusters scatter to higher [Na,Al/Fe] and lower [O/Fe], and the field stars do not exhibit the same light element (anti–)correlations that are prevalent in the globular clusters. Despite sharing similar α, Fe–peak, and heavy element abundances, the light elements rule out that a large fraction of bulge field stars could have originated from self–enriched but now dissolved globular clusters.

Following the discovery of a double red HB in NGC 6569 by Mauro et al. (2012), we investigated the radial velocity, metallicity, and light element abundances of each population. The velocity and [Fe/H] measurements indicate that both HBs contain cluster members, but unlike the case of Terzan 5 we did not detect a large metallicity spread. We found the brighter HB to have a mean [Fe/H] that is higher by 0.13 dex, but we do not consider the [Fe/H] difference to be significant given the small samples sizes ($\sim$5 stars in each HB group), the $\sim$0.15 dex CaT measurement uncertainties of individual stars, and the small 0.05 dex [Fe/H] dispersion observed for the M2FS RGB sample. A further comparison of the co–added spectra revealed that the line strengths vary by $\lesssim 3\%$ between the two HB groups, and we did not detect significant differences in mean light element composition. By extension, we infer that both HB populations have similar He abundances. However, we cannot rule out He abundance differences as small as $\Delta Y \sim 0.02$ that may be sufficient to reproduce the observed double red HB feature.

This research has made use of NASA's Astrophysics Data System Bibliographic Services. This research has made use of the services of the ESO Science Archive Facility. This publication has made use of data products from the Two Micron All Sky Survey, which is a joint project of the University of Massachusetts and the Infrared Processing and Analysis Center/California Institute of Technology, funded by the National Aeronautics and Space Administration and the National Science Foundation. C.I.J. gratefully acknowledges support from the Clay Fellowship, administered by the Smithsonian Astrophysical Observatory. M.M. is grateful for support from the National Science Foundation to develop M2FS (AST–0923160) and carry out the observations reported here (AST–1312997), and to the University of Michigan for its direct support of M2FS construction and operation. M.G.W. is supported by National Science Foundation grants AST–1313045 and AST–1412999. R.M.R acknowledges support from grant AST–1413755 from the National Science Foundation.

REFERENCES

Alonso, A., Arribas, S., & Martínez-Roger, C. 1999, A&AS, 140, 261

Alves-Brito, A., Barbuy, B., Zoccali, M., et al. 2006, A&A, 460, 269

Alves-Brito, A., Meléndez, J., Asplund, M., Ramírez, I., & Yong, D. 2010, A&A, 513, A35

Armandroff, T. E., & Da Costa, G. S. 1991, AJ, 101, 1329

Barbuy, B., Zoccali, M., Ortolani, S., et al. 2006, A&A, 449, 349

Barbuy, B., Zoccali, M., Ortolani, S., et al. 2007, AJ, 134, 1613

Barbuy, B., Chiappini, C., Cantelli, E., et al. 2014, A&A, 570, A76

Barbuy, B., Cantelli, E., Vemado, A., et al. 2016, A&A, 591, A53

Bastian, N., Lamers, H. J. G. L. M., de Mink, S. E., et al. 2013, MNRAS, 436, 2398

Battaglia, G., Irwin, M., Tolstoy, E., et al. 2008, MNRAS, 383, 183

Bekki, K., & Tsujimoto, T. 2016, ApJ, 831, 70

Bellazzini, M., Ibata, R. A., Chapman, S. C., et al. 2008, AJ, 136, 1147

Bensby, T., Yee, J. C., Feltzing, S., et al. 2013, A&A, 549, A147

Bergemann, M., Lind, K., Collet, R., Magic, Z., & Asplund, M. 2012, MNRAS, 427, 27

Bica, E. L. D., & Pastoriza, M. G. 1983, Ap&SS, 91, 99

Bisterzo, S., Gallino, R., Straniero, O., Cristallo, S., & Käppeler, F. 2010, MNRAS, 404, 1529

Bragaglia, A., Carretta, E., Gratton, R., et al. 2010a, A&A, 519, A60

Bragaglia, A., Carretta, E., Gratton, R. G., et al. 2010b, ApJ, 720, L41

Busso, M., Gallino, R., & Wasserburg, G. J. 1999, ARA&A, 37, 239

Carrera, R., Gallart, C., Pancino, E., & Zinn, R. 2007, AJ, 134, 1298

Carrera, R., Pancino, E., Gallart, C., & del Pino, A. 2013, MNRAS, 434, 1681

Carretta, E., Cohen, J. G., Gratton, R. G., & Behr, B. B. 2001, AJ, 122, 1469

Carretta, E., Bragaglia, A., Gratton, R. G., et al. 2007a, A&A, 464, 967

Carretta, E., Recio-Blanco, A., Gratton, R. G., Piotto, G., & Bragaglia, A. 2007b, ApJ, 671, L125

Carretta, E., Bragaglia, A., Gratton, R., D'Orazi, V., & Lucatello, S. 2009a, A&A, 508, 695

Carretta, E., Bragaglia, A., Gratton, R. G., et al. 2009b, A&A, 505, 117

Carretta, E., Bragaglia, A., Gratton, R., & Lucatello, S. 2009c, A&A, 505, 139

Carretta, E., Bragaglia, A., Gratton, R., et al. 2010a, ApJ, 712, L21

Carretta, E., Bragaglia, A., Gratton, R. G., et al. 2010b, ApJ, 714, L7

Castelli, F., & Kurucz, R. L. 2004, arXiv:astro-ph/0405087

Charbonnel, C. 1995, ApJ, 453, L41

Cole, A. A., Smecker-Hane, T. A., Tolstoy, E., Bosler, T. L., & Gallagher, J. S. 2004, MNRAS, 347, 367

D'Antona, F., & Ventura, P. 2007, MNRAS, 379, 1431

D'Antona, F., Vesperini, E., D'Ercole, A., et al. 2016, MNRAS, 458, 2122

D'Orazi, V., Gratton, R., Lucatello, S., et al. 2010, ApJ, 719, L213

Da Costa, G. S. 2016a, The General Assembly of Galaxy Halos: Structure, Origin and Evolution, 317, 110

Da Costa, G. S. 2016b, MNRAS, 455, 199

Decressin, T., Charbonnel, C., & Meynet, G. 2007, A&A, 475, 859

de Mink, S. E., Pols, O. R., Langer, N., & Izzard, R. G. 2009, A&A, 507, L1

Denissenkov, P. A., & VandenBerg, D. A. 2003, ApJ, 593, 509

Denissenkov, P. A., & Hartwick, F. D. A. 2014, MNRAS, 437, L21

Dias, B., Barbuy, B., Saviane, I., et al. 2016, A&A, 590, A9

Dinescu, D. I., van Altena, W. F., Girard, T. M., & López, C. E. 1999, AJ, 117, 277

Dobrovolskas, V., Kučinskas, A., Bonifacio, P., et al. 2015, A&A, 576, A128

Dotter, A., Chaboyer, B., Jevremović, D., et al. 2008, ApJS, 178, 89

Dupree, A. K., Strader, J., & Smith, G. H. 2011, ApJ, 728, 155

Dutra, C. M., & Bica, E. 2000, A&A, 359, 347

Feltzing, S., Primas, F., & Johnson, R. A. 2009, A&A, 493, 913

Ferraro, F. R., Dalessandro, E., Mucciarelli, A., et al. 2009, Nature, 462, 483

Ferraro, F. R., Massari, D., Dalessandro, E., et al. 2016, ApJ, 828, 75

Frischknecht, U., Hirschi, R., Pignatari, M., et al. 2016, MNRAS, 456, 1803

Fulbright, J. P., McWilliam, A., & Rich, R. M. 2007, ApJ, 661, 1152

Gallino, R., Arlandini, C., Busso, M., et al. 1998, ApJ, 497, 388

García Pérez, A. E., Cunha, K., Shetrone, M., et al. 2013, ApJ, 767, L9

González Hernández, J. I., & Bonifacio, P. 2009, A&A, 497, 497

Gonzalez, O. A., Rejkuba, M., Zoccali, M., et al. 2011, A&A, 530, A54

Gonzalez, O. A., Rejkuba, M., Zoccali, M., et al. 2012, A&A, 543, A13

Gratton, R., Sneden, C., & Carretta, E. 2004, ARA&A, 42, 385

Gratton, R. G., Lucatello, S., Bragaglia, A., et al. 2006, A&A, 455, 271

Gratton, R. G., Lucatello, S., Bragaglia, A., et al. 2007, A&A, 464, 953

Gratton, R. G., Carretta, E., Bragaglia, A., Lucatello, S., & D'Orazi, V. 2010, A&A, 517, A81

Gratton, R. G., Carretta, E., & Bragaglia, A. 2012, A&A Rev., 20, 50

Gratton, R. G., Lucatello, S., Sollima, A., et al. 2015, A&A, 573, A92

Harris, W. E. 1996, AJ, 112, 1487

Hill, V., Lecureur, A., Gómez, A., et al. 2011, A&A, 534, A80

Howes, L. M., Asplund, M., Casey, A. R., et al. 2014, MNRAS, 445, 4241

Howes, L. M., Casey, A. R., Asplund, M., et al. 2015, Nature, 527, 484

Idiart, T. P., Thevenin, F., & de Freitas Pacheco, J. A. 1997, AJ, 113, 1066

James, G., François, P., Bonifacio, P., et al. 2004, A&A, 427, 825

Johnson, C. I., & Pilachowski, C. A. 2010, ApJ, 722, 1373

Johnson, C. I., Rich, R. M., Kobayashi, C., & Fulbright, J. P. 2012, ApJ, 749, 175

Johnson, C. I., Rich, R. M., Kobayashi, C., Kunder, A., & Koch, A. 2014, AJ, 148, 67

Johnson, C. I., Rich, R. M., Pilachowski, C. A., et al. 2015a, AJ, 150, 63

Johnson, C. I., McDonald, I., Pilachowski, C. A., et al. 2015b, AJ, 149, 71

Johnson, C. I., Caldwell, N., Rich, R. M., Pilachowski, C. A., & Hsyu, T. 2016, AJ, 152, 21

Johnson, C. I., Caldwell, N., Rich, R. M., et al. 2017a, ApJ, 836, 168

Johnson, C. I., Caldwell, N., Rich, R. M., & Walker, M. G. 2017b, AJ, 154, 155

Johnson, C. I., Caldwell, N., Rich, R. M., et al. 2017c, ApJ, 842, 24

Jönsson, H., Ryde, N., Nordlander, T., et al. 2017, A&A, 598, A100

Kraft, R. P. 1994, PASP, 106, 553

Kunder, A., Koch, A., Rich, R. M., et al. 2012, AJ, 143, 57

Kurtz, M. J., & Mink, D. J. 1998, PASP, 110, 934

Lardo, C., Mucciarelli, A., & Bastian, N. 2016, MNRAS, 457, 51

Lawler, J. E., Bonvallet, G., & Sneden, C. 2001a, ApJ, 556, 452

Lawler, J. E., Wickliffe, M. E., den Hartog, E. A., & Sneden, C. 2001b, ApJ, 563, 1075

Lee, J.-W., & Carney, B. W. 2002, AJ, 124, 1511

Lee, J.-W. 2015, ApJS, 219, 7

Lind, K., Asplund, M., Barklem, P. S., & Belyaev, A. K. 2011, A&A, 528, A103

Marino, A. F., Sneden, C., Kraft, R. P., et al. 2011a, A&A, 532, A8

Marino, A. F., Milone, A. P., Piotto, G., et al. 2011b, ApJ, 731, 64

Marino, A. F., Milone, A. P., Karakas, A. I., et al. 2015, MNRAS, 450, 815

Massari, D., Mucciarelli, A., Dalessandro, E., et al. 2012, ApJ, 755, L32

Massari, D., Mucciarelli, A., Ferraro, F. R., et al. 2014, ApJ, 795, 22

Massari, D., Dalessandro, E., Ferraro, F. R., et al. 2015, ApJ, 810, 69

Massari, D., Mucciarelli, A., Dalessandro, E., et al. 2017, MNRAS, 468, 1249

Mateo, M., Bailey, J. I., Crane, J., et al. 2012, Proc. SPIE, 8446, 84464Y

Mauro, F., Moni Bidin, C., Cohen, R., et al. 2012, ApJ, 761, L29

Mauro, F., Moni Bidin, C., Geisler, D., et al. 2014, A&A, 563, A76

McWilliam, A., & Rich, R. M. 1994, ApJS, 91, 749

McWilliam, A. 2016, PASA, 33, e040

Meléndez, J., Asplund, M., Alves-Brito, A., et al. 2008, A&A, 484, L21

Milone, A. P., Marino, A. F., Dotter, A., et al. 2014, ApJ, 785, 21

Mucciarelli, A., Lapenna, E., Massari, D., et al. 2015, ApJ, 809, 128

Muñoz, C., Villanova, S., Geisler, D., et al. 2017, A&A, 605, A12

Ness, M., Freeman, K., Athanassoula, E., et al. 2013, MNRAS, 432, 2092

Ness, M., Asplund, M., & Casey, A. R. 2014, MNRAS, 445, 2994

Norris, J. E., & Da Costa, G. S. 1995, ApJ, 447, 680

Olszewski, E. W., Schommer, R. A., Suntzeff, N. B., & Harris, H. C. 1991, AJ, 101, 515

O'Malley, E. M., Knaizev, A., McWilliam, A., & Chaboyer, B. 2017, ApJ, 846, 23

Origlia, L., & Rich, R. M. 2004, AJ, 127, 3422

Origlia, L., Valenti, E., & Rich, R. M. 2005a, MNRAS, 356, 1276

Origlia, L., Valenti, E., Rich, R. M., & Ferraro, F. R. 2005b, MNRAS, 363, 897

Origlia, L., Valenti, E., & Rich, R. M. 2008, MNRAS, 388, 1419

Origlia, L., Rich, R. M., Ferraro, F. R., et al. 2011, ApJ, 726, L20

Origlia, L., Massari, D., Rich, R. M., et al. 2013, ApJ, 779, L5

Ortolani, S., Bica, E., & Barbuy, B. 2001, A&A, 374, 564

Prantzos, N., Charbonnel, C., & Iliadis, C. 2007, A&A, 470, 179

Ramírez, I., & Allende Prieto, C. 2011, ApJ, 743, 135

Rich, R. M., Origlia, L., & Valenti, E. 2012, ApJ, 746, 59

Roederer, I. U., Cowan, J. J., Karakas, A. I., et al. 2010, ApJ, 724, 975

Roederer, I. U. 2011, ApJ, 732, L17

Rojas-Arriagada, A., Zoccali, M., Vásquez, S., et al. 2016, A&A, 587, A95

Rutledge, G. A., Hesser, J. E., Stetson, P. B., et al. 1997, PASP, 109, 883

Ryde, N., Gustafsson, B., Edvardsson, B., et al. 2010, A&A, 509, A20

Saito, R. K., Hempel, M., Minniti, D., et al. 2012, A&A, 537, A107

Santos, J. F. C., Jr., & Piatti, A. E. 2004, A&A, 428, 79

Saviane, I., da Costa, G. S., Held, E. V., et al. 2012, A&A, 540, A27

Schiavon, R. P., Johnson, J. A., Frinchaboy, P. M., et al. 2017a, MNRAS, 466, 1010

Schiavon, R. P., Zamora, O., Carrera, R., et al. 2017b, MNRAS, 465, 501

Simmerer, J., Sneden, C., Cowan, J. J., et al. 2004, ApJ, 617, 109

Skrutskie, M. F., Cutri, R. M., Stiening, R., et al. 2006, AJ, 131, 1163

Smith, V. V., Suntzeff, N. B., Cunha, K., et al. 2000, AJ, 119, 1239

Sneden, C. 1973, ApJ, 184, 839

Sneden, C. 2004, Mem. Soc. Astron. Italiana, 75, 267

Sneden, C., Lucatello, S., Ram, R. S., Brooke, J. S. A., & Bernath, P. 2014, ApJS, 214, 26

Starkenburg, E., Hill, V., Tolstoy, E., et al. 2010, A&A, 513, A34

Tang, B., Cohen, R. E., Geisler, D., et al. 2017, MNRAS, 465, 19

Tsuchiya, T., Dinescu, D. I., & Korchagin, V. I. 2003, ApJ, 589, L29

Valcarce, A. A. R., Catelan, M., & Sweigart, A. V. 2012, A&A, 547, A5

Valenti, E., Origlia, L., & Ferraro, F. R. 2005, MNRAS, 361, 272

Valenti, E., Origlia, L., & Rich, R. M. 2011, MNRAS, 414, 2690

Valenti, E., Origlia, L., Mucciarelli, A., & Rich, R. M. 2015, A&A, 574, A80

Van der Swaelmen, M., Barbuy, B., Hill, V., et al. 2016, A&A, 586, A1

Ventura, P., & D'Antona, F. 2009, A&A, 499, 835

Ventura, P., Di Criscienzo, M., Carini, R., & D'Antona, F. 2013, MNRAS, 431, 3642

Villanova, S., Geisler, D., & Piotto, G. 2010, ApJ, 722, L18

Villanova, S., Moni Bidin, C., Mauro, F., Munoz, C., & Monaco, L. 2017, MNRAS, 464, 2730

Yong, D., Alves Brito, A., Da Costa, G. S., et al. 2014, MNRAS, 439, 2638

Yong, D., Da Costa, G. S., & Norris, J. E. 2016, MNRAS, 460, 1846

Yoon, S.-J., Joo, S.-J., Ree, C. H., et al. 2008, ApJ, 677, 1080-1090

Zinn, R. 1980, ApJS, 42, 19

Zoccali, M., Hill, V., Lecureur, A., et al. 2008, A&A, 486, 177

Zoccali, M., Gonzalez, O. A., Vasquez, S., et al. 2014, A&A, 562, A66

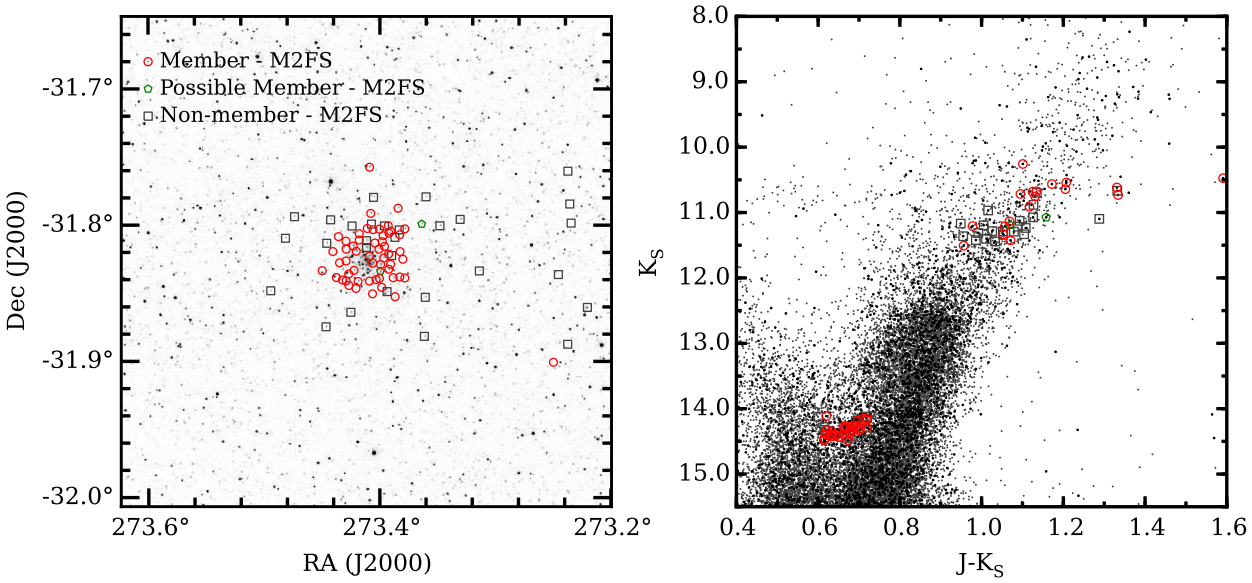

Fig. 1.— Left: the sky coordinates of all member (open red circles), possible member (open green pentagons), and non–member (open grey boxes) stars observed with M2FS are overplotted on a 2MASS J–band image centered on NGC 6569. The stars designated as possible members have radial velocities consistent with cluster membership but lack [Fe/H] measurements. Right: the member, possible member, and non–member stars observed with M2FS are plotted on a K_S versus J–K_S color–magnitude diagram using data from the VVV survey. For stars where VVV J and/or K_S photometry was unavailable, we have substituted 2MASS magnitudes. Note that the few member stars with J–$K_S > 1.3$ either have large magnitude errors or exhibit significant differences between their VVV and 2MASS magnitudes. The filled black circles indicate all stars within 5′ of the cluster center, and the open grey circles indicate stars with projected radial distances between 5–15′ from the cluster center. The remaining colors and symbols are the same as in the left panel.

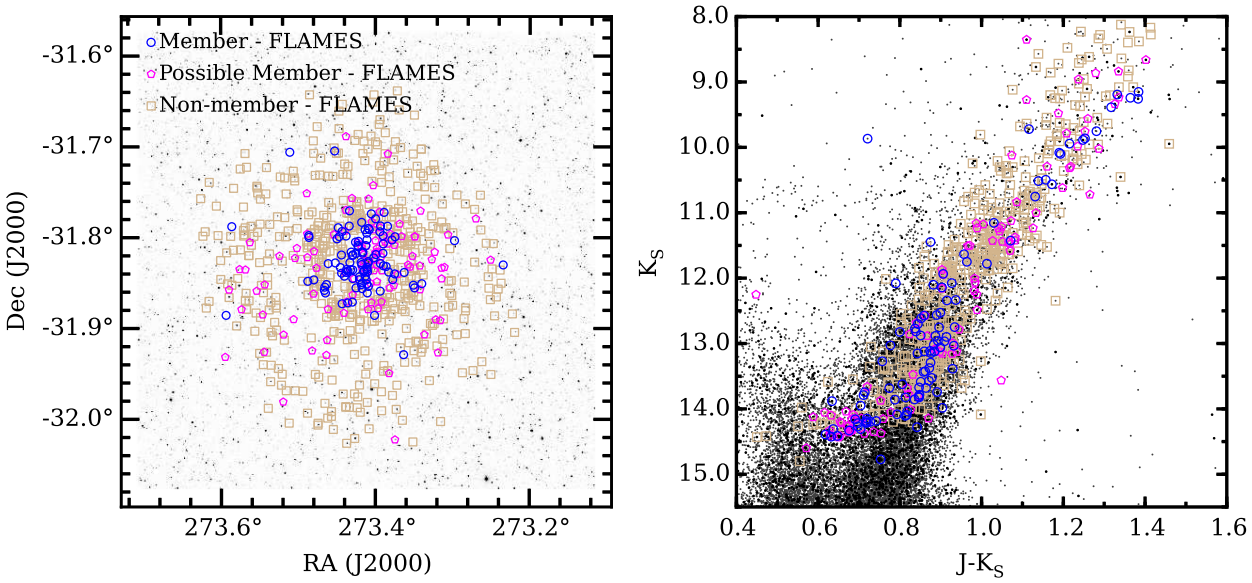

Fig. 2.— Similar to Figure 1, the left and right panels show the sky coordinates and VVV colors and magnitudes for NGC 6569 member (open blue circles), possible member (open magenta pentagons), and non–member (open tan boxes) stars observed with FLAMES.

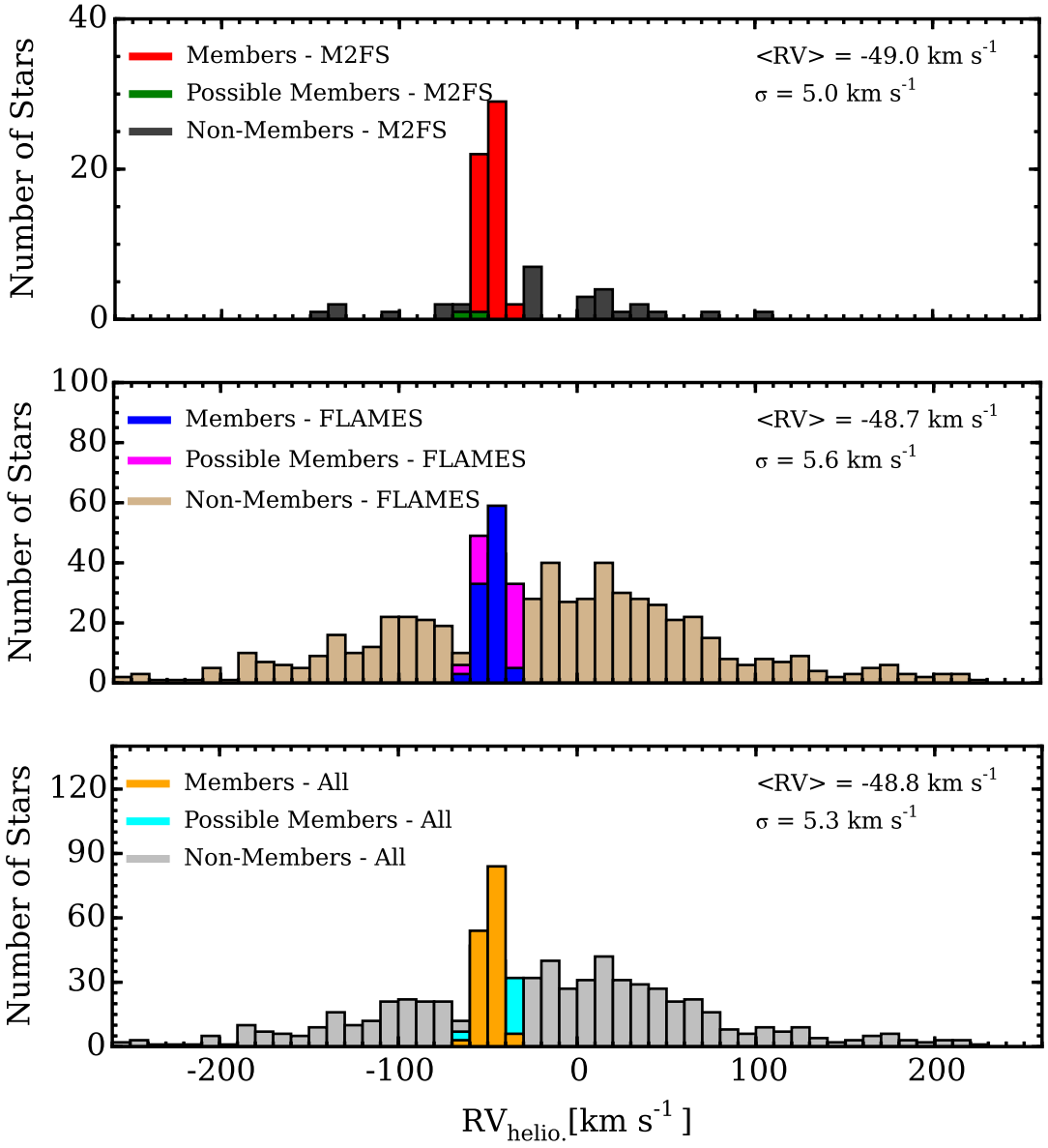

Fig. 3.— The top, middle, and bottom panels illustrate the heliocentric radial velocity distributions of member, possible member, and non–member stars observed with M2FS, FLAMES, and the combined sample, respectively. For the bottom panel, we averaged the velocities for stars in common between the M2FS and FLAMES data sets. All data are sampled into 10 km s^{-1} bins. Note that the mean velocity and dispersion values only include member stars.

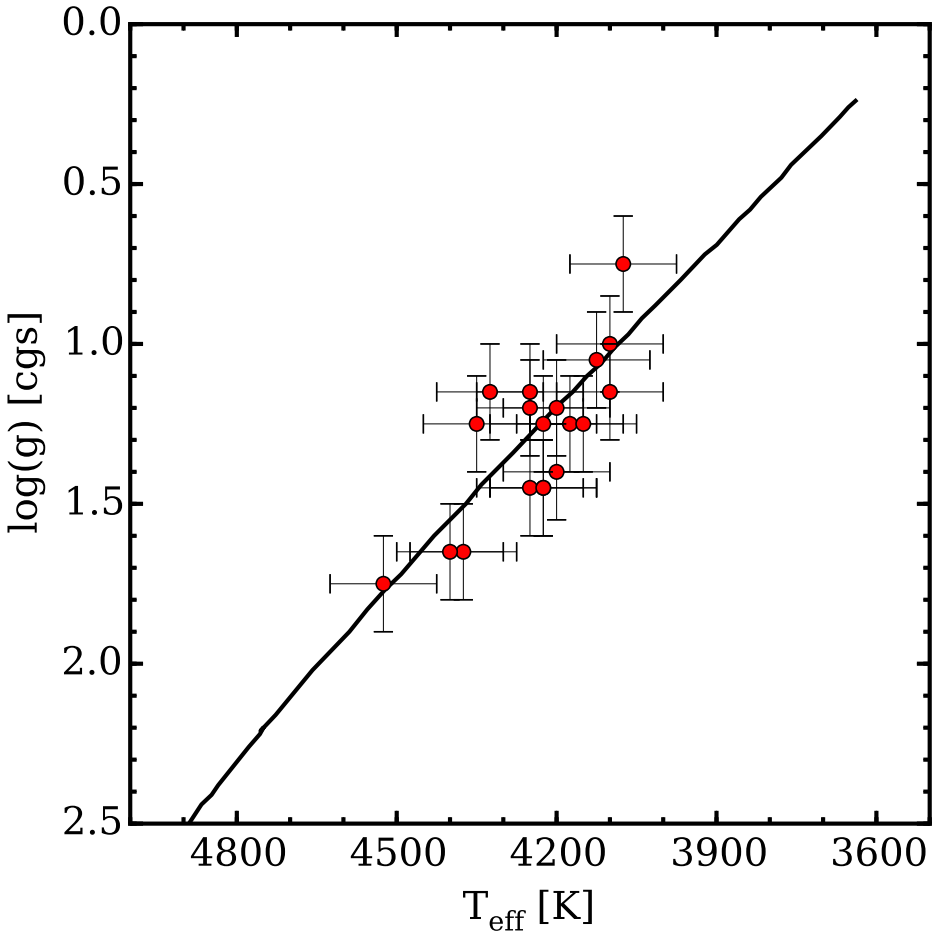

Fig. 4.— The spectroscopically determined T_{eff} and log(g) values for all M2FS stars are compared against a 10.9 Gyr α–enhanced Dartmouth isochrone (Dotter et al. 2008) with [Fe/H] = –0.85. The error bars on each star represent the adopted T_{eff} and log(g) uncertainties adopted for this analysis. See text for details.

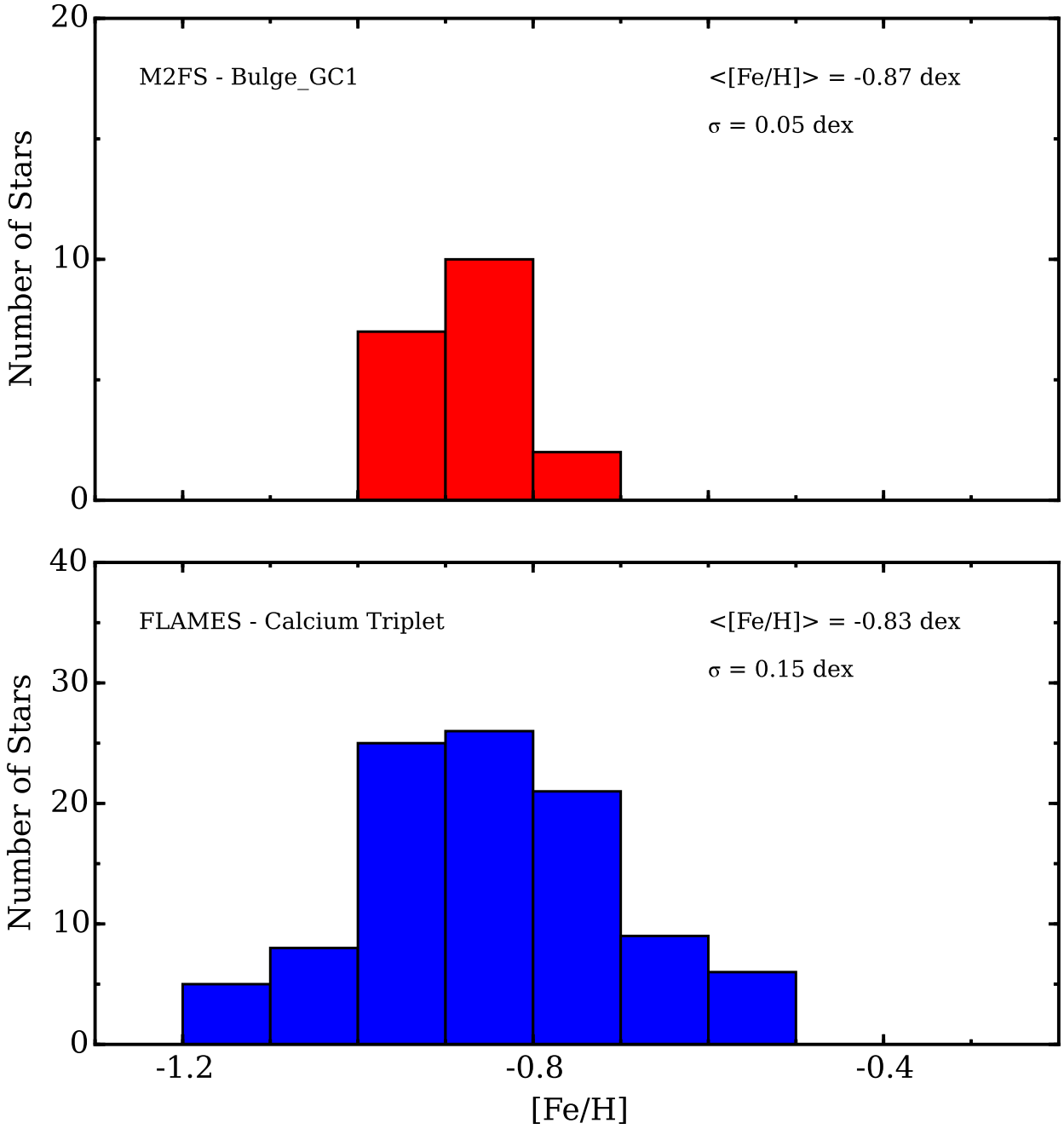

Fig. 5.— The top and bottom panels illustrate the [Fe/H] distribution functions for the M2FS and FLAMES samples, respectively. The data are sampled into 0.1 dex bins. The mean uncertainty in [Fe/H] for the Calcium Triplet data is 0.15 dex, which is comparable to the [Fe/H] dispersion shown here. Therefore, both the M2FS and FLAMES samples are consistent with NGC 6569 being a monometallic cluster.

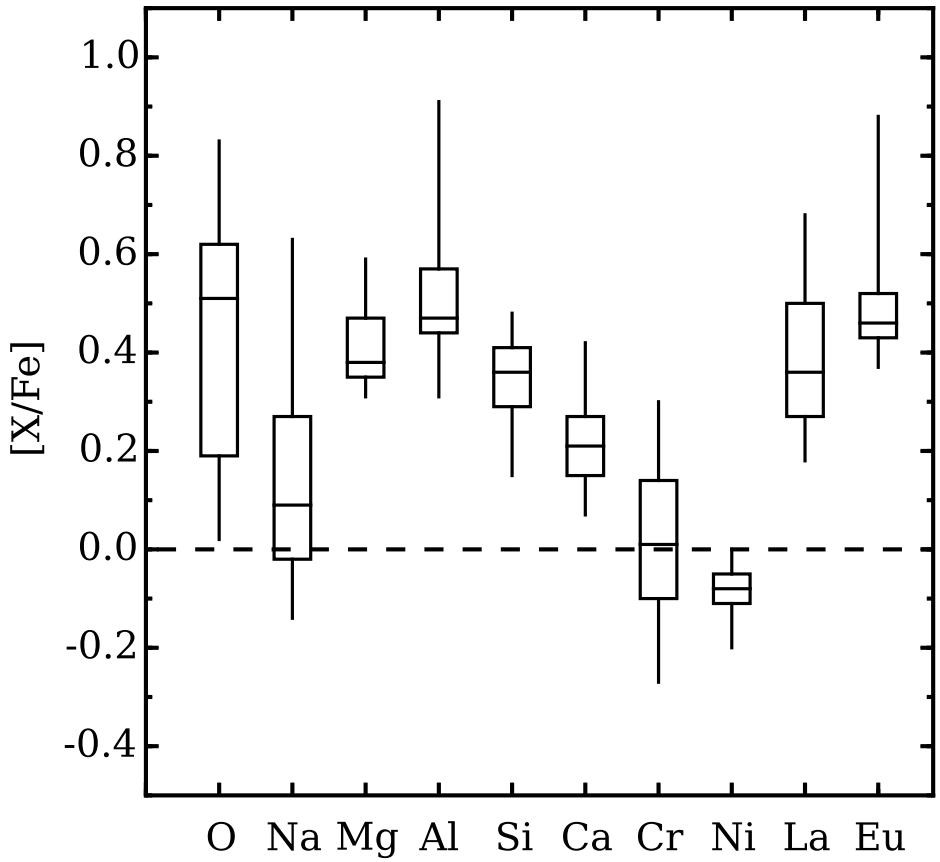

Fig. 6.— A box plot is shown to illustrate the overall composition pattern of NGC 6569. For each element, the top, middle, and bottom horizontal lines represent the third quartile, median, and first quartile [X/Fe] abundances, respectively. Similarly, the vertical solid lines indicate the maximum and minimum [X/Fe] ratios of each element.

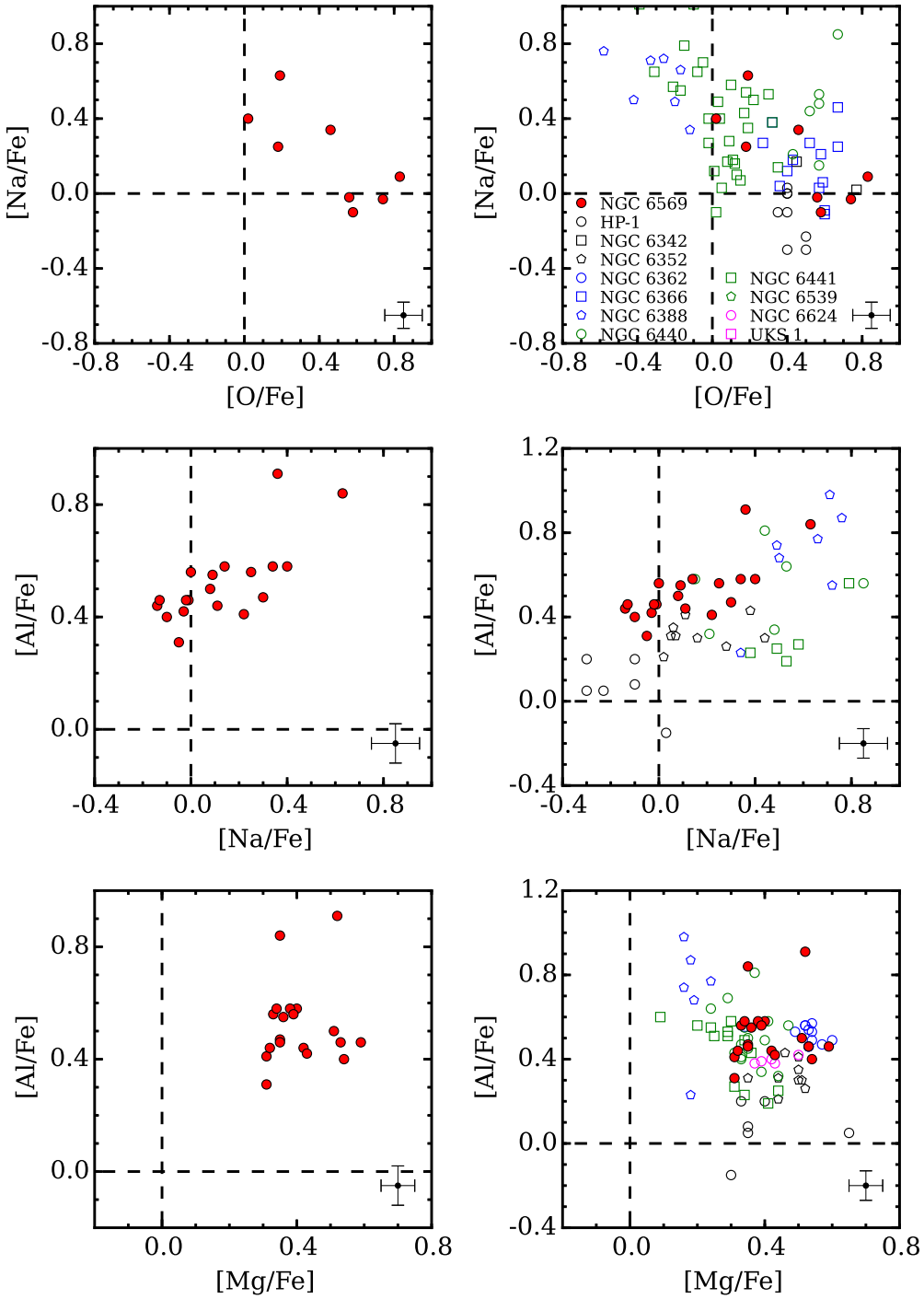

Fig. 7.— Left: plots of [O/Fe] versus [Na/Fe], [Al/Fe] versus [Na/Fe], and [Al/Fe] versus [Mg/Fe] are shown for NGC 6569. The data indicate an anti–correlation between [O/Fe] and [Na/Fe] and a correlation between [Na/Fe] and [Al/Fe], but [Mg/Fe] and [Al/Fe] do not exhibit any correlation. Right: similar plots are shown comparing the light element [X/Fe] ratios of NGC 6569 against those of similar metallicity (–1.0 $\lesssim$ [Fe/H] $\lesssim$ –0.5) inner Galaxy (|l| $\lesssim$ 20°; |b| $\lesssim$ 20°; R_{GC} $\lesssim$ 3 kpc) clusters. The data sources are provided in Table 8. Representative error bars are included for each panel.

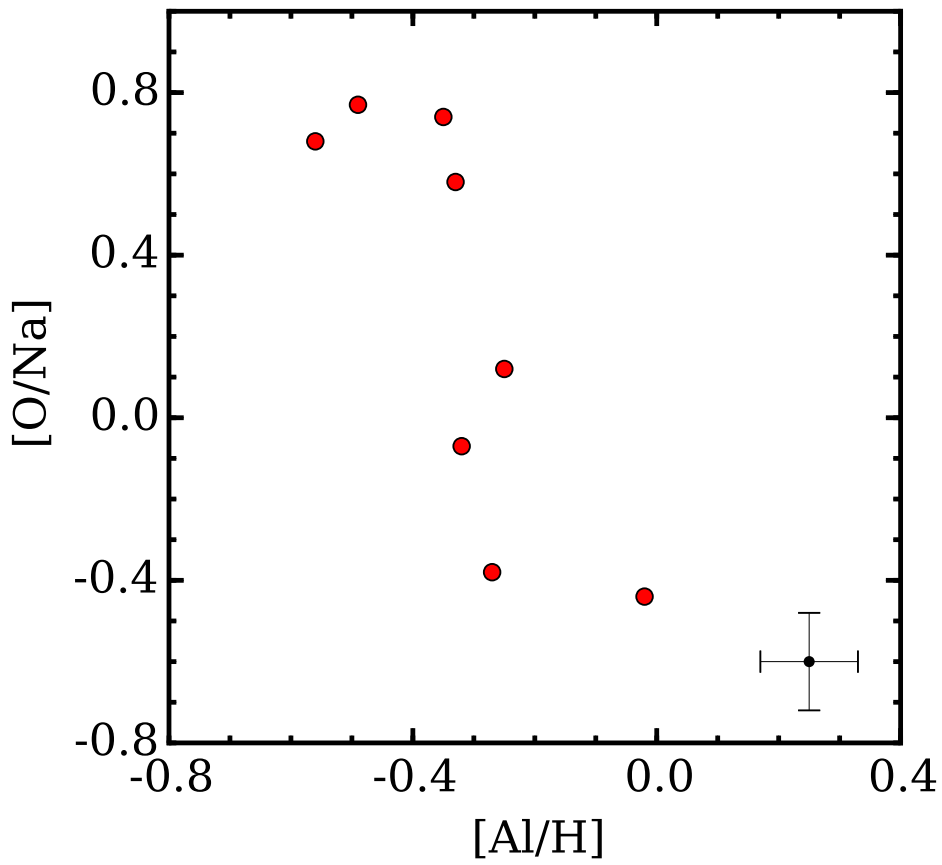

Fig. 8.— [O/Na] is plotted as a function of [Al/H] for NGC 6569. The data are consistent with NGC 6569 hosting at least two distinct populations.

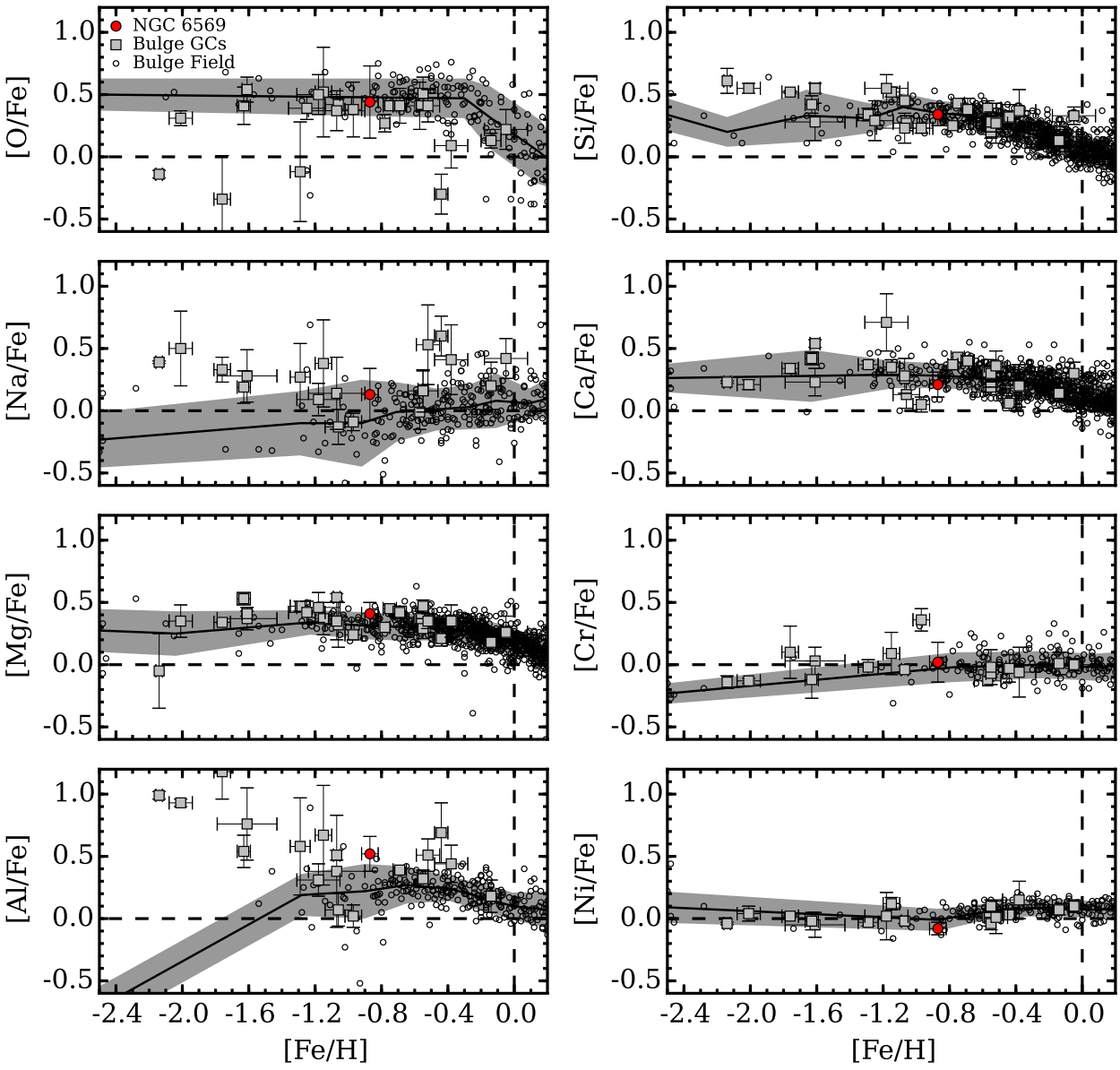

Fig. 9.— The [X/Fe] ratios of elements ranging from O to Eu are plotted as a function of [Fe/H] for NGC 6569 (filled red circle), several Galactic bulge globular clusters (filled grey boxes), and a representative sample of bulge field stars (open black circles). The cluster symbols represent the mean [X/Fe] abundances and the error bars trace the standard deviation within each cluster. The solid black lines trace moving averages of the bulge field star data, and the filled dark grey regions illustrate the 1σ variations. The data sources are listed in Table 8.

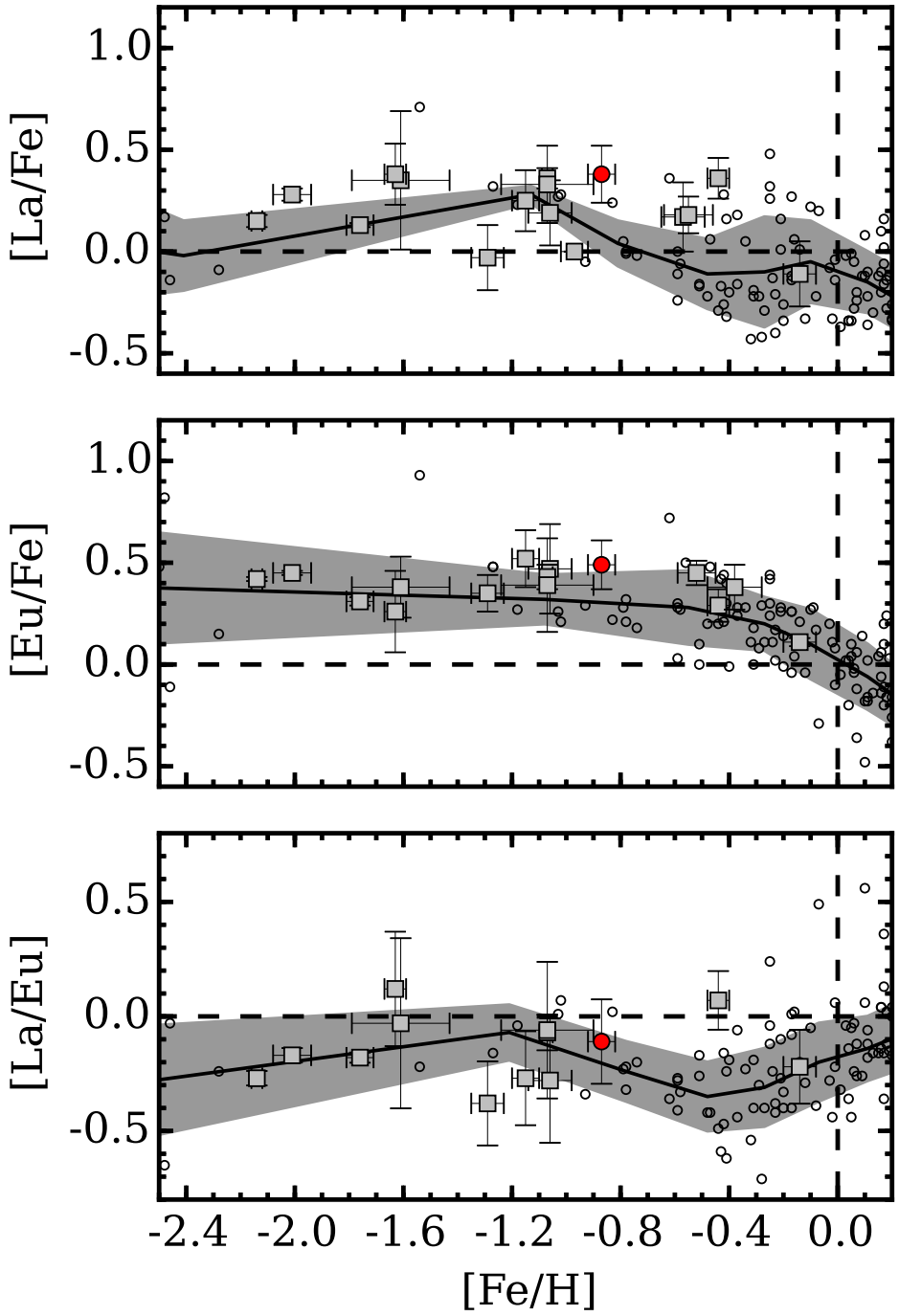

Fig. 10.— Similar to Figure 9, the [La/Fe], [Eu/Fe], and [La/Eu] ratios of Galactic bulge clusters and field stars are plotted as a function of [Fe/H].

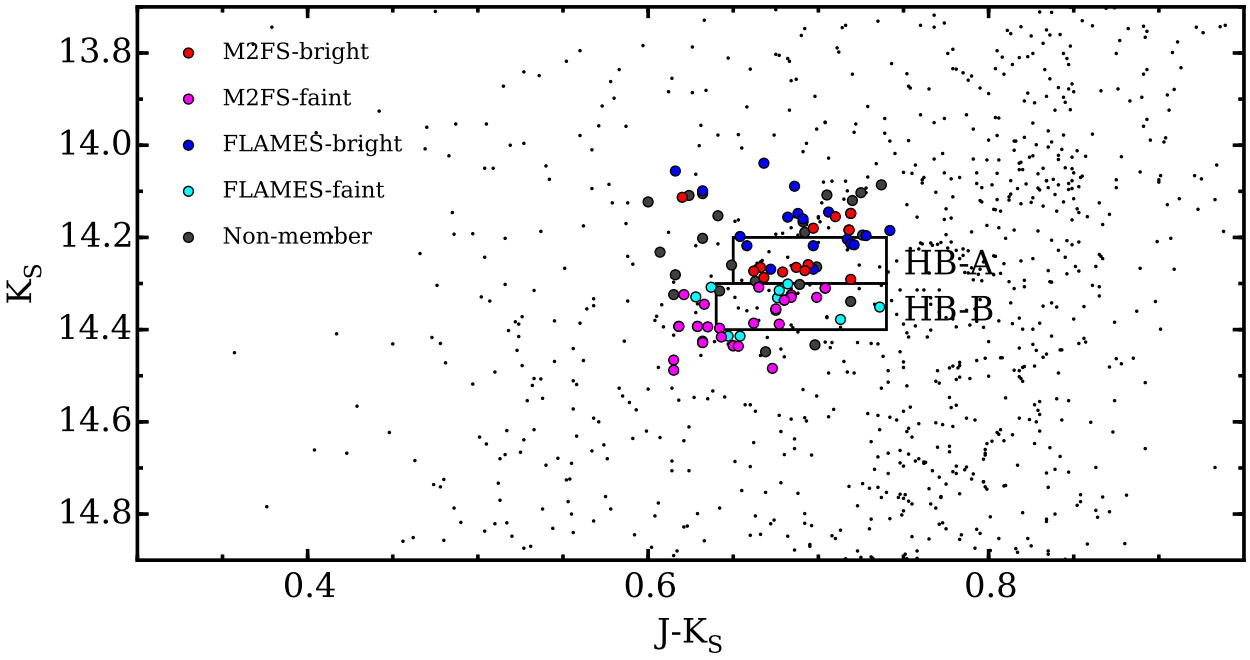

Fig. 11.— A VVV K_S versus J–K_S color–magnitude diagram is shown for the HB region of NGC 6569. The two large boxes indicate the magnitude and color ranges where Mauro et al. (2012) identified a possible double HB. The filled red and magenta circles indicate stars observed with M2FS that may belong to the "bright" (HB–A) and "faint" (HB–B) populations, respectively. Similarly, the filled blue and cyan circles show stars observed with FLAMES that may belong to the HB–A and HB–B populations. The filled grey circles indicate stars with radial velocities that are inconsistent with cluster membership.

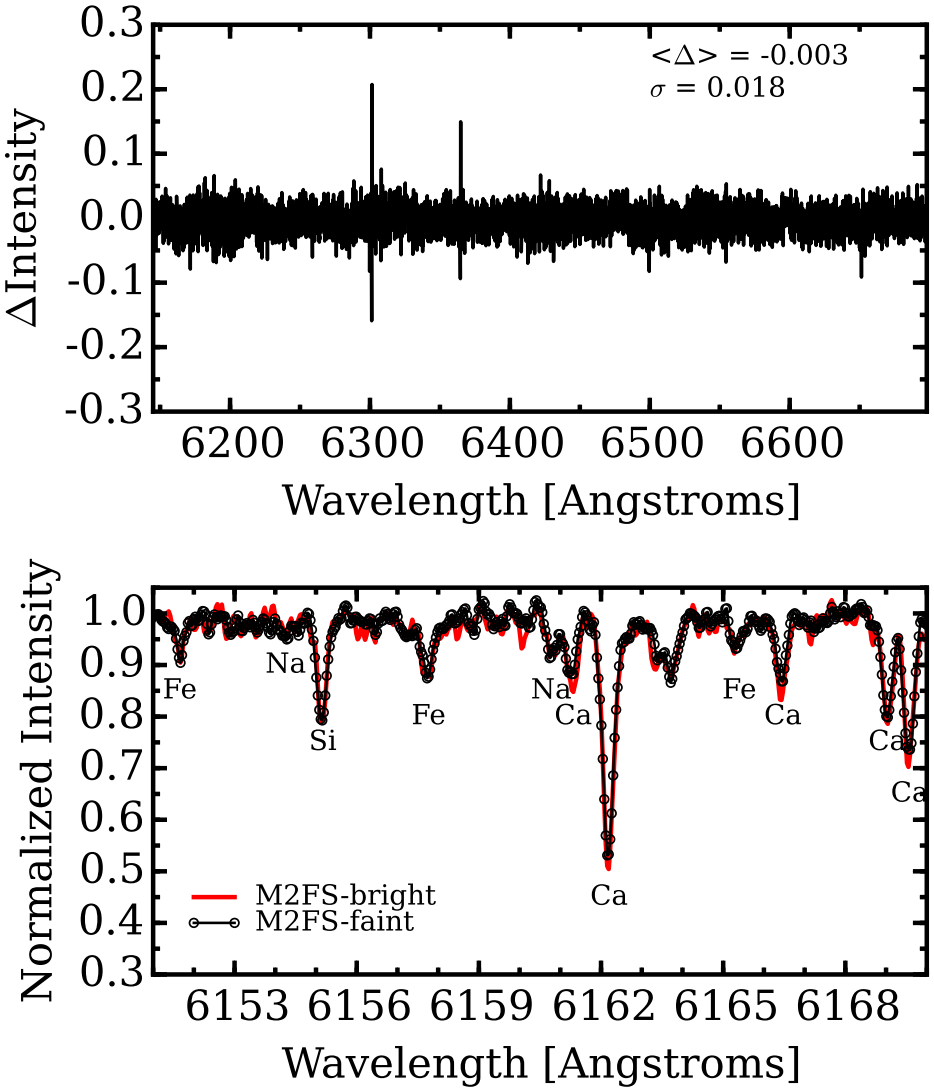

Fig. 12.— Top: after co–adding all M2FS spectra for stars residing in the bright and faint HB boxes of Figure 11, this panel shows the difference in normalized line strength (ΔIntensity) between the mean bright and faint HB populations as a function of wavelength. Except for spectral regions near the 6300 and 6363 Å telluric features, the two populations have mean spectra that agree to within 1.8%. Bottom: a sample of the spectral region near the 6154/6160 Na I lines compared the co–added M2FS–bright (red lines) and M2FS–faint (open black circles and lines) populations. The data do not present strong evidence favoring [Fe/H], [α/Fe], or light element abundance variations as the cause of the double HB.

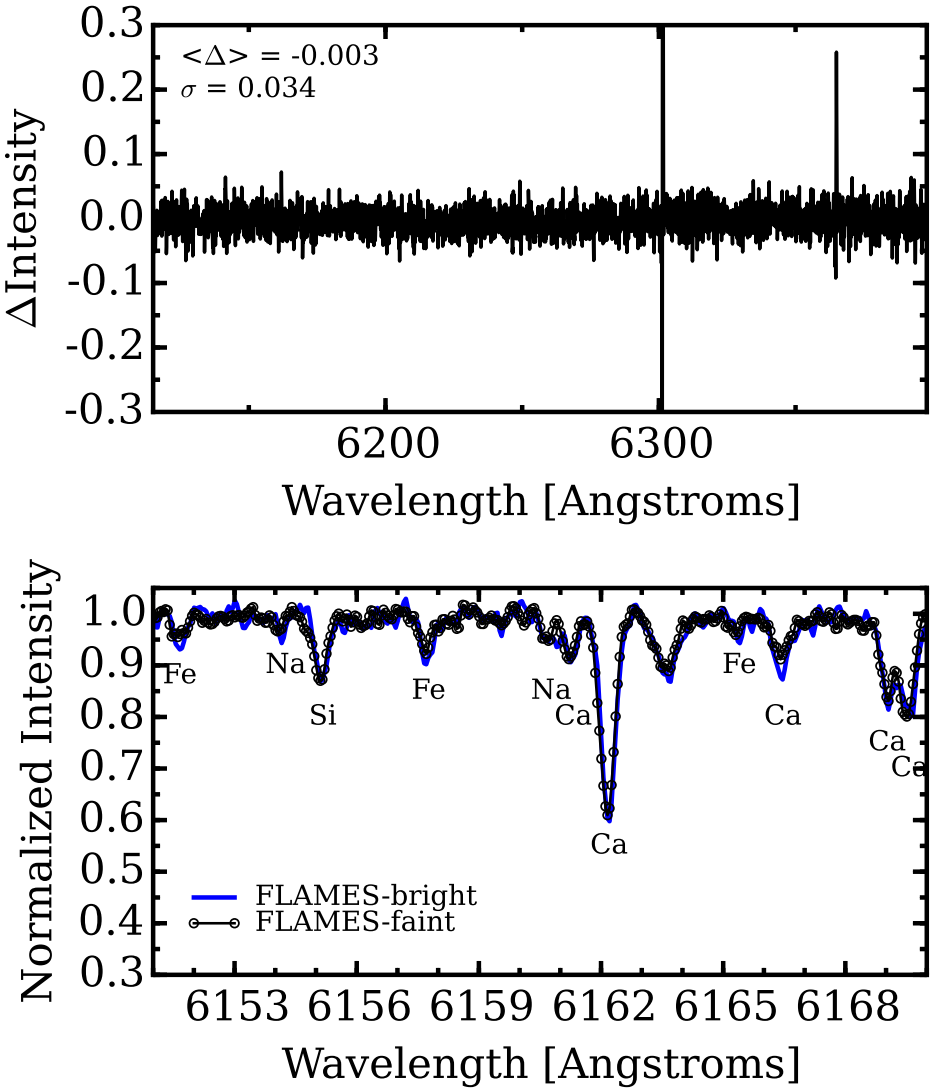

Fig. 13.— Top: similar to Figure 12, the difference in line strength between the co–added FLAMES HR13 spectra of bright and faint HB stars is plotted as a function of wavelength. The mean spectra agree to within 3.4%. Bottom: a comparison of the spectral region near the 6154/6160 Na I lines shows that the bright and faint HB stars exhibit similar mean [Fe/H], [α/Fe], and light element abundances.

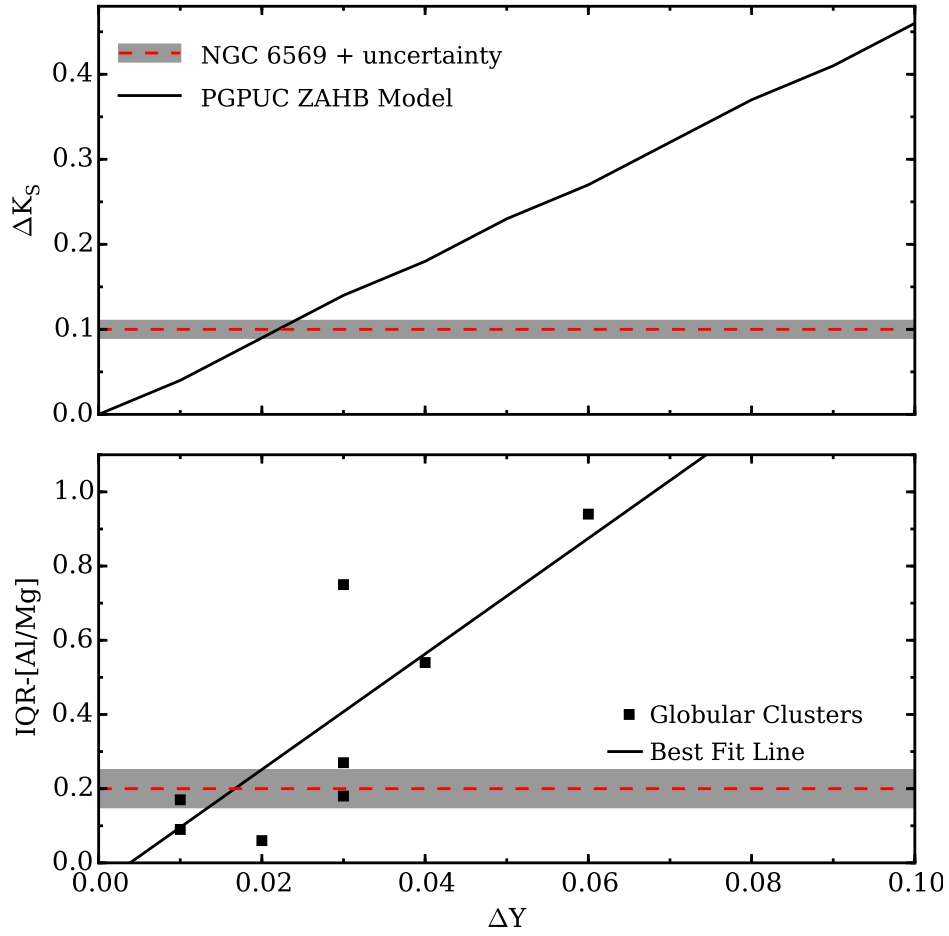

Fig. 14.— *Top:* the solid black line shows the predicted change in a 0.7 $M_\odot$ red HB star's K_S–band magnitude (ΔK_S) on the zero age HB (ZAHB) as a function of He enhancement (ΔY) where $\Delta Y = 0$ corresponds to $Y = 0.25$. The isochrone model was obtained from the Princeton–Goddard–PUC (PGPUC) stellar evolution database (Valcarce et al. 2012) assuming an age of 10.9 Gyr, [Fe/H] = –0.87 dex, [α/Fe] = +0.3 dex, and metallicity (Z) values that scale with changes in Y. The dashed red line indicates the measured difference in K_S between the two red HBs in NGC 6569, and the grey shaded region indicates the ∼0.01 magnitude uncertainty. *Bottom:* the observed change in a cluster's [Al/Mg] interquartile range (IQR) as a function of ΔY is shown using the compilation of Gratton et al. (2010). The red dashed line indicates the [Al/Mg] IQR for NGC 6569, and the shaded uncertainty region was calculated by drawing 10^3 random samples from the observed [Al/Mg] distribution and determining the standard deviations of the IQR values. Note that the Gratton et al. (2010) ΔY values refer to the difference between a cluster's median and maximum He abundances. The combined panels indicate that $\Delta Y \sim 0.02$ may be sufficient to produce a ZAHB K_S–band difference of ∼0.1 magnitudes, and that the [Al/Mg] spread in NGC 6569 is compatible with $\Delta Y \sim 0.01$–0.03, at least when compared to other clusters in the Gratton et al. (2010) compilation.

Table 1. Observation Log

Field Number	Instrument	Filter	UT Date	Exposure Time (s)
1	M2FS	Bulge_GC1	2014 June 03	3 × 2400
2	FLAMES	HR13	2014 July 03	1 × 2775
2	FLAMES	HR13	2014 August 01	1 × 2775
3	FLAMES	HR21	2015 June 22	1 × 1800
4	FLAMES	HR21	2015 June 27	1 × 2700
5	FLAMES	HR21	2015 June 27	1 × 2700
6	FLAMES	HR21	2015 June 28	1 × 2700
7	FLAMES	HR21	2015 July 26	1 × 1800
8	FLAMES	HR21	2015 July 26	1 × 1800
6	FLAMES	HR21	2015 July 26	1 × 2700
9	M2FS	Bulge_GC1	2016 June 28	3 × 1800
9	M2FS	Bulge_GC1	2016 June 30	3 × 1800
9	M2FS	Bulge_GC1	2016 July 01	3 × 2000
9	M2FS	Bulge_GC1	2016 July 01	1 × 1800

Note. — Observations with matching field numbers indicate that the same fiber and instrument configurations were used.

Table 2. M2FS Star Identifiers, Coordinates, Photometry, and Velocities

Star Name (2MASS)	RA (J2000)	DEC (J2000)	J (mag)	K_S (mag)	Star Name (VVV)	RA (J2000)	DEC (J2000)	J (mag)	K_S (mag)	$RV_{helio.}$ (km s^{-1})	RV Error (km s^{-1})
Cluster Members											
18125997−3154025	273.249915	−31.900700	15.021	14.285	J181259.99−315402.48	273.249967	−31.900692	14.952	14.265	−52.6	0.3
18133083−3148103[a]	273.378474	−31.802876	11.759	10.628	J181330.83−314810.39	273.378486	−31.802886	11.737	10.565	−48.7	0.2
18133123−3149306	273.380141	−31.825172	15.076	14.308	J181331.23−314930.67	273.380129	−31.825189	14.955	14.287	−52.0	0.4
18133181−3149104	273.382578	−31.819578	15.109	14.343	J181331.82−314910.62	273.382596	−31.819618	15.014	14.330	−57.6	0.4
18133187−3148259	273.382802	−31.807209	15.010	14.361	J181331.87−314825.98	273.382799	−31.807219	14.931	14.265	−42.7	0.3
18133187−3150175[a]	273.382816	−31.838215	14.457	13.917	J181331.90−315017.56	273.382939	−31.838213	14.902	14.184	−60.6	0.4
18133222−3147158[a]	273.384260	−31.787737	12.526	11.434	J181332.22−314715.86	273.384264	−31.787739	12.497	11.426	−49.3	0.2
18133324−3150194	273.388522	−31.838749	12.101	10.925	J181333.24−315019.50	273.388507	−31.838752	12.066	10.732	−55.2	0.3
18133375−3148167	273.390662	−31.804651	15.202	14.551	J181333.75−314816.74	273.390664	−31.804651	15.059	14.416	−41.7	0.5
18133377−3149437	273.390744	−31.828823	14.939	14.386	J181333.77−314943.66	273.390718	−31.828796	15.029	14.330	−49.8	0.4
18133412−3148218	273.392179	−31.806067	12.258	11.153	J181334.12−314821.82	273.392196	−31.806064	12.204	11.136	−56.9	0.2
18133417−3149571	273.392380	−31.832544	12.199	11.093	J181334.17−314957.21	273.392375	−31.832559	12.185	11.207	−55.2	0.2
18133419−3149168[a]	273.392467	−31.821350	14.931	14.253	J181334.17−314916.96	273.392391	−31.821379	15.022	14.393	−51.7	0.6
18133504−3148567[a]	273.396034	−31.815771	15.122	14.369	J181335.06−314856.77	273.396084	−31.815771	15.009	14.325	−45.4	0.4
18133519−3149272	273.396659	−31.824236	12.392	11.307	J181335.20−314927.26	273.396682	−31.824240	12.387	11.334	−52.3	0.2
18133531−3148284	273.397158	−31.807911	15.239	14.521	J181335.31−314828.47	273.397139	−31.807909	15.065	14.388	−48.0	0.5
18133550−3148442[a]	273.397925	−31.812286	14.519	14.104	J181335.50−314843.57	273.397941	−31.812105	15.016	14.336	−50.7	0.3
18133562−3150448	273.398452	−31.845791	15.063	14.344	J181335.63−315044.83	273.398464	−31.845787	14.964	14.272	−51.5	0.4
18133584−3149447	273.399346	−31.829111	11.805	10.680	···	···	···	···	···	−45.2	0.2
18133609−3150214	273.400381	−31.839294	14.856	14.228	J181336.09−315021.44	273.400396	−31.839289	14.978	14.345	−55.4	0.5
18133610−3148112	273.400431	−31.803118	11.756	10.553	J181336.10−314811.20	273.400436	−31.803112	11.750	10.543	−55.3	0.3
18133620−3149040	273.400847	−31.817795	12.329	11.293	J181336.20−314904.09	273.400846	−31.817805	12.267	11.210	−41.0	0.2
18133678−3150244	273.403282	−31.840132	11.950	10.775	J181336.78−315024.51	273.403289	−31.840143	11.811	10.716	−43.3	0.2
18133704−3148478	273.404372	−31.813278	15.069	14.535	J181337.04−314847.71	273.404364	−31.813254	15.010	14.291	−52.3	0.4
18133741−3148125	273.405896	−31.803486	15.190	14.592	J181337.42−314812.58	273.405922	−31.803496	14.865	14.155	−48.6	0.5
18133747−3149410	273.406129	−31.828081	11.851	10.754	J181337.46−314941.16	273.406112	−31.828102	11.358	10.257	−49.3	0.2
18133753−3151020[a]	273.406387	−31.850573	15.123	14.420	J181337.53−315102.16	273.406397	−31.850600	15.085	14.435	−51.4	0.5
18133789−3147295[a]	273.407892	−31.791531	11.935	10.857	J181337.89−314729.53	273.407909	−31.791538	11.884	10.753	−49.9	0.2
18133813−3145274[a]	273.408907	−31.757622	11.818	10.620	J181338.13−314527.31	273.408888	−31.757588	11.790	···	−39.7	0.3
18133816−3150285	273.409001	−31.841270	14.627	14.140	J181338.12−315028.27	273.408860	−31.841186	14.945	14.324	−44.3	0.5
18133819−3149224	273.409140	−31.822895	12.041	10.938	J181338.19−314922.45	273.409159	−31.822904	12.066	10.475	−45.4	0.2
18134028−3148398[a]	273.417840	−31.811069	15.087	14.467	J181340.27−314839.83	273.417819	−31.811064	15.060	14.428	−43.1	0.5
18134051−3150295	273.418833	−31.841536	11.901	10.771	J181340.52−315029.57	273.418846	−31.841548	11.948	10.617	−42.5	0.2
18134089−3149095	273.420377	−31.819328	12.029	10.912	J181340.89−314909.61	273.420384	−31.819339	···	10.883	−47.5	0.2
18134095−3150478[a]	273.420639	−31.846621	14.967	14.201	J181340.92−315047.91	273.420524	−31.846644	15.011	14.393	−50.0	0.3
18134136−3150001	273.422368	−31.833385	12.453	11.438	J181341.37−315000.19	273.422399	−31.833388	12.464	11.508	−47.6	0.3
18134151−3148556	273.422976	−31.815470	11.809	10.675	J181341.50−314855.52	273.422950	−31.815423	···	10.685	−54.8	0.2
18134243−3150400	273.426801	−31.844469	15.108	14.383	J181342.43−315040.06	273.426800	−31.844463	15.081	14.466	−44.7	0.4
18134246−3150095	273.426954	−31.835979	15.006	14.333	J181342.45−315009.62	273.426911	−31.836007	15.029	14.394	−35.9	0.4
18134298−3149042	273.429103	−31.817842	14.829	14.204	J181342.97−314904.36	273.429043	−31.817879	14.953	14.259	−49.0	0.4
18134300−3150280	273.429191	−31.841112	11.831	10.684	J181343.00−315028.01	273.429196	−31.841116	11.847	10.642	−49.2	0.2
18134301−3149352	273.429248	−31.826460	15.242	14.594	J181343.02−314935.12	273.429259	−31.826423	15.157	14.484	−52.4	0.4
18134304−3148429	273.429340	−31.811918	15.185	14.499	J181343.03−314842.92	273.429330	−31.811925	15.039	14.397	−48.4	0.4
18134377−3150254	273.432414	−31.840395	14.985	14.340	J181343.77−315025.45	273.432394	−31.840403	14.935	14.273	−49.0	0.4
18134436−3149400	273.434845	−31.827801	15.037	14.537	J181344.36−314940.10	273.434852	−31.827808	14.954	14.275	−46.5	0.4
18134457−3148308	273.435739	−31.808580	15.108	14.307	J181344.58−314831.00	273.435766	−31.808614	15.030	14.355	−54.2	0.4
18134502−3150190[a]	273.437598	−31.838614	14.824	14.026	J181345.01−315019.20	273.437581	−31.838669	14.867	14.148	−48.6	0.3
18134573−3149103	273.440580	−31.819548	15.227	14.588	J181345.73−314910.36	273.440557	−31.819545	15.089	14.436	−45.7	0.4
18134796−3150008	273.449838	−31.833578	14.828	14.178	J181347.95−315000.79	273.449812	−31.833553	14.877	14.180	−53.8	0.4

Table 2—Continued

Star Name (2MASS)	RA (J2000)	DEC (J2000)	J (mag)	K_S (mag)	Star Name (VVV)	RA (J2000)	DEC (J2000)	J (mag)	K_S (mag)	$RV_{helio.}$ (km s^{-1})	RV Error (km s^{-1})
...	...	...	...	...	J181334.27−314801.91	273.392804	−31.800531	14.733	14.113	−46.5	0.6
...	...	...	...	...	J181332.83−315109.69	273.386828	−31.852693	14.973	14.308	−50.7	0.4
...	...	...	...	...	J181338.61−314809.34[a]	273.410888	−31.802595	15.014	14.310	−40.1	0.3
...	...	...	...	...	J181340.26−314823.25	273.417788	−31.806460	15.048	14.386	−50.5	0.3
...	...	...	...	...	J181330.82−315020.13	273.378438	−31.838925	15.103	14.488	−52.6	0.5
Possible Members											
18132732−3147575	273.363857	−31.799313	12.325	11.246	J181327.32−314757.50	273.363861	−31.799307	12.259	11.190	−60.7	0.4
18133588−3150021	273.399531	−31.833939	12.207	11.165	J181335.88−315002.30	273.399522	−31.833973	12.232	11.074	−56.4	0.2
Non−Members											
18125295−3151374	273.220631	−31.860401	14.943	12.158	J181252.94−315137.37	273.220605	−31.860383	14.897	14.281	70.8	0.6
18125636−3147547	273.234865	−31.798529	15.178	14.433	J181256.36−314754.73	273.234846	−31.798536	15.117	14.448	−78.6	0.5
18125664−3147042	273.236026	−31.784521	15.224	14.244	J181256.64−314704.40	273.236009	−31.784556	15.058	14.339	31.0	0.9
18125704−3145375	273.237680	−31.760426	14.976	14.297	J181257.04−314537.60	273.237690	−31.760447	14.939	14.324	15.6	0.5
18125898−3150107	273.245769	−31.836323	14.666	14.001	J181258.95−315011.00	273.245665	−31.836390	14.723	14.123	−68.9	0.5
18131537−3150014[a]	273.314071	−31.833729	12.521	11.455	J181315.37−315001.51	273.314083	−31.833756	12.414	11.403	−30.0	0.3
18131936−3147453[a]	273.330669	−31.795921	11.890	10.709	J181319.35−314745.37	273.330665	−31.795938	11.834	10.699	−23.4	0.4
18132355−3148021[a]	273.348153	−31.800611	12.010	10.883	J181323.55−314802.24	273.348164	−31.800622	...	10.845	38.2	0.5
18132643−3146457[a]	273.360136	−31.779375	12.372	11.323	J181326.43−314645.76	273.360151	−31.779380	12.311	11.285	−144.9	0.4
18132658−3151113[a]	273.360760	−31.853144	12.251	11.250	J181326.58−315111.33	273.360755	−31.853150	12.200	11.195	43.1	0.4
18132676−3152544[a]	273.361509	−31.881792	12.384	11.308	J181326.76−315254.40	273.361532	−31.881779	12.306	11.314	−100.4	0.5
18133199−3148132	273.383324	−31.803673	12.414	11.281	J181331.99−314813.22	273.383321	−31.803672	12.344	11.236	3.8	0.4
18133288−3148328	273.387023	−31.809113	12.246	11.129	J181332.89−314832.84	273.387045	−31.809125	12.220	11.127	−39.3	0.4
18133356−3149210	273.389865	−31.822510	11.995	10.907	J181333.56−314920.96	273.389872	−31.822491	11.999	10.667	−24.6	0.3
18133451−3150561	273.393817	−31.848944	12.436	11.332	J181334.51−315056.24	273.393806	−31.848958	...	11.302	−61.6	0.3
18133504−3148024	273.396004	−31.800678	12.422	11.306	J181335.04−314802.44	273.396012	−31.800679	12.372	11.293	−20.5	0.4
18133731−3146471	273.405493	−31.779770	12.416	11.332	J181337.32−314647.21	273.405508	−31.779781	12.385	11.097	−26.0	0.4
18133774−3147577	273.407276	−31.799366	14.884	14.084	J181337.74−314757.87	273.407267	−31.799411	14.840	14.120	107.0	0.4
18133877−3148416	273.411578	−31.811575	12.429	11.310	J181338.78−314841.62	273.411606	−31.811564	12.341	11.289	−72.7	0.4
18133878−3148597	273.411591	−31.816603	12.306	11.217	J181338.78−314859.77	273.411605	−31.816604	...	11.551	20.4	0.2
18134177−3148027	273.424056	−31.800774	15.207	14.403	J181341.78−314802.70	273.424085	−31.800750	15.131	14.433	0.7	0.4
18134201−3151508[a]	273.425070	−31.864120	12.184	11.177	J181342.01−315150.85	273.425057	−31.864125	12.118	11.169	−20.6	0.3
18134620−3147464[a]	273.442541	−31.796238	12.523	11.463	J181346.21−314746.43	273.442549	−31.796232	12.475	11.442	16.6	0.4
18134701−3148484	273.445905	−31.813461	12.271	11.099	J181347.01−314848.46	273.445889	−31.813461	12.200	11.074	7.2	0.5
18134717−3152291[a]	273.446558	−31.874754	11.990	10.955	J181347.17−315229.09	273.446561	−31.874747	11.985	10.969	11.8	0.3
18135369−3147381[a]	273.473741	−31.793930	12.461	11.346	J181353.70−314738.13	273.473754	−31.793926	12.394	11.341	−130.9	0.4
18135557−3148351	273.481567	−31.809771	12.374	11.388	J181355.57−314835.15	273.481577	−31.809766	12.317	11.362	−29.8	0.2
18135863−3150538[a]	273.494319	−31.848305	12.464	11.410	J181358.63−315053.81	273.494330	−31.848282	12.408	11.422	−133.8	0.4
...	...	...	...	...	J181257.02−315314.90	273.237590	−31.887473	14.881	14.189	14.7	0.3

[a]Observed with both M2FS and FLAMES.

Note. — The first set of coordinates and photometry are on the 2MASS system and the second set are on the VVV system.

Table 3. FLAMES Star Identifiers, Coordinates, Photometry, and Velocities

Star Name (2MASS)	RA (J2000)	DEC (J2000)	J (mag)	K_S (mag)	Star Name (VVV)	RA (J2000)	DEC (J2000)	J (mag)	K_S (mag)	Star Name (VLT)	RA (J2000)	DEC (J2000)	$RV_{helio.}$ (km s^{-1})	RV Error (km s^{-1})
Cluster Members														
18131138−3148128	273.297457	−31.803564	11.104	9.921	J181311.39−314812.91	273.297464	−31.803588	11.034	9.753	3002910	273.297	−31.8036	−47.8	0.7
18132157−3151036	273.339884	−31.851017	14.125	13.269	J181321.57−315103.68	273.339885	−31.851023	14.024	13.148	3001489	273.340	−31.8510	−40.4	0.6
18132381−3151202	273.349243	−31.855625	12.237	11.177	J181323.81−315120.31	273.349248	−31.855644	12.185	11.155	3001323	273.349	−31.8556	−52.4	0.6
18132416−3151095	273.350701	−31.852650	14.167	13.292	...	...	...	...	...	3001259	273.351	−31.8526	−44.9	0.7
18132703−3150191	273.362656	−31.838642	14.063	13.102	J181327.03−315019.17	273.362653	−31.838660	13.980	13.120	3000849	273.363	−31.8386	−52.5	0.9
18132719−3155450	273.363333	−31.929184	10.640	9.786	J181327.19−315545.14	273.363331	−31.929206	10.588	9.867	3003469	273.363	−31.9292	−40.2	0.6
18132987−3147575	273.374495	−31.799328	14.487	13.547	J181329.88−314757.53	273.374508	−31.799314	14.435	13.584	2000503	273.374	−31.7993	−43.1	0.8
18132999−3150248	273.374966	−31.840237	14.950	14.219	J181329.98−315024.90	273.374944	−31.840251	14.945	14.308	2000789	273.375	−31.8402	−42.3	1.9
18133061−3150479	273.377564	−31.846657	13.033	12.098	J181330.61−315048.09	273.377573	−31.846693	13.045	12.142	2000151	273.378	−31.8467	−49.9	0.6
18133083−3148103[a]	273.378474	−31.802876	11.759	10.628	J181330.83−314810.39	273.378486	−31.802886	11.737	10.565	2000042	273.378	−31.8029	−50.9	0.7
18133187−3150175[a]	273.382816	−31.838215	14.457	13.917	J181331.90−315017.56	273.382939	−31.838213	14.902	14.184	2000707	273.383	−31.8382	−61.1	0.1
18133222−3147158[a]	273.384260	−31.787737	12.526	11.434	J181332.22−314715.86	273.384264	−31.787739	12.497	11.426	3000888	273.384	−31.7877	−49.7	0.6
18133329−3146211	273.388747	−31.772543	13.546	12.702	...	...	...	...	...	3001237	273.389	−31.7725	−52.7	0.7
18133354−3148257	273.389787	−31.807146	15.049	14.307	J181333.54−314825.65	273.389782	−31.807128	14.933	14.214	2000735	273.390	−31.8071	−58.2	1.0
18133365−3149030	273.390220	−31.817518	14.469	13.496	J181333.65−314903.02	273.390242	−31.817507	14.404	13.526	2000486	273.390	−31.8175	−45.0	0.8
18133419−3149168[a]	273.392467	−31.821350	14.931	14.253	J181334.17−314916.96	273.392391	−31.821379	15.022	14.393	RHB.200046493	273.392	−31.8214	−51.4	1.1
18133439−3147146	273.393312	−31.787409	14.940	14.250	J181334.39−314714.64	273.393298	−31.787402	14.851	14.160	3000816	273.393	−31.7874	−50.5	0.1
18133444−3149435	273.393530	−31.828775	14.182	13.314	J181334.25−314943.33	273.392737	−31.828705	15.525	14.772	2000412	273.393	−31.8287	−44.8	0.7
18133449−3151332	273.393736	−31.859224	14.848	13.818	J181334.49−315133.27	273.393718	−31.859242	14.672	13.825	2000606	273.394	−31.8592	−45.1	0.6
18133459−3147379	273.394141	−31.793882	13.105	12.113	J181334.59−314737.98	273.394162	−31.793885	13.003	12.076	2000135	273.394	−31.7939	−49.5	0.6
18133504−3148567[a]	273.396034	−31.815771	15.122	14.369	J181335.06−314856.77	273.396084	−31.815771	15.009	14.325	RHB.200049021	273.396	−31.8158	−46.2	0.9
18133550−3148442[a]	273.397925	−31.812286	14.519	14.104	J181335.50−314843.57	273.397941	−31.812105	15.016	14.336	RHB.200050301	273.398	−31.8121	−50.3	0.1
18133584−3149081	273.399354	−31.818924	15.122	14.280	J181335.83−314908.37	273.399309	−31.818994	...	14.160	2000784	273.399	−31.8190	−49.8	1.3
18133592−3146465	273.399706	−31.779596	12.659	11.670	J181335.92−314646.53	273.399697	−31.779594	12.591	11.634	3000968	273.400	−31.7796	−54.7	0.6
18133625−3153094	273.401076	−31.885963	14.663	13.831	J181336.25−315309.54	273.401052	−31.885985	14.633	13.742	3001304	273.401	−31.8859	−43.6	0.1
18133726−3146267	273.405268	−31.774097	14.834	14.237	J181337.24−314626.87	273.405203	−31.774132	14.915	14.218	3001104	273.405	−31.7741	−47.6	1.5
18133753−3151020[a]	273.406387	−31.850573	15.123	14.420	J181337.53−315102.16	273.406397	−31.850600	15.085	14.435	1402137	273.406	−31.8506	−52.3	0.8
18133789−3147295[a]	273.407892	−31.791531	11.935	10.857	J181337.89−314729.53	273.407909	−31.791538	11.884	10.753	2000048	273.408	−31.7915	−50.9	0.6
18133813−3145274[a]	273.408907	−31.757622	11.818	10.620	J181338.13−314527.31	273.408888	−31.757588	11.790	...	3001594	273.409	−31.7576	−41.4	0.7
18133817−3149355	273.409077	−31.826529	11.158	9.943	...	...	...	...	...	1101214	273.409	−31.8265	−61.4	0.7
18133818−3147243	273.409100	−31.790108	13.786	12.826	J181338.19−314724.38	273.409129	−31.790107	13.683	12.749	2000295	273.409	−31.7901	−54.5	0.7
18133820−3151145	273.409182	−31.854034	13.895	12.997	J181338.20−315114.55	273.409187	−31.854043	13.813	12.899	1402110	273.409	−31.8540	−49.6	0.6
18133827−3149413	273.409493	−31.828146	11.293	10.100	...	...	...	...	...	1100865	273.409	−31.8281	−49.2	0.6
18133843−3150157	273.410133	−31.837715	14.375	13.545	J181338.44−315015.87	273.410195	−31.837742	14.459	13.745	1401475	273.410	−31.8377	−58.9	0.7
18133851−3151401	273.410469	−31.861151	14.798	13.846	J181338.51−315140.18	273.410480	−31.861163	14.633	13.785	2000595	273.410	−31.8611	−53.1	0.8
18133859−3149585	273.410797	−31.832939	10.704	9.387	...	...	...	...	...	1401160	273.411	−31.8329	−48.8	0.8
18133863−3150077	273.410995	−31.835491	10.590	9.213	J181338.63−315007.84	273.410968	−31.835511	10.536	9.152	1401269	273.411	−31.8355	−50.0	0.8
18133865−3151050	273.411051	−31.851400	14.941	14.068	J181338.66−315104.99	273.411093	−31.851386	14.911	14.094	1401944	273.411	−31.8514	−47.7	0.6
18133867−3147435	273.411136	−31.795427	14.697	13.860	J181338.67−314743.55	273.411162	−31.795432	14.544	13.680	2000548	273.411	−31.7954	−51.9	0.3
18133884−3150488	273.411862	−31.846895	13.608	12.771	...	...	...	...	...	1401759	273.412	−31.8469	−52.8	0.7
18133895−3148326	273.412305	−31.809074	14.913	13.131	J181338.97−314832.34	273.412401	−31.808984	15.057	14.425	1200710	273.412	−31.8090	−38.7	1.3
18133914−3150341	273.413089	−31.842831	14.253	13.299	J181339.14−315034.26	273.413085	−31.842851	14.924	14.196	1401485	273.413	−31.8428	−48.9	0.7
18133920−3147297	273.413350	−31.791588	14.830	13.958	J181339.20−314729.71	273.413345	−31.791587	14.692	13.856	2000575	273.413	−31.7916	−51.2	0.7
18133940−3150132	273.414174	−31.837006	10.606	9.242	...	...	...	...	...	1401068	273.414	−31.8370	−48.3	0.7
18133967−3150152	273.415306	−31.837580	11.115	9.862	...	...	...	...	...	1400994	273.415	−31.8376	−50.7	0.7
18133989−3148580	273.416226	−31.816122	14.429	13.623	...	...	...	...	...	1200629	273.416	−31.8161	−59.2	0.7
18134008−3149023	273.417031	−31.817314	14.456	13.682	...	...	...	...	...	1200659	273.417	−31.8173	−49.9	1.5
18134010−3151232	273.417117	−31.856449	14.048	13.091	J181340.10−315123.24	273.417109	−31.856457	13.987	13.113	2000364	273.417	−31.8564	−46.0	0.7
18134025−3149477	273.417717	−31.829926	11.267	10.040	J181340.25−314947.76	273.417727	−31.829934	11.135	9.887	1400288	273.418	−31.8299	−50.6	0.7

Table 3—Continued

Star Name (2MASS)	RA (J2000)	DEC (J2000)	J (mag)	K_S (mag)	Star Name (VVV)	RA (J2000)	DEC (J2000)	J (mag)	K_S (mag)	Star Name (VLT)	RA (J2000)	DEC (J2000)	$RV_{helio.}$ (km s^{-1})	RV Error (km s^{-1})
18134027−3147004	273.417805	−31.783447	11.733	10.540	J181340.27−314700.40	273.417799	−31.783446	11.655	10.516	3000839	273.418	−31.7834	−47.1	0.7
18134028−3148398[a]	273.417840	−31.811069	15.087	14.467	J181340.27−314839.83	273.417819	−31.811064	15.060	14.428	1201183	273.418	−31.8111	−41.4	0.4
18134035−3151076	273.418164	−31.852137	13.650	12.754	...	...	...	...	...	1401524	273.418	−31.8521	−52.5	0.7
18134042−3149401	273.418451	−31.827816	11.160	10.052	J181340.41−314940.17	273.418412	−31.827825	10.837	9.721	1100182	273.418	−31.8278	−47.6	0.7
18134095−3150365	273.420640	−31.843498	10.564	9.270	J181340.95−315036.62	273.420637	−31.843506	10.524	9.192	1400828	273.421	−31.8435	−59.6	0.7
18134095−3150478[a]	273.420639	−31.846621	14.967	14.201	J181340.92−315047.91	273.420524	−31.846644	15.011	14.393	1401013	273.420	−31.8466	−50.0	0.0
18134124−3148156	273.421862	−31.804356	13.806	13.029	...	...	...	...	...	2000628	273.422	−31.8041	−52.0	0.0
18134133−3148374	273.422233	−31.810408	13.723	12.835	J181341.33−314837.50	273.422234	−31.810417	13.655	12.816	1201513	273.422	−31.8104	−58.8	0.7
18134145−3148318	273.422722	−31.808847	13.966	13.034	...	...	...	...	...	1201617	273.423	−31.8088	−46.6	0.7
18134202−3151202	273.425099	−31.855635	14.820	13.886	J181342.02−315120.31	273.425098	−31.855643	14.658	13.812	2000623	273.425	−31.8556	−47.8	0.7
18134207−3149041	273.425325	−31.817812	15.441	14.806	J181342.07−314904.22	273.425325	−31.817840	14.927	14.185	1201418	273.425	−31.8178	−53.2	1.5
18134218−3148191	273.425759	−31.805326	13.938	13.015	J181342.17−314819.16	273.425740	−31.805324	13.875	12.966	1201884	273.426	−31.8053	−45.9	0.7
18134302−3150431	273.429257	−31.845325	13.476	12.600	J181343.02−315043.15	273.429282	−31.845320	13.466	12.614	1400043	273.429	−31.8453	−50.0	0.7
18134306−3150091	273.429419	−31.835871	10.710	9.387	J181343.06−315009.19	273.429422	−31.835888	10.641	9.258	1300949	273.429	−31.8359	−42.6	0.8
18134315−3152167	273.429828	−31.871311	14.055	13.152	J181343.15−315216.77	273.429833	−31.871325	13.958	13.059	3000949	273.430	−31.8713	−49.5	0.6
18134318−3149121	273.429958	−31.820038	13.455	12.565	...	...	...	...	...	1201631	273.430	−31.8200	−55.2	0.7
18134352−3148584	273.431348	−31.816242	11.272	10.082	...	...	...	...	...	1201846	273.431	−31.8162	−46.0	0.6
18134370−3150080	273.432120	−31.835583	14.382	13.504	J181343.70−315008.10	273.432108	−31.835586	14.292	13.434	1300986	273.432	−31.8356	−46.6	0.7
18134393−3149397	273.433043	−31.827715	15.221	13.994	J181343.92−314939.89	273.433039	−31.827748	15.061	14.414	1300460	273.433	−31.8277	−48.1	1.1
18134405−3146148	273.433543	−31.770781	14.063	13.199	J181344.05−314614.85	273.433549	−31.770794	14.007	13.122	3001272	273.434	−31.7708	−43.7	0.8
18134412−3147150	273.433850	−31.787525	14.770	13.935	J181344.12−314715.13	273.433843	−31.787538	14.654	13.950	3000837	273.434	−31.7875	−54.9	0.2
18134457−3152197	273.435720	−31.872147	14.867	14.058	J181344.56−315219.81	273.435698	−31.872171	14.857	14.039	3001031	273.436	−31.8721	−47.2	0.1
18134493−3150073	273.437230	−31.835386	14.959	14.200	J181344.93−315007.53	273.437247	−31.835426	14.921	14.204	1301091	273.437	−31.8354	−36.4	0.3
18134502−3150190[a]	273.437598	−31.838614	14.824	14.026	J181345.01−315019.20	273.437581	−31.838669	14.867	14.148	1301234	273.438	−31.8387	−47.7	1.1
18134511−3147546	273.437987	−31.798519	13.530	12.633	J181345.11−314754.60	273.437979	−31.798502	13.432	12.573	2000220	273.438	−31.7985	−40.0	0.6
18134563−3150339	273.440162	−31.842756	14.722	14.071	J181345.63−315033.89	273.440160	−31.842748	14.919	14.106	1301431	273.440	−31.8427	−59.7	1.3
18134635−3147366	273.443130	−31.793505	13.459	12.536	J181346.35−314736.61	273.443136	−31.793503	13.428	12.529	2000218	273.443	−31.7935	−50.0	0.6
18134635−3152231	273.443138	−31.873098	14.951	14.436	J181346.37−315223.33	273.443216	−31.873150	14.966	14.269	3001136	273.443	−31.8731	−44.7	1.3
18134651−3150219	273.443793	−31.839417	14.617	13.834	J181346.51−315021.93	273.443802	−31.839427	14.500	13.789	1301369	273.444	−31.8394	−42.2	1.0
18134689−3149595	273.445375	−31.833202	13.033	12.126	J181346.89−314959.58	273.445387	−31.833219	12.984	12.102	1301147	273.445	−31.8332	−41.9	0.6
18134725−3147570	273.446879	−31.799189	13.274	12.281	J181347.25−314757.14	273.446878	−31.799206	13.272	12.335	2000177	273.447	−31.7992	−47.8	0.9
18134754−3147217	273.448116	−31.789373	14.117	13.127	J181347.54−314721.78	273.448121	−31.789384	13.994	13.151	2000390	273.448	−31.7894	−46.6	1.0
18134793−3148059	273.449744	−31.801643	14.029	13.272	...	...	...	...	...	2000408	273.450	−31.8016	−37.7	1.1
18134846−3149413	273.451952	−31.828156	14.315	13.386	...	...	...	...	...	2000460	273.452	−31.8281	−53.2	0.8
18134865−3142176	273.452736	−31.704897	11.705	10.561	J181348.65−314217.70	273.452742	−31.704918	11.653	10.496	3004381	273.453	−31.7049	−48.9	0.7
18135069−3149440	273.461210	−31.828894	13.973	13.020	J181350.69−314944.03	273.461231	−31.828900	13.903	13.020	3000812	273.461	−31.8289	−42.7	0.7
18135122−3151068	273.463417	−31.851910	13.734	12.882	J181351.21−315106.85	273.463409	−31.851905	13.623	12.823	3001045	273.463	−31.8519	−47.6	0.7
18135154−3151406	273.464755	−31.861294	13.272	12.289	J181351.53−315140.65	273.464743	−31.861292	13.256	12.341	3001219	273.465	−31.8613	−49.1	0.6
18135174−3151173	273.465613	−31.854813	14.716	13.914	J181351.74−315117.26	273.465600	−31.854796	14.639	13.825	3001138	273.466	−31.8548	−49.1	0.9
18135186−3151302	273.466119	−31.858412	14.931	14.050	J181351.86−315130.29	273.466115	−31.858415	14.876	14.083	3001200	273.466	−31.8584	−44.2	0.8
18135512−3150484	273.479706	−31.846800	13.769	12.876	J181355.13−315048.42	273.479713	−31.846784	13.729	12.878	3001330	273.480	−31.8468	−36.3	0.7
18135665−3148002	273.486075	−31.800068	13.785	12.880	J181356.65−314800.24	273.486068	−31.800068	13.771	12.884	3001570	273.486	−31.8001	−47.7	0.6
18135670−3147531	273.486281	−31.798088	12.614	11.640	J181356.70−314753.20	273.486277	−31.798113	12.714	11.750	3001607	273.486	−31.7981	−56.4	0.8
18135701−3150541	273.487583	−31.848385	14.712	13.865	J181357.02−315054.14	273.487587	−31.848373	14.647	13.859	3001557	273.488	−31.8484	−46.5	1.8
18140259−3142225	273.510792	−31.706253	12.886	11.959	J181402.58−314222.48	273.510773	−31.706246	12.841	11.935	3005733	273.511	−31.7062	−42.3	1.4
18142065−3147172	273.586057	−31.788113	12.874	11.832	J181420.65−314717.18	273.586072	−31.788107	12.792	11.779	3006184	273.586	−31.7881	−47.5	0.6
18142246−3153087	273.593593	−31.885777	12.967	12.071	J181422.46−315308.76	273.593598	−31.885769	12.870	12.080	3007155	273.594	−31.8858	−61.2	0.6
...	...	...	...	...	J181256.24−314948.95	273.234342	−31.830267	12.322	11.447	3006051	273.234	−31.8302	−57.7	0.6
...	...	...	...	...	J181333.61−314753.37	273.390059	−31.798161	13.854	12.961	2000318	273.390	−31.7982	−40.7	0.7
...	...	...	...	...	J181346.54−314909.97	273.443923	−31.819438	14.248	13.376	2000440	273.444	−31.8194	−50.2	0.7

Table 3—Continued

Star Name (2MASS)	RA (J2000)	DEC (J2000)	J (mag)	K_S (mag)	Star Name (VVV)	RA (J2000)	DEC (J2000)	J (mag)	K_S (mag)	Star Name (VLT)	RA (J2000)	DEC (J2000)	$RV_{helio.}$ (km s^{-1})	RV Error (km s^{-1})
...	...	...	...	...	J181344.55−315013.55	273.435644	−31.837099	14.287	13.425	1301128	273.436	−31.8371	−47.1	1.0
...	...	...	...	...	J181333.51−314952.71	273.389655	−31.831309	14.440	13.569	2000495	273.390	−31.8313	−46.2	0.7
...	...	...	...	...	J181332.65−314955.58	273.386069	−31.832106	14.519	13.672	2000534	273.386	−31.8321	−41.9	0.0
...	...	...	...	...	J181336.52−314921.39	273.402198	−31.822609	14.515	13.881	2000779	273.402	−31.8226	−42.1	1.2
...	...	...	...	...	J181340.05−315100.27	273.416880	−31.850078	14.888	13.984	1401526	273.417	−31.8501	−52.9	1.1
...	...	...	...	...	J181338.61−314809.34[a]	273.410888	−31.802595	15.014	14.310	2000842	273.411	−31.8026	−38.8	1.2
...	...	...	...	...	J181342.97−314909.73	273.429080	−31.819371	15.007	14.331	1201600	273.429	−31.8194	−52.1	0.1
Possible Members														
18130016−3149292	273.250682	−31.824804	11.493	10.230	J181300.16−314929.40	273.250688	−31.824835	11.454	10.294	3005101	273.251	−31.8248	−39.5	0.8
18130474−3146459	273.269784	−31.779423	12.381	11.230	J181304.74−314645.97	273.269767	−31.779437	12.362	11.236	3004577	273.270	−31.7794	−40.8	0.8
18131340−3147497	273.305866	−31.797157	15.269	14.663	J181313.41−314749.79	273.305901	−31.797166	15.087	14.351	RHB.200005636	273.306	−31.7972	−42.9	0.0
18131450−3149583	273.310455	−31.832874	13.138	12.179	J181314.51−314958.43	273.310459	−31.832899	13.052	12.068	RGB.100049420	273.310	−31.8329	−54.5	0.4
18131539−3150436	273.314157	−31.845472	12.500	11.524	J181315.40−315043.72	273.314176	−31.845479	12.472	11.501	3002220	273.314	−31.8455	−40.2	0.6
18131581−3153294	273.315882	−31.891508	11.226	10.071	J181315.81−315329.50	273.315882	−31.891530	11.197	10.123	3003154	273.316	−31.8915	−45.1	0.7
18131651−3155372	273.318830	−31.927010	11.338	10.091	J181316.52−315537.29	273.318834	−31.927025	11.308	10.021	3004467	273.319	−31.9270	−49.4	0.5
18131721−3153259	273.321719	−31.890545	10.822	9.562	...	...	...	...	...	3002907	273.322	−31.8905	−38.6	0.8
18131754−3148585	273.323103	−31.816261	15.056	14.366	J181317.54−314858.67	273.323102	−31.816300	14.957	14.329	RHB.100056023	273.323	−31.8163	−46.4	0.5
18131844−3149277	273.326847	−31.824368	12.204	11.007	J181318.44−314927.83	273.326847	−31.824398	12.136	11.003	3001715	273.327	−31.8244	−42.0	0.7
18132074−3154256	273.336425	−31.907122	14.964	14.155	J181320.74−315425.68	273.336421	−31.907136	14.838	14.012	RGB.100062827	273.336	−31.9071	−53.8	0.9
18132197−3146151	273.341578	−31.770863	14.931	12.521	J181321.97−314615.15	273.341583	−31.770877	14.852	14.198	RHB.200017606	273.342	−31.7709	−47.0	0.6
18132208−3151269	273.342035	−31.857489	9.556	8.155	J181322.09−315127.04	273.342083	−31.857512	9.463	8.353	3001527	273.342	−31.8575	−58.7	1.6
18132217−3149525	273.342394	−31.831272	14.904	14.216	J181322.17−314952.77	273.342408	−31.831328	14.836	14.148	RHB.100065932	273.342	−31.8313	−53.8	1.0
18132372−3147569	273.348866	−31.799154	14.067	13.180	J181323.72−314757.04	273.348859	−31.799179	13.971	13.085	RGB.200020984	273.349	−31.7992	−39.6	0.2
18132448−3149140	273.352006	−31.820574	10.200	8.883	J181324.47−314914.21	273.351992	−31.820616	10.174	8.839	3001064	273.352	−31.8206	−52.5	0.9
18132525−3149572	273.355243	−31.832577	13.547	12.699	J181325.25−314957.28	273.355245	−31.832580	13.524	12.684	3000984	273.355	−31.8326	−57.8	0.8
18132582−3149489	273.357610	−31.830252	14.872	13.945	J181326.01−314948.02	273.358396	−31.830008	17.897	17.406	3000918	273.358	−31.8302	−57.4	0.5
18132786−3147564	273.366086	−31.799006	14.672	13.930	J181327.86−314756.45	273.366098	−31.799014	14.625	13.872	2000627	273.366	−31.7990	−60.2	0.0
18132849−3147068	273.368714	−31.785225	10.193	8.913	J181328.49−314706.81	273.368717	−31.785226	10.197	8.960	3001179	273.369	−31.7852	−30.1	0.7
18132914−3150265	273.371458	−31.840719	14.371	13.493	J181329.15−315026.66	273.371465	−31.840741	14.308	13.476	2000469	273.371	−31.8407	−36.2	0.8
18132989−3201220	273.374559	−32.022781	12.012	10.783	J181329.89−320121.93	273.374554	−32.022758	11.986	10.721	3010313	273.375	−32.0228	−42.6	0.7
18133010−3148307	273.375449	−31.808546	13.792	12.929	J181330.11−314830.74	273.375473	−31.808539	13.681	12.857	2000282	273.375	−31.8085	−39.8	0.7
18133025−3151104	273.376065	−31.852909	12.700	12.252	J181330.25−315110.57	273.376078	−31.852938	...	12.247	2000163	273.376	−31.8529	−61.1	0.8
18133126−3147477	273.380282	−31.796598	12.907	11.960	J181331.26−314747.72	273.380288	−31.796591	12.849	11.943	2000115	273.380	−31.7966	−40.5	0.8
18133157−3151205	273.381556	−31.855698	13.884	12.960	J181331.57−315120.48	273.381542	−31.855689	13.750	12.883	2000302	273.382	−31.8557	−35.6	0.6
18133170−3156592	273.382120	−31.949793	10.506	9.274	J181331.70−315659.28	273.382118	−31.949801	10.384	9.274	3004355	273.382	−31.9498	−36.3	0.8
18133213−3142292	273.383903	−31.708124	12.276	11.159	J181332.13−314229.27	273.383911	−31.708133	12.196	11.124	3004036	273.384	−31.7081	−40.6	0.6
18133221−3148261	273.384224	−31.807261	14.775	14.089	...	...	...	...	...	2000721	273.384	−31.8072	−54.4	0.4
18133298−3148174	273.387440	−31.804859	14.912	14.153	...	...	...	...	...	RHB.200043404	273.387	−31.8048	−52.5	0.1
18133368−3147591	273.390340	−31.799763	14.381	13.661	...	...	...	...	...	RHB.200045255	273.390	−31.7997	−53.7	0.1
18133402−3150116	273.391764	−31.836567	15.014	14.144	...	...	...	...	...	RHB.200046064	273.392	−31.8366	−45.3	0.3
18133408−3152157	273.392028	−31.871042	12.413	11.310	J181334.08−315215.74	273.392034	−31.871039	12.328	11.284	3000960	273.392	−31.8710	−60.1	0.7
18133444−3147215	273.393519	−31.789310	15.126	14.372	...	...	...	...	...	RHB.200047272	273.393	−31.7893	−51.6	1.3
18133521−3152417	273.396728	−31.878265	13.434	12.572	...	...	...	...	...	RHB.100094388	273.397	−31.8780	−52.9	1.8
18133561−3148588	273.398395	−31.816339	14.149	13.193	J181335.62−314858.70	273.398421	−31.816307	14.083	13.155	2000358	273.398	−31.8163	−38.9	0.8
18133562−3149495	273.398447	−31.830442	14.996	12.490	...	...	...	...	...	RHB.200050550	273.398	−31.8306	−43.9	0.4
18133646−3150116	273.401952	−31.836569	12.025	10.870	J181336.58−315009.92	273.402454	−31.836090	14.713	14.125	RHB.200053506	273.402	−31.8361	−44.5	2.0
18133665−3144339	273.402741	−31.742764	14.058	13.154	...	...	...	...	...	RGB.200053794	273.403	−31.7427	−38.8	0.4
18133666−3147294	273.402768	−31.791521	14.860	12.260	J181336.66−314729.53	273.402782	−31.791537	14.876	14.218	RHB.200053762	273.403	−31.7915	−48.0	3.1
18133714−3146585	273.404766	−31.782940	15.209	14.513	J181337.14−314658.57	273.404773	−31.782937	15.068	14.414	RHB.200055162	273.405	−31.7829	−50.7	0.9
18133723−3152181	273.405144	−31.871717	13.239	12.268	J181337.23−315218.21	273.405166	−31.871728	13.177	12.195	3000898	273.405	−31.8717	−38.4	0.6

Table 3—Continued

Star Name (2MASS)	RA (J2000)	DEC (J2000)	J (mag)	K_S (mag)	Star Name (VVV)	RA (J2000)	DEC (J2000)	J (mag)	K_S (mag)	Star Name (VLT)	RA (J2000)	DEC (J2000)	$RV_{helio.}$ (km s^{-1})	RV Error (km s^{-1})
18133828−3152459	273.409509	−31.879433	14.838	14.156	···	···	···	···	···	3001120	273.409	−31.8794	−49.7	0.9
18133865−3149392	273.411055	−31.827576	11.221	9.986	···	···	···	···	···	1100841	273.411	−31.8276	−60.9	0.7
18133876−3150190	273.411514	−31.838612	14.543	13.774	J181338.79−315018.54	273.411633	−31.838485	14.707	14.039	RHB.200059652	273.412	−31.8385	−53.3	1.1
18133968−3149090	273.415342	−31.819180	10.995	9.787	···	···	···	···	···	1200191	273.415	−31.8192	−48.6	0.7
18133968−3149452	273.415356	−31.829241	10.144	8.865	···	···	···	···	···	1100167	273.415	−31.8292	−51.1	0.8
18134149−3148215	273.422913	−31.805981	10.734	9.380	J181341.49−314821.58	273.422911	−31.805995	10.662	9.336	1201738	273.423	−31.8060	−44.8	0.8
18134264−3150441	273.427694	−31.845606	15.220	14.589	J181342.64−315044.17	273.427681	−31.845605	15.171	14.600	1400231	273.428	−31.8456	−33.0	1.4
18134329−3145247	273.430392	−31.756886	11.994	10.828	J181343.29−314524.71	273.430405	−31.756864	11.922	10.836	3001675	273.430	−31.7569	−47.3	0.5
18134497−3152156	273.437409	−31.871016	15.000	13.873	J181344.97−315215.61	273.437390	−31.871005	14.941	14.269	RHB.100112863	273.437	−31.8710	−51.7	0.4
18134513−3141199	273.438082	−31.688875	10.646	9.499	J181345.14−314120.07	273.438085	−31.688909	10.668	9.480	3005244	273.438	−31.6889	−42.3	0.7
18134515−3146119	273.438144	−31.769983	13.474	12.449	J181345.15−314611.99	273.438136	−31.769998	13.476	12.487	3001317	273.438	−31.7700	−50.3	0.8
18134545−3147347	273.439408	−31.792992	14.754	13.886	J181345.45−314734.80	273.439384	−31.793000	14.645	13.801	2000609	273.439	−31.7930	−36.6	0.7
18134554−3150170	273.439756	−31.838083	10.057	8.802	J181345.53−315017.12	273.439747	−31.838091	10.064	8.662	1301251	273.440	−31.8381	−37.8	1.1
18134579−3153001	273.440797	−31.883375	14.593	13.772	···	···	···	···	···	3001362	273.441	−31.8834	−34.6	1.0
18134890−3147487	273.453776	−31.796877	13.278	12.314	J181348.90−314748.75	273.453769	−31.796877	13.237	12.249	2000176	273.454	−31.7969	−46.5	0.7
18135074−3152450	273.461446	−31.879173	14.829	14.051	···	···	···	···	···	3001539	273.461	−31.8792	−58.1	0.3
18135433−3150016	273.476382	−31.833801	13.013	12.033	J181354.34−315001.67	273.476417	−31.833799	12.988	12.005	3001178	273.476	−31.8338	−55.9	0.8
18135509−3148554	273.479582	−31.815399	13.924	13.072	J181355.10−314855.47	273.479599	−31.815409	13.923	12.994	3001270	273.480	−31.8154	−59.7	0.7
18135525−3151440	273.480243	−31.862228	13.662	12.703	J181355.25−315143.91	273.480230	−31.862200	13.729	12.784	3001566	273.480	−31.8622	−51.0	0.8
18135715−3149194	273.488165	−31.822075	14.582	13.742	J181357.15−314919.48	273.488157	−31.822078	14.501	13.683	3001456	273.488	−31.8221	−50.3	0.3
18135720−3147462	273.488362	−31.796192	12.780	11.821	J181357.21−314746.25	273.488385	−31.796183	12.774	11.871	3001686	273.488	−31.7962	−52.4	0.8
18135732−3145057	273.488863	−31.751608	11.517	10.247	J181357.32−314505.82	273.488862	−31.751618	11.531	10.316	3002886	273.489	−31.7516	−48.6	0.9
18140040−3148430	273.501708	−31.811947	12.287	11.243	J181400.41−314842.98	273.501709	−31.811940	12.262	11.213	3001904	273.502	−31.8119	−54.8	0.7
18140097−3149226	273.504050	−31.822968	10.648	9.345	J181400.97−314922.67	273.504056	−31.822964	10.572	9.236	3001937	273.504	−31.8229	−37.4	0.6
18140144−3153250	273.506028	−31.890287	12.590	11.447	J181401.44−315325.08	273.506024	−31.890302	12.547	11.477	3003043	273.506	−31.8903	−36.9	0.8
18140458−3154261	273.519093	−31.907253	12.505	11.423	···	···	···	···	···	3004100	273.519	−31.9072	−31.9	0.8
18140469−3158520	273.519551	−31.981127	12.197	11.150	J181404.69−315852.06	273.519554	−31.981128	12.149	11.162	3008430	273.520	−31.9811	−43.3	0.7
18140583−3149137	273.524310	−31.820473	11.070	9.808	J181405.83−314913.74	273.524310	−31.820485	11.010	9.757	3002697	273.524	−31.8205	−36.1	0.8
18141044−3151075	273.543507	−31.852108	12.459	11.377	···	···	···	···	···	RGB.200134033	273.543	−31.8521	−31.3	0.2
18141059−3155346	273.544161	−31.926294	12.601	11.491	J181410.60−315534.72	273.544167	−31.926313	12.493	11.442	3005995	273.544	−31.9263	−47.6	0.7
18141103−3153066	273.545976	−31.885168	12.638	11.513	J181411.03−315306.57	273.545967	−31.885159	12.651	11.581	3004476	273.546	−31.8852	−55.8	0.8
18141293−3151325	273.553904	−31.859037	14.042	13.163	J181412.92−315132.46	273.553871	−31.859019	14.024	13.126	RGB.200138578	273.554	−31.8590	−34.2	0.3
18141505−3148199	273.562725	−31.805555	12.522	11.535	J181415.05−314819.98	273.562738	−31.805551	12.473	11.507	3004583	273.563	−31.8056	−53.4	0.7
18141642−3150082	273.568454	−31.835613	12.247	11.180	J181416.43−315008.19	273.568478	−31.835611	12.181	11.177	3004815	273.568	−31.8356	−34.1	0.7
18141765−3152457	273.573557	−31.879368	14.612	13.564	···	···	···	···	···	RGB.200145723	273.574	−31.8794	−56.2	0.4
18141824−3150065	273.576007	−31.835150	12.509	11.459	J181418.24−315006.46	273.576001	−31.835129	12.456	11.429	RGB.200146534	273.576	−31.8351	−46.5	0.3
18142153−3151275	273.589745	−31.857647	12.351	11.246	J181421.54−315127.45	273.589755	−31.857627	12.279	11.238	3006276	273.590	−31.8576	−55.8	0.7
18142273−3155544	273.594720	−31.931795	12.245	11.196	J181422.73−315554.37	273.594715	−31.931770	12.226	11.237	3009183	273.595	−31.9318	−51.2	0.7
···	···	···	···	···	J181355.69−315529.43	273.482079	−31.924843	11.513	10.295	3003716	273.482	−31.9248	−47.9	0.7
···	···	···	···	···	J181343.06−315148.40	273.429440	−31.863445	13.062	12.159	2000156	273.429	−31.8634	−42.3	0.6
···	···	···	···	···	J181335.98−314813.07	273.399940	−31.803633	14.064	13.125	2000446	273.400	−31.8036	−44.1	0.8
···	···	···	···	···	J181334.66−314618.94	273.394417	−31.771928	14.672	14.056	RHB.200047940	273.394	−31.7719	−57.0	1.1
···	···	···	···	···	J181351.03−315447.79	273.462634	−31.913276	14.731	14.099	RHB.100122946	273.463	−31.9133	−36.9	0.1
···	···	···	···	···	J181340.20−315001.20	273.417527	−31.833667	14.851	14.145	1400549	273.417	−31.8336	−43.7	0.0
···	···	···	···	···	J181338.84−314834.56	273.411847	−31.809601	14.937	14.216	RHB.200059803	273.412	−31.8096	−51.4	0.9
···	···	···	···	···	J181335.53−315056.05	273.398069	−31.848905	14.983	14.301	RHB.100094881	273.398	−31.8489	−56.3	0.2
···	···	···	···	···	J181335.83−314929.75	273.399322	−31.824933	14.992	14.315	RHB.200051231	273.399	−31.8249	−50.5	1.0
···	···	···	···	···	J181351.25−315546.84	273.463544	−31.929680	15.033	14.358	RHB.100123245	273.464	−31.9297	−48.7	0.2
···	···	···	···	···	J181336.02−314900.40	273.400105	−31.816780	15.091	14.378	RHB.200051801	273.400	−31.8168	−58.4	0.4
···	···	···	···	···	···	···	···	···	···	RHB.200059094	273.411	−31.8178	−54.3	1.7

Table 3—Continued

Star Name (2MASS)	RA (J2000)	DEC (J2000)	J (mag)	K_S (mag)	Star Name (VVV)	RA (J2000)	DEC (J2000)	J (mag)	K_S (mag)	Star Name (VLT)	RA (J2000)	DEC (J2000)	$RV_{helio.}$ (km s^{-1})	RV Error (km s^{-1})
...	...	...	...	...	...	...	...	...	...	RHB.200046840	273.393	−31.8332	−50.3	1.5
...	...	...	...	...	...	...	...	...	...	RGB.200011463	273.326	−31.7720	−37.2	0.2
...	...	...	...	...	...	...	...	...	...	1101453	273.413	−31.8234	−53.5	0.8
...	...	...	...	...	...	...	...	...	...	3001342	273.482	−31.8097	−30.7	0.6
...	...	...	...	...	...	...	...	...	...	1201075	273.424	−31.8235	−42.1	0.8
...	...	...	...	...	...	...	...	...	...	2000160	273.454	−31.8315	−39.9	0.6
...	...	...	...	...	...	...	...	...	...	3000834	273.362	−31.8308	−38.8	0.8
...	...	...	...	...	...	...	...	...	...	2000316	273.377	−31.8476	−51.0	0.8
...	...	...	...	...	...	...	...	...	...	2000258	273.369	−31.8161	−51.9	0.6
...	...	...	...	...	...	...	...	...	...	3004768	273.264	−31.7832	−44.3	0.8
...	...	...	...	...	...	...	...	...	...	3001014	273.435	−31.7814	−31.4	0.7
...	...	...	...	...	...	...	...	...	...	1200380	273.416	−31.8184	−51.4	0.6
...	...	...	...	...	...	...	...	...	...	3003865	273.417	−31.7086	−60.7	0.7
...	...	...	...	...	...	...	...	...	...	3003691	273.543	−31.8521	−32.2	0.8
...	...	...	...	...	...	...	...	...	...	3004576	273.555	−31.8707	−58.7	0.8
...	...	...	...	...	...	...	...	...	...	3001129	273.397	−31.8782	−33.7	0.9
...	...	...	...	...	...	...	...	...	...	1100285	273.417	−31.8279	−51.9	0.7
...	...	...	...	...	...	...	...	...	...	3003123	273.532	−31.8054	−60.7	0.6
...	...	...	...	...	...	...	...	...	...	3005060	273.564	−31.8712	−40.7	0.6
...	...	...	...	...	...	...	...	...	...	3007498	273.553	−31.9459	−51.0	0.7
...	...	...	...	...	...	...	...	...	...	3003141	273.289	−31.8245	−37.1	0.7
...	...	...	...	...	...	...	...	...	...	1200500	273.416	−31.8170	−45.9	1.0
...	...	...	...	...	...	...	...	...	...	2000463	273.403	−31.8328	−41.4	0.7
...	...	...	...	...	...	...	...	...	...	1200474	273.411	−31.8099	−48.9	0.7
...	...	...	...	...	...	...	...	...	...	2000448	273.451	−31.8388	−41.5	0.7
...	...	...	...	...	...	...	...	...	...	2000701	273.412	−31.8177	−52.1	1.4
...	...	...	...	...	...	...	...	...	...	1400911	273.415	−31.8362	−56.8	0.6
...	...	...	...	...	...	...	...	...	...	1401445	273.411	−31.8390	−51.2	0.6
...	...	...	...	...	...	...	...	...	...	2000586	273.401	−31.8339	−41.7	1.3
...	...	...	...	...	...	...	...	...	...	1400901	273.414	−31.8333	−47.3	2.3
...	...	...	...	...	...	...	...	...	...	2000697	273.395	−31.8334	−48.3	0.5
Non−Members														
18125266−3154163	273.219425	−31.904547	12.017	10.914	J181252.66−315416.47	273.219441	−31.904576	11.955	10.870	3008586	273.219	−31.9045	53.7	0.8
18125335−3153029	273.222293	−31.884144	12.455	11.344	...	...	...	...	...	3007661	273.222	−31.8841	166.1	0.7
18125690−3151014	273.237098	−31.850410	14.287	13.360	J181256.90−315101.52	273.237089	−31.850423	14.203	13.331	RGB.100013964	273.237	−31.8504	90.4	0.3
18125779−3151247	273.240815	−31.856886	13.724	12.782	J181257.79−315124.75	273.240814	−31.856876	13.684	12.762	RGB.100015373	273.241	−31.8569	−140.1	0.3
18125835−3151558	273.243155	−31.865511	11.948	10.878	J181258.35−315155.85	273.243146	−31.865514	11.898	10.854	3005890	273.243	−31.8655	−89.2	0.6
18125890−3153107	273.245438	−31.886318	12.079	11.105	J181258.91−315310.72	273.245463	−31.886314	12.047	11.007	3006241	273.245	−31.8863	−99.2	0.6
18125932−3148244	273.247192	−31.806784	11.468	10.360	J181259.32−314824.41	273.247186	−31.806783	11.406	10.359	3005394	273.247	−31.8068	−93.8	0.8
18125971−3150047	273.248800	−31.834660	12.220	11.143	J181259.71−315004.83	273.248819	−31.834676	12.152	11.120	3005215	273.249	−31.8346	21.7	0.8
18130001−3157032	273.250057	−31.950899	12.338	11.272	J181300.01−315703.31	273.250064	−31.950921	12.292	11.264	3008959	273.250	−31.9509	119.3	0.6
18130021−3152065	273.250903	−31.868483	9.726	8.353	J181300.21−315206.59	273.250887	−31.868499	9.709	8.570	3005494	273.251	−31.8685	113.7	1.0
18130067−3151211	273.252809	−31.855888	12.666	11.571	J181300.67−315121.23	273.252820	−31.855898	12.585	11.541	3005180	273.253	−31.8559	22.5	0.8
18130090−3150356	273.253763	−31.843246	10.868	9.743	J181300.90−315035.70	273.253751	−31.843251	10.803	9.806	3004984	273.254	−31.8432	43.1	0.8
18130154−3148229	273.256428	−31.806374	12.745	11.627	J181301.54−314823.06	273.256418	−31.806406	12.706	11.638	3004856	273.256	−31.8064	71.5	0.7
18130284−3156125	273.261858	−31.936832	12.190	10.999	...	...	...	...	...	3007436	273.262	−31.9368	−27.1	0.8
18130321−3147302	273.263406	−31.791742	12.786	11.869	J181303.21−314730.37	273.263395	−31.791771	12.798	11.876	3004657	273.263	−31.7917	−16.9	1.1
18130335−3145125	273.263981	−31.753483	12.454	11.389	J181303.35−314512.52	273.263971	−31.753480	12.402	11.380	3005653	273.264	−31.7535	13.6	0.8
18130513−3149378	273.271394	−31.827190	10.764	9.532	J181305.13−314937.93	273.271382	−31.827205	10.774	9.680	3003956	273.271	−31.8272	−109.2	0.7
18130515−3146088	273.271494	−31.769129	11.782	10.615	J181305.15−314608.87	273.271492	−31.769131	11.767	10.662	3004760	273.271	−31.7691	−69.8	0.7

Table 3—Continued

Star Name (2MASS)	RA (J2000)	DEC (J2000)	J (mag)	K_S (mag)	Star Name (VVV)	RA (J2000)	DEC (J2000)	J (mag)	K_S (mag)	Star Name (VLT)	RA (J2000)	DEC (J2000)	$RV_{helio.}$ (km s^{-1})	RV Error (km s^{-1})
18130558−3156477	273.273267	−31.946594	12.935	11.902	J181305.57−315647.74	273.273245	−31.946597	12.893	11.877	3007403	273.273	−31.9466	−3.5	0.6
18130791−3152396	273.282976	−31.877670	14.320	13.472	J181307.91−315239.51	273.282970	−31.877642	14.375	13.532	RGB.100035050	273.283	−31.8776	35.3	0.9
18130795−3152505	273.283145	−31.880707	13.896	12.994	J181307.95−315250.58	273.283155	−31.880719	13.851	12.951	RGB.100035136	273.283	−31.8807	28.4	0.5
18130800−3154213	273.283356	−31.905922	12.696	11.654	J181308.01−315421.36	273.283379	−31.905934	12.668	11.641	3004958	273.283	−31.9059	17.9	0.7
18130802−3145470	273.283457	−31.763075	10.017	8.691	J181308.02−314547.10	273.283446	−31.763085	9.947	8.709	3004376	273.283	−31.7631	−13.1	0.8
18130833−3150568	273.284748	−31.849117	11.847	10.847	J181308.34−315056.80	273.284754	−31.849112	11.782	10.825	3003461	273.285	−31.8491	−107.2	0.6
18130839−3153217	273.284996	−31.889376	12.103	10.943	J181308.39−315321.78	273.284986	−31.889384	12.061	10.956	3004295	273.285	−31.8894	7.0	0.8
18130888−3156565	273.287027	−31.949036	14.860	14.245	J181308.89−315656.49	273.287060	−31.949027	14.839	14.232	RHB.100037026	273.287	−31.9490	39.0	0.2
18131062−3154259	273.294269	−31.907221	13.723	13.537	J181310.62−315425.95	273.294268	−31.907210	14.336	13.490	RGB.100040954	273.294	−31.9072	77.7	4.8
18131066−3145118	273.294436	−31.753292	12.757	11.846	J181310.64−314511.36	273.294348	−31.753158	13.172	12.326	3004238	273.294	−31.7533	64.3	0.6
18131189−3147416	273.299573	−31.794897	9.764	8.336	J181311.89−314741.72	273.299562	−31.794923	9.765	8.380	3002948	273.300	−31.7949	12.0	1.1
18131222−3151501	273.300921	−31.863934	14.648	13.842	J181312.21−315150.13	273.300912	−31.863927	14.600	13.757	RGB.100044395	273.301	−31.8639	−10.8	0.4
18131240−3150508	273.301669	−31.847464	12.596	11.619	...	...	...	...	...	3002716	273.302	−31.8474	−16.0	0.7
18131282−3151413	273.303453	−31.861485	10.484	9.129	J181312.82−315141.40	273.303443	−31.861503	10.428	9.248	3002853	273.303	−31.8615	64.2	0.8
18131285−3148444	273.303561	−31.812353	14.672	14.314	J181312.88−314844.36	273.303692	−31.812323	14.958	14.295	RHB.100045970	273.304	−31.8123	48.0	0.4
18131315−3150539	273.304821	−31.848316	12.897	11.973	J181313.15−315054.01	273.304813	−31.848336	12.803	11.877	3002603	273.305	−31.8483	−117.0	0.6
18131319−3152358	273.304986	−31.876623	12.306	11.353	J181313.20−315235.81	273.305014	−31.876615	12.271	11.292	3003126	273.305	−31.8766	120.1	0.6
18131405−3147211	273.308563	−31.789206	12.740	11.674	J181314.05−314721.11	273.308580	−31.789198	12.753	11.731	3002690	273.309	−31.7892	−73.6	0.7
18131465−3147261	273.311072	−31.790606	14.769	13.963	J181314.66−314726.19	273.311085	−31.790610	14.611	13.759	RGB.200006936	273.311	−31.7906	−142.7	0.4
18131477−3155326	273.311558	−31.925730	12.989	12.069	J181314.78−315532.65	273.311596	−31.925738	12.920	11.999	3004652	273.312	−31.9257	−164.8	0.7
18131479−3153232	273.311636	−31.889786	14.021	13.136	J181314.79−315323.29	273.311665	−31.889804	13.943	13.055	RGB.100049993	273.312	−31.8898	56.1	0.3
18131503−3154443	273.312631	−31.912315	11.897	10.868	J181315.02−315444.37	273.312610	−31.912327	11.888	10.882	3004021	273.313	−31.9123	27.5	0.7
18131518−3145476	273.313273	−31.763226	11.503	10.376	J181315.18−314547.54	273.313283	−31.763206	11.086	9.866	3003186	273.313	−31.7632	106.8	0.7
18131537−3150014[a]	273.314071	−31.833729	12.521	11.455	J181315.37−315001.51	273.314083	−31.833756	12.414	11.403	3002139	273.314	−31.8337	−31.4	0.7
18131538−3146588	273.314102	−31.783022	14.492	13.555	J181315.38−314658.88	273.314122	−31.783023	14.425	13.571	RGB.200007762	273.314	−31.7830	−121.5	0.6
18131631−3147225	273.317978	−31.789589	12.820	11.896	J181316.31−314722.52	273.317991	−31.789590	12.749	11.844	3002337	273.318	−31.7896	−210.9	0.7
18131682−3155102	273.320106	−31.919514	14.448	13.608	J181316.83−315510.19	273.320127	−31.919498	14.405	13.567	RGB.100054381	273.320	−31.9195	−160.6	2.6
18131754−3143335	273.323112	−31.725981	12.710	11.624	J181317.54−314333.51	273.323094	−31.725976	12.640	11.627	3004346	273.323	−31.7260	105.7	0.8
18131757−3144424	273.323240	−31.745125	12.566	11.529	J181317.58−314442.47	273.323255	−31.745132	12.534	11.532	3003477	273.323	−31.7451	−240.2	0.9
18131770−3153420	273.323785	−31.895014	12.332	11.288	J181317.71−315342.10	273.323809	−31.895028	12.295	11.249	3003010	273.324	−31.8950	−14.8	0.8
18131778−3152354	273.324118	−31.876507	13.211	12.349	...	...	...	...	...	RGB.100056585	273.324	−31.8769	−240.4	0.1
18131786−3143118	273.324440	−31.719961	14.764	13.828	J181317.86−314311.81	273.324436	−31.719948	14.699	13.832	RGB.200011020	273.324	−31.7199	−110.8	0.1
18131813−3147164	273.325547	−31.787897	11.899	10.733	J181318.13−314716.46	273.325545	−31.787906	11.793	10.639	3002115	273.326	−31.7879	−12.3	0.7
18131825−3153489	273.326052	−31.896929	14.711	13.794	J181318.24−315349.00	273.326020	−31.896947	14.557	13.716	RGB.100057455	273.326	−31.8969	172.8	5.9
18131849−3146347	273.327047	−31.776318	12.155	11.051	J181318.49−314634.75	273.327044	−31.776322	12.116	10.938	3002332	273.327	−31.7763	118.3	1.0
18131880−3143355	273.328344	−31.726538	10.863	9.609	J181318.80−314335.51	273.328341	−31.726531	10.864	9.614	3004157	273.328	−31.7265	16.8	0.8
18131886−3153413	273.328598	−31.894823	9.926	8.554	J181318.86−315341.43	273.328592	−31.894843	9.901	8.656	3002842	273.329	−31.8948	15.8	1.4
18131889−3148270	273.328728	−31.807505	10.275	8.917	J181318.89−314827.02	273.328718	−31.807508	...	8.836	3001745	273.329	−31.8075	−72.9	0.9
18131917−3157276	273.329907	−31.957693	12.087	10.952	J181319.18−315727.65	273.329924	−31.957682	12.051	10.909	3005882	273.330	−31.9577	31.9	0.7
18131936−3147453[a]	273.330669	−31.795921	11.890	10.709	J181319.35−314745.37	273.330665	−31.795938	11.834	10.699	3001825	273.331	−31.7959	−24.1	0.7
18131982−3148543	273.332596	−31.815094	13.210	12.294	J181319.82−314854.44	273.332584	−31.815123	13.123	12.210	3001575	273.333	−31.8151	32.4	0.6
18132013−3154230	273.333892	−31.906399	10.351	9.090	J181320.13−315423.09	273.333884	−31.906414	10.330	9.133	3003132	273.334	−31.9064	−119.8	0.8
18132073−3144398	273.336384	−31.744389	14.434	13.496	J181320.73−314439.77	273.336409	−31.744382	14.256	13.390	RGB.200015439	273.336	−31.7444	48.0	0.3
18132107−3143567	273.337810	−31.732422	11.759	10.596	J181321.07−314356.66	273.337809	−31.732406	11.708	10.561	3003599	273.338	−31.7324	9.0	0.8
18132112−3150290	273.338028	−31.841400	14.568	13.642	J181321.12−315029.07	273.338038	−31.841410	14.481	13.621	3001447	273.338	−31.8414	−11.6	0.6
18132138−3148439	273.339098	−31.812202	13.666	12.823	J181321.38−314843.99	273.339118	−31.812220	13.663	12.831	3001416	273.339	−31.8122	13.9	0.8
18132173−3142100	273.340550	−31.702801	12.569	11.552	J181321.73−314210.05	273.340564	−31.702793	12.536	11.501	RGB.200017201	273.341	−31.7028	−107.7	0.3
18132175−3150093	273.340651	−31.835926	14.209	13.285	...	...	...	...	...	3001341	273.341	−31.8359	−101.6	0.7
18132176−3155353	273.340708	−31.926487	11.850	10.660	J181321.76−315535.41	273.340700	−31.926504	11.772	10.704	3003820	273.341	−31.9265	41.7	0.7
18132181−3147373	273.340876	−31.793713	14.900	14.338	J181321.82−314737.30	273.340926	−31.793695	14.829	14.241	3001590	273.341	−31.7937	2.1	0.8

Table 3—Continued

Star Name (2MASS)	RA (J2000)	DEC (J2000)	J (mag)	K_S (mag)	Star Name (VVV)	RA (J2000)	DEC (J2000)	J (mag)	K_S (mag)	Star Name (VLT)	RA (J2000)	DEC (J2000)	$RV_{helio.}$ (km s^{-1})	RV Error (km s^{-1})
18132194−3143462	273.341422	−31.729509	12.960	12.043	J181321.94−314346.20	273.341418	−31.729501	12.885	11.985	3003643	273.341	−31.7295	−10.6	0.7
18132215−3152307	273.342321	−31.875198	11.725	10.696	J181322.15−315230.67	273.342304	−31.875188	11.675	10.692	3001870	273.342	−31.8752	84.9	0.7
18132264−3154552	273.344342	−31.915335	10.575	9.361	J181322.63−315455.24	273.344307	−31.915347	10.582	9.353	3003224	273.344	−31.9153	39.1	0.7
18132265−3151077	273.344403	−31.852142	13.534	12.624	J181322.65−315107.67	273.344411	−31.852131	13.432	12.559	3001385	273.344	−31.8521	−28.3	0.8
18132266−3151541	273.344448	−31.865046	14.078	13.246	J181322.66−315154.16	273.344432	−31.865046	14.016	13.177	3001605	273.344	−31.8650	152.5	0.6
18132279−3144369	273.344987	−31.743595	12.992	11.918	J181322.79−314436.93	273.344993	−31.743594	12.912	11.861	3002941	273.345	−31.7436	−13.0	0.9
18132282−3147212	273.345105	−31.789227	14.925	14.089	J181322.82−314721.21	273.345114	−31.789226	14.828	14.103	3001560	273.345	−31.7892	31.1	0.2
18132302−3143180	273.345936	−31.721670	11.314	10.165	J181323.02−314318.07	273.345958	−31.721688	11.329	10.134	3003920	273.346	−31.7217	68.7	0.7
18132325−3150421	273.346902	−31.845043	12.551	11.497	...	...	...	...	...	3001263	273.347	−31.8450	16.5	0.7
18132328−3148138	273.347025	−31.803841	13.608	12.718	J181323.28−314813.82	273.347036	−31.803839	...	12.676	3001295	273.347	−31.8038	−23.4	0.8
18132335−3156139	273.347299	−31.937218	11.983	10.855	J181323.34−315614.01	273.347291	−31.937227	11.955	10.813	3004220	273.347	−31.9372	6.8	0.7
18132337−3154514	273.347386	−31.914280	14.613	13.886	J181323.37−315451.40	273.347393	−31.914280	14.603	13.754	RGB.100068499	273.347	−31.9143	−170.0	0.4
18132355−3148021[a]	273.348153	−31.800611	12.010	10.883	J181323.55−314802.24	273.348164	−31.800622	...	10.845	3001300	273.348	−31.8006	36.9	0.8
18132363−3149005	273.348479	−31.816814	13.997	13.185	...	...	...	...	...	3001171	273.348	−31.8168	−28.4	0.9
18132387−3139553	273.349468	−31.665373	13.841	12.957	J181323.87−313955.41	273.349483	−31.665394	13.750	12.831	RGB.200021399	273.349	−31.6654	−25.1	0.3
18132391−3150009	273.349646	−31.833586	14.214	13.392	J181323.92−315001.00	273.349686	−31.833612	14.143	13.380	3001130	273.350	−31.8336	−1.8	0.7
18132396−3155292	273.349843	−31.924795	10.484	9.169	J181323.95−315529.29	273.349833	−31.924805	10.444	9.252	3003514	273.350	−31.9248	−88.4	0.9
18132406−3150052	273.350290	−31.834799	14.731	13.863	J181324.07−315005.31	273.350306	−31.834809	14.616	13.835	3001122	273.350	−31.8348	−93.5	0.7
18132406−3151362	273.350263	−31.860058	14.879	14.086	...	...	...	...	...	3001372	273.350	−31.8601	39.8	1.8
18132422−3142294	273.350929	−31.708185	14.954	14.240	J181324.22−314229.49	273.350927	−31.708193	14.859	14.009	RGB.200022135	273.351	−31.7082	−109.7	0.5
18132424−3151203	273.351012	−31.855642	13.479	12.577	...	...	...	...	...	3001291	273.351	−31.8556	−135.2	0.8
18132426−3152094	273.351107	−31.869287	12.819	11.880	J181324.27−315209.39	273.351141	−31.869275	12.757	11.830	3001532	273.351	−31.8693	14.6	0.7
18132430−3201308	273.351259	−32.025249	14.792	13.955	J181324.30−320130.73	273.351279	−32.025205	14.733	14.109	RHB.100070450	273.351	−32.0252	28.1	0.5
18132445−3146550	273.351905	−31.781948	12.807	11.761	...	...	...	...	...	3001552	273.352	−31.7819	−76.8	0.8
18132485−3151491	273.353576	−31.863653	14.373	13.608	J181324.86−315149.10	273.353590	−31.863640	14.335	13.601	3001364	273.354	−31.8636	−87.0	0.7
18132487−3149321	273.353638	−31.825600	13.273	12.234	J181324.88−314932.24	273.353670	−31.825623	...	12.225	3001020	273.354	−31.8256	−25.2	0.8
18132493−3147549	273.353895	−31.798599	12.781	11.873	J181324.94−314755.01	273.353929	−31.798617	12.749	11.835	3001217	273.354	−31.7986	−126.4	0.6
18132498−3148247	273.354092	−31.806879	14.744	13.852	J181324.97−314824.82	273.354063	−31.806895	14.830	13.993	3001115	273.354	−31.8069	127.5	0.9
18132502−3148163	273.354281	−31.804529	9.901	8.542	J181325.02−314816.35	273.354272	−31.804542	9.879	8.616	3001140	273.354	−31.8045	42.4	0.9
18132517−3147386	273.354886	−31.794073	14.443	13.684	J181325.17−314738.61	273.354888	−31.794060	14.386	13.614	3001262	273.355	−31.7941	136.4	0.7
18132536−3150138	273.355668	−31.837193	14.977	14.517	J181325.36−315013.93	273.355694	−31.837204	14.881	14.431	3001000	273.356	−31.8372	−24.3	1.1
18132552−3154577	273.356365	−31.916033	12.515	11.556	J181325.53−315457.67	273.356391	−31.916022	12.469	11.531	3002988	273.356	−31.9160	−83.7	0.6
18132563−3152005	273.356817	−31.866825	13.958	13.082	J181325.63−315200.64	273.356807	−31.866847	13.947	13.091	3001360	273.357	−31.8668	−4.7	0.8
18132585−3148152	273.357716	−31.804230	12.954	12.052	J181325.85−314815.23	273.357743	−31.804232	12.893	11.988	3001060	273.358	−31.8042	215.9	0.6
18132585−3151431	273.357739	−31.861984	14.967	14.296	J181325.85−315143.12	273.357733	−31.861979	14.818	14.267	3001254	273.358	−31.8620	28.2	1.1
18132596−3143457	273.358189	−31.729387	10.392	9.038	J181325.96−314345.76	273.358186	−31.729378	10.416	9.080	3003309	273.358	−31.7294	5.0	0.8
18132597−3147099	273.358215	−31.786093	13.670	12.800	J181325.97−314709.94	273.358245	−31.786095	13.611	12.733	3001328	273.358	−31.7861	−157.0	0.8
18132607−3148318	273.358638	−31.808834	14.171	13.361	J181326.07−314831.77	273.358652	−31.808827	14.124	13.361	3000987	273.359	−31.8088	−109.9	0.7
18132634−3154010	273.359760	−31.900291	11.484	10.362	J181326.34−315401.06	273.359759	−31.900296	11.460	10.399	3002254	273.360	−31.9003	189.6	0.7
18132643−3146457[a]	273.360136	−31.779375	12.372	11.323	J181326.43−314645.76	273.360151	−31.779380	12.311	11.285	3001444	273.360	−31.7794	−146.9	0.8
18132658−3151113[a]	273.360760	−31.853144	12.251	11.250	J181326.58−315111.33	273.360755	−31.853150	12.200	11.195	3001055	273.361	−31.8531	42.9	0.8
18132676−3152544[a]	273.361509	−31.881792	12.384	11.308	J181326.76−315254.40	273.361532	−31.881779	12.306	11.314	3001636	273.361	−31.8818	−100.9	0.8
18132685−3148584	273.361878	−31.816225	14.681	13.871	J181326.85−314858.36	273.361909	−31.816214	14.643	13.878	3000853	273.362	−31.8162	153.8	0.9
18132689−3148155	273.362054	−31.804312	14.729	13.903	J181326.89−314815.53	273.362069	−31.804315	14.681	13.942	3000964	273.362	−31.8043	−94.6	0.1
18132698−3150531	273.362431	−31.848093	14.861	14.116	J181326.98−315053.25	273.362447	−31.848126	14.836	14.075	3000948	273.362	−31.8481	65.6	1.0
18132736−3152312	273.364037	−31.875340	12.772	11.741	J181327.36−315231.23	273.364039	−31.875344	12.699	11.715	3001418	273.364	−31.8753	−21.9	0.7
18132754−3146183	273.364775	−31.771776	13.781	12.854	...	...	...	...	...	3001556	273.365	−31.7717	−14.7	0.8
18132756−3200052	273.364865	−32.001450	11.483	10.393	J181327.56−320005.13	273.364868	−32.001426	11.454	10.389	3008418	273.365	−32.0014	−136.5	0.6
18132774−3150498	273.365603	−31.847183	12.509	11.446	J181327.74−315049.86	273.365607	−31.847183	12.411	11.398	2000085	273.366	−31.8472	−7.2	0.8
18132779−3148209	273.365803	−31.805817	14.340	13.461	J181327.79−314820.97	273.365800	−31.805827	14.293	13.423	2000474	273.366	−31.8058	−74.5	1.0

Table 3—Continued

Star Name (2MASS)	RA (J2000)	DEC (J2000)	J (mag)	K_S (mag)	Star Name (VVV)	RA (J2000)	DEC (J2000)	J (mag)	K_S (mag)	Star Name (VLT)	RA (J2000)	DEC (J2000)	$RV_{helio.}$ (km s^{-1})	RV Error (km s^{-1})
18132779−3152454	273.365833	−31.879290	13.865	13.033	J181327.80−315245.44	273.365836	−31.879289	13.757	12.934	3001479	273.366	−31.8793	−206.8	0.8
18132786−3145363	273.366116	−31.760096	12.261	11.232	J181327.86−314536.29	273.366118	−31.760082	12.201	11.188	3001880	273.366	−31.7601	58.4	0.6
18132805−3149592	273.366895	−31.833120	11.499	10.482	J181328.05−314959.30	273.366892	−31.833140	11.347	10.303	2000032	273.367	−31.8331	63.7	0.7
18132807−3148033	273.366988	−31.800928	13.489	12.570	J181328.08−314803.32	273.367005	−31.800925	13.407	12.516	2000211	273.367	−31.8009	24.3	0.6
18132818−3142039	273.367443	−31.701099	9.877	8.518	J181328.18−314203.96	273.367442	−31.701103	9.982	8.640	3004655	273.367	−31.7011	−75.8	0.8
18132822−3155176	273.367597	−31.921583	9.688	8.274	···	···	···	···	···	3003049	273.368	−31.9216	18.3	1.1
18132837−3148555	273.368213	−31.815439	13.966	13.034	···	···	···	···	···	2000369	273.368	−31.8154	53.2	0.8
18132847−3146495	273.368635	−31.780428	13.209	12.213	J181328.46−314649.54	273.368620	−31.780429	13.136	12.185	3001281	273.369	−31.7804	−186.3	0.7
18132852−3151537	273.368863	−31.864925	13.807	12.878	J181328.52−315153.72	273.368853	−31.864925	13.681	12.825	2000287	273.369	−31.8649	124.9	0.8
18132861−3139348	273.369244	−31.659689	12.985	11.914	J181328.61−313935.04	273.369238	−31.659734	12.898	11.879	3007606	273.369	−31.6597	22.9	0.7
18132878−3146047	273.369946	−31.767998	13.759	12.860	J181328.79−314604.77	273.369964	−31.767993	13.689	12.814	3001579	273.370	−31.7680	−208.2	0.7
18132916−3147488	273.371508	−31.796906	14.088	13.300	J181329.16−314748.95	273.371502	−31.796932	14.016	13.196	2000381	273.371	−31.7969	−13.5	0.4
18132919−3138192	273.371625	−31.638683	14.890	14.334	J181329.19−313819.29	273.371637	−31.638694	14.921	14.195	RHB.200033714	273.372	−31.6387	−98.6	0.0
18132925−3147315	273.371876	−31.792086	13.180	12.319	J181329.24−314731.53	273.371873	−31.792093	13.128	12.267	2000159	273.372	−31.7921	50.3	0.7
18132928−3157460	273.372037	−31.962799	12.827	11.836	J181329.28−315746.01	273.372040	−31.962781	12.786	11.805	3005333	273.372	−31.9628	−139.5	0.7
18132938−3147441	273.372435	−31.795584	14.040	13.187	J181329.38−314744.15	273.372424	−31.795598	14.016	13.209	2000391	273.372	−31.7956	−254.8	0.9
18132950−3159218	273.372953	−31.989399	10.022	8.626	J181329.49−315921.76	273.372887	−31.989379	9.908	8.720	3007246	273.373	−31.9894	59.5	0.9
18132977−3141406	273.374059	−31.694616	14.895	14.181	J181329.77−314140.58	273.374057	−31.694607	14.834	14.202	RHB.200035147	273.374	−31.6946	56.5	0.5
18132995−3152429	273.374822	−31.878599	13.369	12.497	J181329.95−315242.95	273.374804	−31.878599	13.247	12.418	3001327	273.375	−31.8786	34.9	0.8
18133004−3142101	273.375177	−31.702833	12.104	11.045	J181330.04−314210.21	273.375181	−31.702839	12.044	11.004	3004440	273.375	−31.7028	106.9	0.6
18133006−3146197	273.375257	−31.772146	13.616	12.744	···	···	···	···	···	3001379	273.375	−31.7721	−115.0	0.7
18133030−3148497	273.376283	−31.813816	14.558	13.693	J181330.30−314849.68	273.376258	−31.813802	14.545	13.637	2000582	273.376	−31.8138	−87.8	0.3
18133034−3142530	273.376421	−31.714727	11.137	9.984	J181330.34−314253.00	273.376430	−31.714724	11.126	10.058	3003754	273.376	−31.7147	77.7	0.7
18133035−3146186	273.376482	−31.771835	13.377	12.343	···	···	···	···	···	3001374	273.376	−31.7718	20.2	0.7
18133036−3148086	273.376526	−31.802393	14.280	13.390	···	···	···	···	···	2000477	273.376	−31.8024	−15.2	0.6
18133041−3150297	273.376712	−31.841606	14.363	13.413	J181330.41−315029.79	273.376731	−31.841610	14.252	13.447	2000429	273.377	−31.8416	176.0	0.7
18133061−3152193	273.377568	−31.872028	14.250	13.416	J181330.61−315219.36	273.377553	−31.872047	14.173	13.402	3001156	273.378	−31.8720	12.5	0.7
18133067−3158267	273.377812	−31.974110	12.956	11.946	J181330.67−315826.74	273.377793	−31.974095	12.896	11.980	3006018	273.378	−31.9741	−63.7	0.8
18133098−3146398	273.379114	−31.777729	14.548	13.782	J181330.99−314639.78	273.379144	−31.777718	14.500	13.740	3001206	273.379	−31.7777	35.6	0.5
18133105−3150358	273.379414	−31.843279	14.357	13.425	J181331.05−315035.79	273.379397	−31.843277	14.189	13.384	2000413	273.379	−31.8433	79.4	0.8
18133110−3153043	273.379619	−31.884535	12.601	11.617	J181331.11−315304.28	273.379631	−31.884524	12.518	11.601	3001439	273.380	−31.8845	80.7	0.7
18133112−3151145	273.379685	−31.854033	13.764	12.621	J181331.13−315114.56	273.379713	−31.854046	13.645	12.799	2000285	273.380	−31.8540	1.0	0.7
18133113−3148031	273.379728	−31.800884	13.648	12.654	J181331.13−314803.11	273.379750	−31.800866	13.592	12.619	2000264	273.380	−31.8009	30.2	0.7
18133121−3147085	273.380050	−31.785719	13.620	12.700	J181331.21−314708.59	273.380064	−31.785721	13.551	12.700	3000997	273.380	−31.7857	−12.6	0.8
18133126−3147264	273.380290	−31.790676	13.247	12.307	J181331.26−314726.34	273.380290	−31.790652	13.186	12.299	2000170	273.380	−31.7907	−29.1	0.7
18133130−3144587	273.380428	−31.749655	12.878	11.912	J181331.30−314458.67	273.380441	−31.749633	12.750	11.822	3002051	273.380	−31.7496	31.6	1.5
18133135−3149459	273.380652	−31.829430	14.182	13.307	J181331.36−314945.95	273.380672	−31.829431	14.084	13.211	2000398	273.381	−31.8294	22.7	0.8
18133158−3151587	273.381586	−31.866306	13.494	12.570	J181331.58−315158.67	273.381602	−31.866299	13.397	12.488	2000213	273.382	−31.8663	−92.6	0.8
18133170−3153311	273.382104	−31.891989	11.330	10.227	J181331.70−315331.20	273.382093	−31.892002	11.223	10.245	3001648	273.382	−31.8920	12.1	0.6
18133172−3143599	273.382184	−31.733311	12.459	11.434	J181331.72−314359.91	273.382205	−31.733310	···	11.357	3002739	273.382	−31.7333	−84.4	0.7
18133173−3148190	273.382243	−31.805304	13.883	13.124	···	···	···	···	···	RHB.200040028	273.382	−31.8049	−86.3	0.2
18133207−3149049	273.383627	−31.818039	14.451	13.518	J181332.07−314904.94	273.383658	−31.818040	14.388	13.531	2000488	273.384	−31.8180	62.8	0.6
18133211−3146103	273.383822	−31.769543	14.661	13.888	J181332.12−314610.35	273.383872	−31.769542	14.512	13.744	3001353	273.384	−31.7695	27.9	0.8
18133212−3147585	273.383869	−31.799595	13.548	12.687	J181332.13−314758.56	273.383901	−31.799602	13.467	12.612	2000217	273.384	−31.7996	−75.0	0.7
18133215−3156483	273.383991	−31.946770	11.122	9.956	···	···	···	···	···	3004158	273.384	−31.9467	14.1	0.7
18133234−3151434	273.384770	−31.862076	13.784	12.753	J181332.34−315143.64	273.384753	−31.862124	13.771	12.862	2000317	273.385	−31.8621	−15.2	0.8
18133242−3151466	273.385123	−31.862968	14.697	12.744	J181332.42−315146.72	273.385092	−31.862978	14.950	14.075	2000798	273.385	−31.8630	−126.9	0.0
18133256−3146384	273.385678	−31.777344	14.303	13.441	J181332.57−314638.43	273.385738	−31.777343	14.266	13.370	3001149	273.386	−31.7773	−6.7	0.7
18133272−3152464	273.386346	−31.879568	11.935	10.731	J181332.72−315246.45	273.386340	−31.879570	11.851	10.751	3001238	273.386	−31.8796	54.7	0.8
18133292−3141052	273.387185	−31.684780	12.625	11.594	J181332.92−314105.25	273.387185	−31.684792	12.554	11.546	3005504	273.387	−31.6848	37.2	0.7

Table 3—Continued

Star Name (2MASS)	RA (J2000)	DEC (J2000)	J (mag)	K_S (mag)	Star Name (VVV)	RA (J2000)	DEC (J2000)	J (mag)	K_S (mag)	Star Name (VLT)	RA (J2000)	DEC (J2000)	$RV_{helio.}$ (km s^{-1})	RV Error (km s^{-1})
18133300−3142283	273.387533	−31.707863	11.973	10.761	J181333.00−314228.31	273.387538	−31.707866	11.915	10.769	3004020	273.387	−31.7079	−130.2	1.1
18133306−3153055	273.387771	−31.884874	14.445	13.630	J181333.06−315305.62	273.387753	−31.884895	14.342	13.503	3001361	273.388	−31.8849	43.4	0.9
18133330−3143005	273.388784	−31.716818	10.298	8.928	J181333.30−314300.56	273.388762	−31.716824	10.264	9.026	3003503	273.389	−31.7168	−10.6	0.8
18133334−3150085	273.388946	−31.835712	14.039	13.109	J181333.35−315008.67	273.388965	−31.835742	13.988	13.065	2000346	273.389	−31.8357	34.7	0.6
18133334−3156279	273.388951	−31.941097	12.696	11.663	J181333.35−315627.99	273.388961	−31.941110	12.636	11.614	3003791	273.389	−31.9411	58.0	0.6
18133347−3156507	273.389494	−31.947439	10.928	9.703	···	···	···	···	···	3004150	273.389	−31.9474	−125.7	0.8
18133367−3152120	273.390323	−31.870026	14.049	13.137	J181333.67−315212.03	273.390318	−31.870009	13.952	13.073	2000349	273.390	−31.8700	−131.6	0.7
18133373−3152005	273.390574	−31.866816	12.788	11.835	J181333.73−315200.52	273.390569	−31.866813	12.726	11.813	2000110	273.391	−31.8668	−0.8	0.8
18133394−3154230	273.391454	−31.906389	9.953	8.629	J181333.94−315422.97	273.391439	−31.906383	9.904	8.771	3002073	273.391	−31.9064	−183.0	0.9
18133395−3145552	273.391463	−31.765337	13.694	12.850	···	···	···	···	···	3001415	273.391	−31.7653	−222.5	0.7
18133396−3143370	273.391502	−31.726946	14.958	14.316	···	···	···	···	···	RHB.200046013	273.392	−31.7269	55.1	0.0
18133405−3159272	273.391889	−31.990900	12.937	11.926	J181334.05−315927.20	273.391886	−31.990890	12.843	11.874	3007162	273.392	−31.9909	−181.0	0.7
18133410−3158119	273.392113	−31.969994	14.657	13.898	J181334.10−315811.95	273.392106	−31.969989	14.605	13.780	RGB.100091633	273.392	−31.9700	66.3	0.1
18133419−3146481	273.392498	−31.780033	14.981	14.198	···	···	···	···	···	3001012	273.392	−31.7800	23.2	2.2
18133438−3152253	273.393291	−31.873718	14.232	13.421	J181334.38−315225.40	273.393269	−31.873724	14.256	13.411	3001030	273.393	−31.8737	40.7	0.7
18133454−3152136	273.393954	−31.870455	14.569	13.663	J181334.54−315213.66	273.393953	−31.870464	14.445	13.522	3000926	273.394	−31.8704	−2.5	0.8
18133458−3140135	273.394097	−31.670439	9.509	8.086	J181334.58−314013.64	273.394094	−31.670457	9.570	8.280	3006484	273.394	−31.6704	80.5	0.7
18133465−3147432	273.394387	−31.795341	14.454	13.553	J181334.65−314743.27	273.394415	−31.795354	14.364	13.492	2000478	273.394	−31.7953	73.4	0.7
18133465−3152235	273.394406	−31.873211	13.910	13.004	J181334.64−315223.59	273.394374	−31.873220	13.873	12.944	3001004	273.394	−31.8732	14.6	0.9
18133472−3143153	273.394703	−31.720926	11.100	9.812	J181334.73−314315.32	273.394730	−31.720923	11.075	9.906	3003258	273.395	−31.7209	57.3	0.7
18133480−3140321	273.395008	−31.675596	12.265	11.236	J181334.81−314032.08	273.395066	−31.675580	12.172	11.177	3006092	273.395	−31.6756	7.9	0.8
18133493−3149459	273.395550	−31.829430	15.327	14.588	J181334.93−314946.03	273.395561	−31.829453	14.950	14.143	2000771	273.396	−31.8294	44.7	0.8
18133518−3152070	273.396602	−31.868622	13.716	12.761	J181335.18−315207.02	273.396614	−31.868619	13.616	12.719	2000279	273.397	−31.8686	55.4	0.8
18133536−3147086	273.397334	−31.785740	13.487	12.474	···	···	···	···	···	3000824	273.397	−31.7857	−78.7	0.8
18133540−3141527	273.397516	−31.697973	13.723	12.801	···	···	···	···	···	RGB.200050122	273.397	−31.6980	64.7	0.4
18133550−3153188	273.397920	−31.888561	13.783	12.743	J181335.49−315318.89	273.397914	−31.888581	13.728	12.764	3001397	273.398	−31.8886	−70.7	0.7
18133561−3147167	273.398384	−31.787992	14.379	13.585	J181335.61−314716.80	273.398384	−31.788002	14.275	13.486	3000759	273.398	−31.7880	−121.2	0.7
18133571−3151162	273.398809	−31.854502	14.212	13.258	J181335.71−315116.19	273.398817	−31.854499	14.108	13.205	2000400	273.399	−31.8545	−123.9	0.7
18133594−3141414	273.399774	−31.694836	11.374	10.270	J181335.94−314141.38	273.399768	−31.694830	11.343	10.283	3004731	273.400	−31.6948	−140.9	0.7
18133603−3146515	273.400164	−31.780989	13.873	12.992	J181336.04−314651.58	273.400176	−31.780997	13.829	12.901	3000922	273.400	−31.7810	−11.5	0.8
18133614−3146182	273.400614	−31.771742	14.223	13.359	J181336.31−314618.89	273.401298	−31.771915	···	···	3001189	273.401	−31.7717	89.0	0.6
18133621−3147046	273.400888	−31.784618	14.438	13.603	J181336.21−314704.62	273.400894	−31.784618	14.374	13.507	3000832	273.401	−31.7846	29.6	0.6
18133621−3157402	273.400906	−31.961189	12.757	11.690	J181336.22−315740.25	273.400918	−31.961183	12.716	11.686	3004953	273.401	−31.9612	−4.6	0.8
18133631−3153323	273.401308	−31.892324	13.278	12.345	···	···	···	···	···	3001506	273.401	−31.8923	−10.1	0.7
18133641−3146164	273.401744	−31.771231	14.092	13.197	J181336.42−314616.39	273.401756	−31.771221	14.152	13.256	3001195	273.402	−31.7712	94.0	0.8
18133643−3138351	273.401806	−31.643084	15.096	14.414	J181336.43−313835.21	273.401821	−31.643114	14.963	14.264	RHB.200053248	273.402	−31.6431	−74.6	0.7
18133646−3147328	273.401948	−31.792446	12.356	11.353	J181336.47−314732.76	273.401969	−31.792436	12.283	11.316	2000078	273.402	−31.7924	−29.2	0.7
18133652−3146447	273.402206	−31.779110	13.902	13.024	J181336.53−314644.80	273.402217	−31.779111	13.834	12.974	3000970	273.402	−31.7791	−180.5	0.8
18133704−3153329	273.404348	−31.892498	13.890	12.948	J181337.03−315333.00	273.404331	−31.892502	13.850	12.934	3001502	273.404	−31.8925	2.7	0.7
18133706−3144179	273.404450	−31.738319	11.444	10.189	J181337.07−314417.96	273.404475	−31.738325	···	10.218	3002356	273.404	−31.7383	−166.1	0.8
18133714−3152325	273.404773	−31.875698	13.746	12.779	J181337.14−315232.48	273.404759	−31.875689	13.688	12.838	3001021	273.405	−31.8757	128.3	0.6
18133717−3152225	273.404889	−31.872929	14.485	13.696	J181337.17−315222.53	273.404877	−31.872926	14.456	13.662	3000938	273.405	−31.8729	7.7	0.7
18133737−3141187	273.405725	−31.688528	12.777	11.703	J181337.37−314118.73	273.405723	−31.688537	12.679	11.647	3005145	273.406	−31.6885	−164.2	0.9
18133763−3151408	273.406809	−31.861340	14.268	13.270	···	···	···	···	···	2000409	273.407	−31.8613	−14.5	1.7
18133784−3146440	273.407701	−31.778896	12.488	11.449	J181337.85−314643.93	273.407733	−31.778871	12.438	11.423	3000958	273.408	−31.7789	−137.3	0.6
18133796−3145495	273.408176	−31.763771	14.624	13.663	J181337.96−314549.58	273.408192	−31.763773	14.508	13.625	3001383	273.408	−31.7637	43.8	0.1
18133821−3152229	273.409230	−31.873039	14.444	13.533	J181338.21−315222.94	273.409232	−31.873041	14.363	13.480	3000927	273.409	−31.8730	51.9	0.7
18133827−3142097	273.409497	−31.702709	11.295	10.100	J181338.27−314209.82	273.409478	−31.702730	11.321	10.118	3004230	273.409	−31.7027	44.6	0.7
18133832−3156253	273.409681	−31.940378	12.518	11.518	J181338.32−315625.34	273.409671	−31.940372	12.476	11.525	3003639	273.410	−31.9404	56.7	0.6
18133899−3157022	273.412489	−31.950619	12.689	11.660	···	···	···	···	···	3004259	273.412	−31.9506	−114.6	0.6

Table 3—Continued

Star Name (2MASS)	RA (J2000)	DEC (J2000)	J (mag)	K_S (mag)	Star Name (VVV)	RA (J2000)	DEC (J2000)	J (mag)	K_S (mag)	Star Name (VLT)	RA (J2000)	DEC (J2000)	$RV_{helio.}$ (km s^{-1})	RV Error (km s^{-1})
18133925−3155301	273.413562	−31.925037	12.620	11.644	···	···	···	···	···	3002848	273.414	−31.9250	24.2	1.0
18133929−3142557	273.413737	−31.715477	10.980	9.716	J181339.29−314255.76	273.413731	−31.715492	10.989	9.749	3003478	273.414	−31.7155	−19.5	0.8
18133930−3150385	273.413780	−31.844038	13.121	12.251	J181339.31−315038.57	273.413824	−31.844049	···	12.246	1401486	273.414	−31.8440	71.9	0.6
18133939−3150258	273.414157	−31.840502	11.210	10.014	J181339.39−315025.81	273.414147	−31.840504	11.242	9.957	1401255	273.414	−31.8405	14.5	0.7
18133953−3141385	273.414738	−31.694042	12.626	11.682	J181339.53−314138.65	273.414746	−31.694070	12.641	11.710	3004757	273.415	−31.6940	16.1	0.6
18133959−3152321	273.414972	−31.875593	13.769	12.787	J181339.59−315232.14	273.414972	−31.875596	13.673	12.735	3001011	273.415	−31.8756	7.4	0.8
18133965−3153001	273.415226	−31.883383	14.716	14.019	J181339.64−315300.14	273.415206	−31.883373	14.539	13.979	3001225	273.415	−31.8834	12.2	4.5
18133987−3142274	273.416138	−31.707617	14.251	13.346	J181339.87−314227.48	273.416145	−31.707635	14.210	13.325	RGB.200062586	273.416	−31.7076	−21.1	0.2
18134015−3147066	273.417306	−31.785175	14.366	13.594	J181340.15−314706.56	273.417306	−31.785158	14.391	···	3000800	273.417	−31.7852	−9.4	0.9
18134030−3150454	273.417954	−31.845949	13.943	13.042	···	···	···	···	···	1401202	273.418	−31.8459	−2.5	0.6
18134031−3147089	273.417976	−31.785828	14.341	13.564	J181340.31−314708.80	273.417982	−31.785780	14.466	13.731	3000783	273.418	−31.7858	25.2	0.7
18134035−3148332	273.418137	−31.809240	14.113	13.173	J181340.36−314833.27	273.418185	−31.809243	13.946	13.098	1201279	273.418	−31.8092	21.5	0.7
18134062−3153269	273.419274	−31.890818	12.181	11.038	J181340.61−315327.02	273.419246	−31.890840	12.121	11.039	3001451	273.419	−31.8908	−11.1	0.8
18134067−3147253	273.419476	−31.790367	14.388	13.529	J181340.67−314725.35	273.419467	−31.790375	14.296	13.459	2000441	273.419	−31.7904	−181.5	0.7
18134070−3159332	273.419594	−31.992577	12.073	10.891	J181340.70−315933.29	273.419590	−31.992583	12.009	10.918	3007239	273.420	−31.9926	67.4	0.7
18134071−3146319	273.419632	−31.775530	10.903	9.682	J181340.71−314631.86	273.419639	−31.775518	10.830	9.547	3001067	273.420	−31.7755	15.8	0.7
18134071−3146534	273.419656	−31.781500	11.319	10.092	J181340.72−314653.41	273.419675	−31.781504	11.405	9.946	3000895	273.420	−31.7815	−143.5	0.7
18134087−3154041	273.420326	−31.901146	12.762	11.631	J181340.87−315404.09	273.420332	−31.901138	12.679	11.590	3001809	273.420	−31.9011	37.2	0.7
18134092−3153334	273.420535	−31.892632	14.493	13.591	···	···	···	···	···	3001511	273.420	−31.8926	36.5	0.8
18134093−3157454	273.420571	−31.962624	12.890	11.881	J181340.92−315745.40	273.420541	−31.962614	12.820	11.893	3005046	273.421	−31.9626	−75.1	0.7
18134097−3146258	273.420748	−31.773848	13.732	12.800	J181340.98−314625.84	273.420763	−31.773846	13.701	12.766	3001124	273.421	−31.7738	−26.0	0.8
18134114−3146077	273.421427	−31.768827	14.290	13.377	J181341.15−314607.73	273.421465	−31.768814	14.204	13.340	3001253	273.421	−31.7688	−90.5	0.6
18134118−3146472	273.421586	−31.779802	13.337	12.432	J181341.18−314647.22	273.421599	−31.779784	13.236	12.328	3000947	273.422	−31.7798	−96.2	0.8
18134137−3141120	273.422378	−31.686684	14.853	13.919	J181341.36−314112.11	273.422340	−31.686698	14.721	13.890	RGB.200066708	273.422	−31.6867	48.6	0.5
18134147−3158324	273.422814	−31.975691	12.513	11.376	J181341.47−315832.43	273.422816	−31.975677	12.446	11.372	3005951	273.423	−31.9757	116.3	0.8
18134175−3147149	273.423977	−31.787491	13.555	12.574	J181341.75−314714.93	273.423995	−31.787481	13.455	12.496	3000765	273.424	−31.7875	61.4	0.8
18134176−3145382	273.424005	−31.760632	11.793	10.598	J181341.76−314538.28	273.424015	−31.760635	11.797	10.678	3001514	273.424	−31.7606	51.0	0.7
18134180−3146441	273.424170	−31.778925	14.373	13.596	J181341.80−314644.12	273.424172	−31.778925	14.252	13.439	3000986	273.424	−31.7789	119.8	0.7
18134183−3145434	273.424300	−31.762074	13.950	13.101	J181341.84−314543.36	273.424342	−31.762046	13.974	13.082	3001463	273.424	−31.7621	13.9	0.7
18134186−3145573	273.424447	−31.765938	13.917	12.974	J181341.86−314557.33	273.424443	−31.765926	13.829	12.901	3001343	273.424	−31.7659	166.7	0.7
18134201−3151508[a]	273.425070	−31.864120	12.184	11.177	J181342.01−315150.85	273.425057	−31.864125	12.118	11.169	2000072	273.425	−31.8641	−22.8	0.7
18134210−3151327	273.425445	−31.859093	13.898	12.743	J181341.96−315132.68	273.424853	−31.859078	14.148	13.314	2000450	273.425	−31.8591	−27.9	0.6
18134234−3147019	273.426428	−31.783880	13.573	12.557	J181342.34−314701.92	273.426437	−31.783867	13.517	12.551	3000865	273.426	−31.7839	−101.4	0.6
18134239−3146293	273.426647	−31.774828	14.793	14.077	J181342.40−314629.26	273.426681	−31.774795	14.689	13.996	3001123	273.427	−31.7748	−18.9	1.6
18134240−3141358	273.426682	−31.693295	12.780	11.778	J181342.40−314135.96	273.426685	−31.693324	12.688	11.702	3004858	273.427	−31.6933	−64.6	0.6
18134245−3201173	273.426880	−32.021496	9.821	8.393	J181342.45−320117.39	273.426877	−32.021499	9.688	8.478	3009983	273.427	−32.0215	−95.6	1.0
18134250−3158205	273.427111	−31.972366	12.847	11.867	J181342.50−315820.47	273.427099	−31.972355	12.818	11.893	3005723	273.427	−31.9724	−11.2	0.7
18134251−3155441	273.427157	−31.928925	12.566	11.421	J181342.51−315544.18	273.427160	−31.928940	12.523	11.393	3003098	273.427	−31.9289	−91.2	0.8
18134263−3147321	273.427625	−31.792273	14.309	13.090	J181342.62−314732.05	273.427617	−31.792237	14.193	13.247	2000435	273.428	−31.7922	−83.1	0.5
18134268−3151123	273.427861	−31.853430	14.160	13.402	J181342.68−315112.38	273.427856	−31.853441	14.147	13.389	2000439	273.428	−31.8534	10.8	0.7
18134304−3153062	273.429349	−31.885078	14.497	13.662	J181343.04−315306.22	273.429344	−31.885064	14.425	13.598	3001307	273.429	−31.8851	−9.9	0.9
18134306−3154429	273.429440	−31.911926	10.857	9.631	J181343.06−315442.96	273.429419	−31.911935	10.816	9.658	3002280	273.429	−31.9119	7.6	0.7
18134309−3149219	273.429559	−31.822756	14.823	12.344	···	···	···	···	···	1201487	273.429	−31.8229	57.2	0.7
18134328−3146476	273.430349	−31.779900	13.832	12.883	J181343.28−314647.59	273.430357	−31.779886	13.716	12.867	3001002	273.430	−31.7799	107.9	0.6
18134337−3151418	273.430736	−31.861631	12.693	11.584	J181343.37−315141.79	273.430734	−31.861611	12.602	11.570	2000103	273.431	−31.8616	−185.2	0.9
18134337−3152371	273.430710	−31.876982	14.793	14.012	J181343.37−315237.22	273.430727	−31.877006	14.716	13.875	3001116	273.431	−31.8770	49.4	1.6
18134344−3145386	273.431000	−31.760736	13.133	12.208	···	···	···	···	···	3001549	273.431	−31.7607	−137.0	1.4
18134348−3153042	273.431167	−31.884525	11.667	10.485	J181343.48−315304.29	273.431187	−31.884528	11.638	10.509	3001306	273.431	−31.8845	−87.4	0.7
18134352−3147212	273.431374	−31.789244	11.308	10.140	J181343.53−314721.29	273.431378	−31.789249	11.300	10.068	2000023	273.431	−31.7892	171.3	0.7
18134360−3151169	273.431678	−31.854715	13.786	12.929	···	···	···	···	···	2000342	273.432	−31.8547	3.6	0.7

Table 3—Continued

Star Name (2MASS)	RA (J2000)	DEC (J2000)	J (mag)	K_S (mag)	Star Name (VVV)	RA (J2000)	DEC (J2000)	J (mag)	K_S (mag)	Star Name (VLT)	RA (J2000)	DEC (J2000)	$RV_{helio.}$ (km s^{-1})	RV Error (km s^{-1})
18134383−3154096	273.432633	−31.902670	12.611	11.461	J181343.83−315409.66	273.432646	−31.902684	12.546	11.429	3001933	273.433	−31.9027	98.6	0.8
18134399−3153171	273.433313	−31.888111	12.856	11.825	J181343.99−315317.21	273.433319	−31.888115	12.776	11.781	3001438	273.433	−31.8881	75.3	0.8
18134406−3159142	273.433617	−31.987284	10.366	9.082	J181344.06−315914.09	273.433611	−31.987250	10.195	9.119	3006890	273.434	−31.9873	−10.2	0.7
18134421−3146251	273.434211	−31.773643	13.621	12.734	J181344.20−314625.10	273.434205	−31.773641	13.592	12.730	3001203	273.434	−31.7736	−187.7	0.8
18134450−3143184	273.435448	−31.721796	12.867	11.853	J181344.50−314318.54	273.435442	−31.721817	12.838	11.787	3003257	273.435	−31.7218	−3.8	0.8
18134451−3147221	273.435492	−31.789494	14.482	13.801	J181344.51−314722.20	273.435483	−31.789500	14.410	13.688	2000508	273.435	−31.7895	8.8	0.9
18134452−3151526	273.435538	−31.864624	13.958	13.082	···	···	···	···	···	2000360	273.435	−31.8646	202.4	1.1
18134472−3154461	273.436370	−31.912809	13.634	12.800	···	···	···	···	···	RGB.100112406	273.436	−31.9129	−3.5	0.5
18134481−3143510	273.436726	−31.730846	12.392	11.415	J181344.81−314351.05	273.436730	−31.730847	12.347	11.413	3002814	273.437	−31.7308	−17.4	0.6
18134486−3146230	273.436953	−31.773058	13.579	12.627	J181344.87−314623.08	273.436985	−31.773079	13.483	12.659	3001239	273.437	−31.7731	−135.4	0.6
18134494−3201363	273.437274	−32.026772	9.583	8.170	···	···	···	···	···	3010576	273.437	−32.0267	−203.7	1.0
18134501−3150324	273.437566	−31.842350	15.548	14.865	J181345.02−315032.52	273.437590	−31.842369	15.355	14.800	1301378	273.438	−31.8424	127.9	1.6
18134508−3152223	273.437839	−31.872868	13.924	13.051	J181345.07−315222.29	273.437826	−31.872859	13.809	13.019	3001069	273.438	−31.8729	74.8	0.7
18134523−3159110	273.438477	−31.986406	11.989	10.943	J181345.23−315910.90	273.438495	−31.986361	11.948	10.924	3006864	273.438	−31.9864	140.1	0.6
18134549−3149305	273.439547	−31.825148	14.640	13.769	···	···	···	···	···	1300490	273.440	−31.8251	−98.2	0.6
18134549−3151142	273.439560	−31.853951	14.333	13.447	J181345.50−315114.18	273.439588	−31.853940	14.234	13.549	2000500	273.440	−31.8539	136.1	0.8
18134554−3143091	273.439776	−31.719217	11.593	10.355	J181345.54−314309.27	273.439787	−31.719242	11.563	10.362	3003419	273.440	−31.7192	41.3	0.8
18134585−3149220	273.441055	−31.822798	13.668	12.730	J181345.85−314922.10	273.441046	−31.822808	13.616	12.764	1300336	273.441	−31.8228	84.5	1.1
18134594−3145334	273.441417	−31.759285	12.683	11.647	J181345.93−314533.37	273.441410	−31.759272	12.597	11.624	3001689	273.441	−31.7593	174.0	0.6
18134601−3158211	273.441747	−31.972536	12.868	11.933	J181346.02−315821.04	273.441756	−31.972513	12.792	11.872	3005847	273.442	−31.9725	−110.4	0.7
18134609−3143504	273.442075	−31.730671	11.333	10.132	J181346.10−314350.38	273.442093	−31.730664	11.347	10.102	3002877	273.442	−31.7307	−139.2	0.7
18134620−3147464[a]	273.442541	−31.796238	12.523	11.463	J181346.21−314746.43	273.442549	−31.796232	12.475	11.442	2000090	273.443	−31.7962	15.8	0.8
18134628−3139126	273.442870	−31.653521	12.373	11.260	J181346.28−313912.68	273.442866	−31.653523	12.340	11.341	3008006	273.443	−31.6535	24.9	0.8
18134662−3148264	273.444254	−31.807360	14.465	13.531	J181346.62−314826.41	273.444267	−31.807339	14.419	13.531	2000494	273.444	−31.8074	−95.4	0.8
18134664−3149053	273.444343	−31.818142	14.302	13.330	J181346.64−314905.29	273.444338	−31.818138	14.226	13.293	2000436	273.444	−31.8181	−64.0	0.8
18134671−3149182	273.444662	−31.821730	12.850	11.911	J181346.71−314918.18	273.444631	−31.821718	12.797	11.908	2000109	273.445	−31.8217	−378.8	1.1
18134702−3147156	273.445927	−31.787691	10.334	9.106	J181347.01−314715.79	273.445896	−31.787721	10.364	9.106	3000978	273.446	−31.7877	44.2	0.7
18134704−3154199	273.446025	−31.905533	9.718	8.338	J181347.05−315419.92	273.446044	−31.905534	10.995	8.472	3002176	273.446	−31.9055	−127.9	0.8
18134717−3152291[a]	273.446558	−31.874754	11.990	10.955	J181347.17−315229.09	273.446561	−31.874747	11.985	10.969	3001214	273.447	−31.8747	10.6	0.7
18134728−3140488	273.447034	−31.680244	12.517	11.563	J181347.29−314048.89	273.447049	−31.680248	12.462	11.528	3005931	273.447	−31.6802	−14.4	0.8
18134732−3139395	273.447193	−31.660988	12.568	11.426	J181347.32−313939.66	273.447181	−31.661017	12.514	11.451	3007391	273.447	−31.6610	15.7	0.5
18134748−3142255	273.447854	−31.707109	12.937	11.899	J181347.48−314225.62	273.447859	−31.707117	12.900	11.862	3004185	273.448	−31.7071	−157.5	0.8
18134749−3153109	273.447884	−31.886387	13.110	12.140	J181347.48−315310.99	273.447865	−31.886388	13.060	12.163	3001534	273.448	−31.8864	143.8	0.6
18134772−3148330	273.448852	−31.809179	13.459	12.627	J181347.73−314833.16	273.448889	−31.809213	13.432	12.614	2000208	273.449	−31.8092	−13.9	0.8
18134776−3150372	273.449029	−31.843681	14.737	14.105	···	···	···	···	···	2000722	273.449	−31.8437	−71.4	1.2
18134812−3142269	273.450501	−31.707474	13.199	12.243	···	···	···	···	···	RGB.200085414	273.450	−31.7075	−202.4	0.5
18134825−3152253	273.451059	−31.873711	14.015	13.092	J181348.25−315225.29	273.451047	−31.873694	13.976	13.049	3001246	273.451	−31.8737	−102.2	0.7
18134831−3153000	273.451301	−31.883360	14.334	13.495	J181348.30−315300.10	273.451279	−31.883362	14.230	13.407	3001484	273.451	−31.8834	−7.6	0.7
18134833−3152487	273.451410	−31.880201	13.761	12.818	J181348.34−315248.75	273.451427	−31.880210	13.691	12.821	3001401	273.451	−31.8802	−96.6	0.7
18134840−3153133	273.451701	−31.887053	14.630	13.679	J181348.41−315313.50	273.451709	−31.887084	14.549	···	3001614	273.452	−31.8870	−20.2	1.7
18134847−3153085	273.451960	−31.885706	12.842	11.887	J181348.46−315308.56	273.451941	−31.885712	12.796	11.896	3001571	273.452	−31.8857	20.8	0.8
18134879−3152487	273.453304	−31.880207	14.192	13.320	J181348.79−315248.76	273.453302	−31.880213	14.151	13.337	3001435	273.453	−31.8802	−9.4	0.7
18134881−3142055	273.453413	−31.701538	11.042	9.751	J181348.81−314205.59	273.453402	−31.701553	11.011	9.827	3004584	273.453	−31.7015	209.2	0.6
18134888−3154134	273.453667	−31.903744	11.908	10.761	J181348.87−315413.42	273.453660	−31.903730	11.867	10.735	3002210	273.454	−31.9037	−163.4	0.7
18134895−3148068	273.453983	−31.801914	14.505	13.754	J181348.95−314806.85	273.453998	−31.801905	14.510	13.798	2000561	273.454	−31.8019	27.9	0.7
18134897−3156052	273.454051	−31.934799	11.320	10.223	J181348.96−315605.29	273.454038	−31.934804	11.316	10.211	3003649	273.454	−31.9348	51.6	0.6
18134909−3200415	273.454550	−32.011555	11.644	10.574	···	···	···	···	···	3009288	273.455	−32.0116	18.4	0.6
18134917−3148186	273.454903	−31.805168	13.932	13.040	J181349.18−314818.59	273.454927	−31.805164	13.894	12.990	2000345	273.455	−31.8052	10.6	0.8
18134919−3152159	273.454986	−31.871098	14.437	13.569	···	···	···	···	···	3001244	273.455	−31.8711	56.8	0.8
18134921−3143582	273.455082	−31.732849	10.516	9.202	···	···	···	···	···	3002940	273.455	−31.7328	−128.2	0.9

Table 3—Continued

Star Name (2MASS)	RA (J2000)	DEC (J2000)	J (mag)	K_S (mag)	Star Name (VVV)	RA (J2000)	DEC (J2000)	J (mag)	K_S (mag)	Star Name (VLT)	RA (J2000)	DEC (J2000)	$RV_{helio.}$ (km s^{-1})	RV Error (km s^{-1})
18134929−3152340	273.455396	−31.876120	13.375	12.495	J181349.29−315234.05	273.455395	−31.876128	13.313	12.463	3001359	273.455	−31.8761	−1.9	0.6
18134948−3157257	273.456192	−31.957150	14.855	14.172	J181349.48−315725.60	273.456185	−31.957112	14.794	14.153	RHB.100120539	273.456	−31.9571	30.2	0.2
18134958−3146032	273.456584	−31.767578	12.702	11.683	J181349.58−314603.27	273.456596	−31.767578	12.630	11.663	3001635	273.457	−31.7676	−6.3	0.6
18134965−3153035	273.456910	−31.884314	13.543	12.572	J181349.66−315303.51	273.456917	−31.884310	13.469	12.571	3001611	273.457	−31.8843	−176.3	0.9
18134966−3152199	273.456934	−31.872206	14.717	13.904	J181349.65−315219.98	273.456906	−31.872218	14.628	13.843	3001294	273.457	−31.8722	−21.8	1.3
18134966−3159306	273.456929	−31.991848	10.755	9.600	J181349.65−315930.56	273.456911	−31.991824	10.705	9.546	3007535	273.457	−31.9918	37.5	0.7
18134969−3159496	273.457048	−31.997124	12.443	11.501	J181349.68−315949.57	273.457030	−31.997105	12.381	11.516	3008008	273.457	−31.9971	−189.5	0.7
18134976−3147112	273.457342	−31.786449	12.947	11.937	J181349.76−314711.31	273.457359	−31.786476	12.962	11.979	3001186	273.457	−31.7864	−108.1	0.7
18135005−3150289	273.458551	−31.841373	12.484	11.349	J181350.04−315028.89	273.458534	−31.841361	12.456	...	3000819	273.459	−31.8414	−14.8	0.8
18135009−3148543	273.458744	−31.815086	14.749	14.019	J181350.10−314854.27	273.458752	−31.815077	14.630	13.876	3000792	273.459	−31.8151	34.7	0.2
18135032−3147250	273.459703	−31.790287	12.583	11.597	J181350.33−314725.00	273.459713	−31.790278	12.519	11.590	3001163	273.460	−31.7903	75.5	0.6
18135050−3145416	273.460455	−31.761564	10.864	9.548	J181350.50−314541.69	273.460443	−31.761582	10.816	9.625	3001873	273.460	−31.7616	−18.7	0.7
18135051−3151104	273.460486	−31.852898	14.346	13.571	J181350.51−315110.44	273.460478	−31.852901	14.210	13.586	3000998	273.460	−31.8529	−75.0	0.8
18135060−3143572	273.460856	−31.732569	11.522	10.279	J181350.60−314357.27	273.460865	−31.732577	11.213	10.048	3003063	273.461	−31.7326	−136.2	0.8
18135071−3147443	273.461322	−31.795643	13.857	12.981	J181350.72−314744.23	273.461339	−31.795622	13.816	12.925	3001089	273.461	−31.7956	−109.9	0.9
18135082−3151337	273.461756	−31.859377	13.551	12.672	J181350.82−315133.74	273.461754	−31.859373	13.497	12.695	3001134	273.462	−31.8594	69.7	0.7
18135085−3159564	273.461882	−31.999016	12.776	11.638	J181350.85−315956.35	273.461889	−31.998989	12.676	11.622	3008248	273.462	−31.9990	22.1	0.7
18135109−3146412	273.462910	−31.778112	12.736	11.814	J181351.10−314641.19	273.462929	−31.778109	12.690	11.843	3001457	273.463	−31.7781	−66.2	0.7
18135120−3153168	273.463337	−31.888021	12.506	11.566	...	...	...	...	...	3001821	273.463	−31.8880	−5.6	0.8
18135131−3148581	273.463794	−31.816149	13.711	12.875	J181351.29−314858.12	273.463717	−31.816145	13.779	13.050	3000886	273.464	−31.8161	−206.9	0.9
18135150−3147178	273.464622	−31.788301	12.802	11.759	J181351.51−314717.92	273.464636	−31.788311	12.732	11.715	3001274	273.465	−31.7883	−25.0	0.7
18135153−3148035	273.464720	−31.800983	14.761	13.958	J181351.52−314803.12	273.464684	−31.800867	15.084	14.086	3001076	273.465	−31.8010	5.8	0.1
18135162−3150578	273.465088	−31.849413	14.004	13.182	J181351.62−315057.80	273.465092	−31.849392	14.042	13.262	3001047	273.465	−31.8494	200.6	0.7
18135171−3158578	273.465463	−31.982746	12.653	11.586	J181351.71−315857.84	273.465459	−31.982734	12.583	11.582	3006958	273.465	−31.9827	128.8	0.8
18135175−3149497	273.465659	−31.830482	13.930	13.063	J181351.76−314949.73	273.465667	−31.830481	13.893	13.116	3000903	273.466	−31.8305	11.1	0.7
18135199−3148336	273.466626	−31.809341	13.374	12.463	...	...	...	...	...	3001017	273.467	−31.8093	−178.3	0.7
18135204−3146325	273.466864	−31.775717	14.153	13.241	J181352.04−314632.58	273.466875	−31.775718	14.118	13.206	3001597	273.467	−31.7757	14.1	0.7
18135236−3148151	273.468206	−31.804222	13.847	12.974	J181352.36−314815.20	273.468208	−31.804223	13.782	12.948	3001105	273.468	−31.8042	42.0	0.6
18135236−3148435	273.468191	−31.812094	13.053	12.122	J181352.37−314843.51	273.468214	−31.812088	12.997	12.149	3001029	273.468	−31.8121	−65.8	0.7
18135237−3150260	273.468236	−31.840578	13.740	12.795	J181352.37−315026.01	273.468232	−31.840559	13.690	12.804	3001028	273.468	−31.8406	−81.0	0.7
18135252−3149103	273.468872	−31.819546	12.010	10.959	J181352.52−314910.32	273.468870	−31.819536	11.975	10.863	3000993	273.469	−31.8195	34.4	0.6
18135280−3152221	273.470034	−31.872814	13.898	12.949	J181352.80−315222.06	273.470032	−31.872797	...	12.912	3001551	273.470	−31.8728	9.5	0.8
18135297−3151069	273.470712	−31.851921	14.017	13.109	J181352.97−315106.91	273.470724	−31.851920	13.974	13.084	3001202	273.471	−31.8519	18.5	0.8
18135299−3142460	273.470831	−31.712784	10.587	9.266	J181352.99−314246.08	273.470828	−31.712802	10.612	9.371	3004260	273.471	−31.7128	−173.6	0.9
18135310−3150133	273.471251	−31.837029	9.595	8.191	J181353.09−315013.33	273.471237	−31.837036	9.597	8.235	3001072	273.471	−31.8370	23.2	1.0
18135317−3150533	273.471566	−31.848145	13.849	12.914	J181353.17−315053.25	273.471583	−31.848127	13.805	12.893	3001176	273.472	−31.8481	32.3	0.7
18135328−3148317	273.472000	−31.808817	13.860	12.990	...	...	...	...	...	3001147	273.472	−31.8088	−6.2	0.8
18135331−3143527	273.472127	−31.731318	12.352	11.266	J181353.31−314352.74	273.472132	−31.731317	12.290	11.263	3003337	273.472	−31.7313	183.5	0.6
18135343−3150178	273.472641	−31.838284	13.600	12.740	J181353.43−315017.83	273.472655	−31.838287	13.605	12.800	3001113	273.473	−31.8383	−18.9	0.7
18135354−3149281	273.473105	−31.824497	14.695	13.743	J181353.54−314928.13	273.473108	−31.824482	14.597	13.845	3001087	273.473	−31.8245	−168.3	1.5
18135360−3147010	273.473368	−31.783628	13.780	12.806	J181353.60−314701.02	273.473368	−31.783619	13.683	12.804	3001541	273.473	−31.7836	30.0	0.8
18135363−3157141	273.473466	−31.953920	12.710	11.651	J181353.63−315714.08	273.473468	−31.953912	12.614	11.634	3005133	273.473	−31.9539	85.0	0.6
18135369−3147381[a]	273.473741	−31.793930	12.461	11.346	J181353.70−314738.13	273.473754	−31.793926	12.394	11.341	3001352	273.474	−31.7939	−131.9	0.8
18135384−3200166	273.474353	−32.004631	12.761	11.719	J181353.84−320016.56	273.474355	−32.004601	12.664	11.696	3008997	273.474	−32.0046	17.7	1.1
18135387−3200241	273.474487	−32.006702	10.837	9.709	J181353.87−320024.00	273.474475	−32.006667	10.747	9.637	3009225	273.474	−32.0067	−102.5	0.6
18135389−3147140	273.474550	−31.787226	12.690	11.699	J181353.89−314714.05	273.474544	−31.787237	12.684	11.710	3001490	273.475	−31.7872	103.9	0.6
18135408−3140411	273.475353	−31.678108	12.502	11.421	J181354.08−314041.27	273.475340	−31.678132	12.490	11.454	3006568	273.475	−31.6781	−8.8	0.8
18135415−3147563	273.475652	−31.798973	13.623	12.610	J181354.15−314756.38	273.475636	−31.798997	13.554	12.606	3001316	273.476	−31.7990	−70.2	0.6
18135420−3148560	273.475839	−31.815571	13.305	12.416	J181354.21−314856.01	273.475889	−31.815561	13.348	12.545	3001180	273.476	−31.8156	63.7	0.6
18135440−3151134	273.476670	−31.853743	10.591	9.238	J181354.39−315113.39	273.476655	−31.853722	10.522	9.218	3001340	273.477	−31.8537	213.3	0.8

Table 3—Continued

Star Name (2MASS)	RA (J2000)	DEC (J2000)	J (mag)	K_S (mag)	Star Name (VVV)	RA (J2000)	DEC (J2000)	J (mag)	K_S (mag)	Star Name (VLT)	RA (J2000)	DEC (J2000)	$RV_{helio.}$ (km s^{-1})	RV Error (km s^{-1})
18135450−3148200	273.477106	−31.805578	14.435	13.570	J181354.50−314820.05	273.477114	−31.805571	14.365	13.527	3001286	273.477	−31.8056	−159.5	0.8
18135466−3149382	273.477789	−31.827288	11.390	10.324	J181354.67−314938.19	273.477797	−31.827276	11.378	10.302	3001196	273.478	−31.8273	−101.5	0.7
18135468−3143545	273.477868	−31.731821	11.827	10.651	J181354.68−314354.58	273.477870	−31.731829	11.828	10.712	3003426	273.478	−31.7318	189.3	0.7
18135469−3157032	273.477905	−31.950909	12.330	11.207	J181354.69−315703.29	273.477893	−31.950916	12.277	11.217	3005052	273.478	−31.9509	−11.7	0.6
18135491−3151546	273.478804	−31.865173	11.781	10.536	J181354.90−315154.56	273.478788	−31.865157	11.793	10.453	3001587	273.479	−31.8652	−131.6	0.8
18135495−3147274	273.478971	−31.790962	14.910	14.066	J181354.94−314727.37	273.478948	−31.790939	14.813	14.108	3001528	273.479	−31.7909	−93.8	0.3
18135497−3151156	273.479044	−31.854343	14.177	13.275	J181354.97−315115.54	273.479050	−31.854318	14.141	13.273	3001408	273.479	−31.8543	−176.3	0.8
18135518−3142270	273.479935	−31.707525	11.299	10.049	J181355.19−314227.11	273.479962	−31.707533	11.306	10.166	3004743	273.480	−31.7075	−17.6	0.8
18135520−3151318	273.480021	−31.858849	13.616	12.633	J181355.20−315131.76	273.480023	−31.858824	13.596	12.650	3001497	273.480	−31.8588	68.9	0.8
18135528−3141373	273.480338	−31.693714	13.752	12.775	J181355.27−314137.44	273.480315	−31.693736	13.667	12.731	RGB.200102688	273.480	−31.6937	40.1	0.2
18135540−3150513	273.480856	−31.847601	12.233	11.246	J181355.40−315051.22	273.480861	−31.847562	12.201	11.226	3001368	273.481	−31.8476	49.1	0.6
18135552−3150214	273.481338	−31.839304	14.993	14.429	J181355.53−315021.37	273.481376	−31.839270	14.890	14.417	3001305	273.481	−31.8393	2.7	1.2
18135569−3146192	273.482070	−31.772007	12.724	11.722	J181355.69−314619.26	273.482073	−31.772017	12.685	11.717	3002033	273.482	−31.7720	48.4	0.8
18135585−3148370	273.482717	−31.810303	14.173	13.260	...	...	...	...	...	3001369	273.483	−31.8103	74.5	0.7
18135596−3154384	273.483186	−31.910667	14.676	13.884	J181355.96−315438.51	273.483198	−31.910699	14.690	13.891	RGB.100129452	273.483	−31.9107	−29.1	6.1
18135603−3147456	273.483499	−31.796000	13.371	12.459	J181356.03−314745.57	273.483483	−31.795992	13.335	12.410	3001563	273.483	−31.7960	43.0	0.6
18135645−3138348	273.485215	−31.643024	12.921	11.859	J181356.45−313834.91	273.485221	−31.643033	12.926	11.850	3009809	273.485	−31.6430	124.2	0.9
18135674−3146303	273.486455	−31.775110	12.580	11.547	...	...	...	...	...	3002056	273.486	−31.7751	64.2	0.6
18135681−3149336	273.486711	−31.826008	14.030	13.139	...	...	...	...	...	3001411	273.487	−31.8260	179.8	0.8
18135689−3148308	273.487045	−31.808575	12.884	11.840	J181356.88−314830.88	273.487040	−31.808580	12.836	11.818	3001494	273.487	−31.8086	64.9	0.6
18135695−3151479	273.487330	−31.863327	10.489	9.140	J181356.95−315147.94	273.487326	−31.863317	10.451	9.080	3001769	273.487	−31.8633	−171.6	0.8
18135714−3159368	273.488121	−31.993561	11.289	10.226	J181357.15−315936.66	273.488131	−31.993517	11.247	10.208	3008390	273.488	−31.9936	69.0	0.6
18135723−3148416	273.488467	−31.811571	14.517	13.588	J181357.23−314841.69	273.488488	−31.811581	14.384	13.537	3001516	273.488	−31.8116	24.8	0.1
18135738−3148179	273.489094	−31.804981	12.702	11.563	J181357.38−314817.95	273.489096	−31.804986	12.621	11.557	3001598	273.489	−31.8050	41.9	0.7
18135859−3158102	273.494133	−31.969509	15.048	14.241	J181358.59−315810.07	273.494150	−31.969465	14.991	14.302	RHB.100132136	273.494	−31.9695	−84.1	0.3
18135863−3150538[a]	273.494319	−31.848305	12.464	11.410	J181358.63−315053.81	273.494330	−31.848282	12.408	11.422	3001748	273.494	−31.8483	−134.7	0.8
18135922−3149274	273.496779	−31.824280	12.638	11.492	J181359.22−314927.41	273.496780	−31.824282	...	11.499	3001706	273.497	−31.8243	−5.6	0.7
18140032−3147248	273.501372	−31.790224	14.317	11.407	J181400.32−314724.77	273.501352	−31.790216	14.277	13.384	RGB.200113808	273.501	−31.7902	−68.3	0.5
18140033−3146106	273.501386	−31.769634	12.451	11.401	J181400.33−314610.74	273.501403	−31.769652	12.418	11.399	3002657	273.501	−31.7696	−122.2	0.7
18140093−3158080	273.503884	−31.968908	12.907	11.934	J181400.93−315807.93	273.503886	−31.968872	12.845	11.918	3006932	273.504	−31.9689	6.2	0.6
18140106−3144161	273.504436	−31.737829	12.086	11.030	...	...	...	...	...	3003899	273.504	−31.7378	−118.1	0.6
18140122−3144040	273.505105	−31.734465	10.113	8.706	J181401.22−314404.14	273.505099	−31.734485	10.183	8.823	3004074	273.505	−31.7344	−83.9	0.5
18140151−3143379	273.506309	−31.727198	12.807	11.760	J181401.51−314337.93	273.506322	−31.727205	12.738	11.725	RGB.200116438	273.506	−31.7272	−76.4	0.4
18140155−3149117	273.506481	−31.819918	12.681	11.563	J181401.55−314911.72	273.506469	−31.819925	12.595	11.561	3002023	273.506	−31.8199	−84.3	0.8
18140285−3200163	273.511890	−32.004555	12.700	11.748	J181402.85−320016.41	273.511915	−32.004561	12.647	11.732	3010168	273.512	−32.0046	−134.9	0.7
18140311−3147345	273.512993	−31.792933	12.030	11.006	J181403.12−314734.59	273.513012	−31.792942	12.004	11.030	3002537	273.513	−31.7929	−82.4	0.6
18140372−3145078	273.515531	−31.752169	14.425	13.470	...	...	...	...	...	RGB.200121028	273.515	−31.7522	45.9	0.1
18140375−3158078	273.515631	−31.968838	13.085	12.142	J181403.76−315808.27	273.515693	−31.968966	13.527	12.346	RGB.100136147	273.516	−31.9690	9.3	0.4
18140399−3147578	273.516649	−31.799389	10.288	8.938	J181403.98−314757.82	273.516622	−31.799395	10.206	8.956	3002572	273.517	−31.7994	9.3	0.8
18140418−3146415	273.517446	−31.778215	15.098	14.316	J181404.18−314641.63	273.517455	−31.778232	15.034	14.203	RGB.200121997	273.517	−31.7782	−82.8	0.3
18140420−3144046	273.517516	−31.734615	13.956	12.986	J181404.20−314404.71	273.517534	−31.734643	13.938	13.013	RGB.200122096	273.518	−31.7346	57.6	0.5
18140434−3154474	273.518087	−31.913168	12.916	11.865	J181404.34−315447.38	273.518085	−31.913162	12.858	11.860	3004306	273.518	−31.9132	16.0	0.7
18140496−3149340	273.520667	−31.826120	12.580	11.532	...	...	...	...	...	3002543	273.521	−31.8261	−67.4	0.8
18140502−3157025	273.520920	−31.950699	14.870	14.018	J181405.02−315702.53	273.520931	−31.950705	14.796	13.998	RGB.100136833	273.521	−31.9507	31.7	0.2
18140524−3157457	273.521834	−31.962715	11.306	10.046	J181405.23−315745.77	273.521832	−31.962714	11.255	10.093	3007144	273.522	−31.9627	−10.0	0.8
18140555−3144003	273.523133	−31.733423	12.874	11.783	J181405.55−314400.36	273.523138	−31.733434	12.788	11.746	3004767	273.523	−31.7334	−146.3	0.7
18140582−3147564	273.524250	−31.799021	12.438	11.391	J181405.82−314756.43	273.524270	−31.799011	12.401	11.350	3002883	273.524	−31.7990	−119.3	0.8
18140620−3156397	273.525854	−31.944372	11.782	10.732	J181406.20−315639.71	273.525854	−31.944366	11.732	10.712	3006160	273.526	−31.9444	−116.7	0.7
18140644−3146380	273.526860	−31.777246	11.486	10.298	J181406.44−314638.18	273.526866	−31.777273	11.493	10.258	3003404	273.527	−31.7772	−192.6	0.9
18140675−3154075	273.528128	−31.902084	12.139	11.034	J181406.75−315407.51	273.528128	−31.902088	12.080	11.084	3004269	273.528	−31.9021	29.5	0.6

Table 3—Continued

Star Name (2MASS)	RA (J2000)	DEC (J2000)	J (mag)	K_S (mag)	Star Name (VVV)	RA (J2000)	DEC (J2000)	J (mag)	K_S (mag)	Star Name (VLT)	RA (J2000)	DEC (J2000)	$RV_{helio.}$ (km s^{-1})	RV Error (km s^{-1})
18140685−3152296	273.528543	−31.874910	12.776	11.763	J181406.84−315229.65	273.528535	−31.874904	12.686	11.738	3003445	273.529	−31.8749	68.9	0.7
18140690−3152398	273.528756	−31.877747	14.441	13.541	J181406.89−315239.82	273.528749	−31.877730	14.341	13.505	RGB.200127337	273.529	−31.8777	19.0	0.2
18140696−3151578	273.529023	−31.866056	13.207	12.143	...	...	...	...	...	RGB.200127514	273.529	−31.8661	−26.8	0.2
18140735−3153369	273.530664	−31.893599	12.570	11.626	J181407.35−315336.94	273.530663	−31.893597	12.529	11.669	3004061	273.531	−31.8936	−95.0	0.6
18140801−3154303	273.533415	−31.908421	12.909	12.012	J181408.02−315430.36	273.533438	−31.908436	12.860	12.002	3004703	273.533	−31.9084	−6.1	0.6
18140842−3156266	273.535109	−31.940744	12.348	11.168	J181408.42−315626.70	273.535099	−31.940752	12.254	11.146	3006328	273.535	−31.9407	219.6	0.7
18140848−3154161	273.535334	−31.904486	11.602	10.416	J181408.47−315416.12	273.535328	−31.904479	11.491	10.345	3004629	273.535	−31.9045	174.3	0.6
18140851−3152190	273.535476	−31.871948	9.754	8.396	...	...	...	...	...	3003669	273.535	−31.8719	22.0	0.8
18140861−3157319	273.535904	−31.958885	10.032	8.673	J181408.61−315732.03	273.535914	−31.958899	10.026	8.857	3007479	273.536	−31.9589	199.0	0.8
18140883−3147081	273.536833	−31.785604	12.764	11.714	J181408.83−314708.25	273.536827	−31.785627	12.671	11.671	3003626	273.537	−31.7856	47.1	0.6
18140893−3149054	273.537212	−31.818180	14.181	13.332	J181408.93−314905.44	273.537234	−31.818178	14.195	13.319	RGB.200131319	273.537	−31.8182	3.8	0.7
18140903−3152471	273.537655	−31.879774	10.984	9.799	...	...	...	...	...	3003950	273.538	−31.8797	194.7	0.7
18140935−3159176	273.538990	−31.988230	12.959	11.941	J181409.35−315917.56	273.538995	−31.988213	12.876	11.935	3009880	273.539	−31.9882	−10.6	0.6
18140952−3151092	273.539698	−31.852560	14.854	14.004	...	...	...	...	...	RGB.200132332	273.540	−31.8526	−105.6	0.3
18140953−3150390	273.539736	−31.844172	12.727	11.805	...	...	...	...	...	3003428	273.540	−31.8442	−66.8	0.8
18140955−3149327	273.539827	−31.825762	15.084	14.247	J181409.56−314932.67	273.539850	−31.825742	14.972	14.159	RGB.200132450	273.540	−31.8257	3.4	0.4
18140983−3143230	273.540972	−31.723059	14.304	13.349	J181409.83−314323.12	273.540974	−31.723090	14.203	13.303	RGB.200133077	273.541	−31.7231	−97.0	0.2
18140989−3155350	273.541219	−31.926414	11.622	10.532	J181409.89−315535.11	273.541225	−31.926421	11.586	10.577	3005865	273.541	−31.9264	165.8	0.6
18141005−3145075	273.541889	−31.752087	14.492	13.678	J181410.05−314507.62	273.541903	−31.752117	14.469	13.624	RGB.200133437	273.542	−31.7521	20.9	2.3
18141081−3151392	273.545062	−31.860907	10.990	9.719	J181410.81−315139.20	273.545068	−31.860892	10.852	9.646	3003890	273.545	−31.8609	78.8	0.8
18141090−3156244	273.545426	−31.940126	12.834	11.828	J181410.89−315624.53	273.545385	−31.940148	12.747	11.790	3006791	273.545	−31.9401	−74.8	0.6
18141145−3151104	273.547729	−31.852905	11.256	9.996	J181411.45−315110.40	273.547745	−31.852891	11.216	9.953	3003896	273.548	−31.8529	26.4	0.8
18141172−3145282	273.548850	−31.757845	12.083	10.962	J181411.72−314528.23	273.548870	−31.757844	12.033	10.949	3004952	273.549	−31.7578	9.3	0.7
18141175−3153176	273.548988	−31.888243	12.898	11.881	...	...	...	...	...	3004704	273.549	−31.8882	−142.5	0.7
18141185−3147073	273.549377	−31.785376	12.965	11.983	J181411.85−314707.32	273.549376	−31.785367	12.845	11.943	3004232	273.549	−31.7854	−5.8	0.7
18141200−3149398	273.550041	−31.827723	12.711	11.778	J181412.01−314939.75	273.550046	−31.827710	12.665	11.781	3003839	273.550	−31.8277	−79.5	0.6
18141203−3155396	273.550148	−31.927675	10.474	9.168	J181412.03−315539.73	273.550143	−31.927703	10.478	9.225	3006333	273.550	−31.9277	48.0	0.7
18141258−3145039	273.552452	−31.751099	13.869	12.946	J181412.58−314503.99	273.552424	−31.751110	13.751	12.840	RGB.200138096	273.552	−31.7511	87.3	0.2
18141265−3147403	273.552723	−31.794538	12.968	12.040	J181412.65−314740.32	273.552745	−31.794534	12.918	11.986	3004233	273.553	−31.7945	−106.6	0.7
18141277−3144438	273.553229	−31.745523	11.440	10.187	J181412.77−314443.95	273.553215	−31.745544	11.415	10.193	3005612	273.553	−31.7455	35.7	0.6
18141281−3144369	273.553411	−31.743584	12.721	11.569	J181412.82−314436.98	273.553432	−31.743607	12.682	11.522	3005690	273.553	−31.7436	−122.1	0.8
18141313−3152596	273.554725	−31.883224	12.879	11.936	J181413.13−315259.66	273.554744	−31.883240	12.838	11.952	3004868	273.555	−31.8832	−98.1	0.6
18141352−3154119	273.556355	−31.903328	14.525	13.566	...	...	...	...	...	RGB.200139483	273.556	−31.9034	127.9	0.5
18141376−3147556	273.557367	−31.798794	12.161	10.989	J181413.77−314755.71	273.557382	−31.798810	12.103	10.967	3004394	273.557	−31.7988	20.8	0.7
18141455−3148309	273.560642	−31.808603	12.938	11.883	J181414.55−314831.02	273.560648	−31.808618	12.855	11.852	3004443	273.561	−31.8086	61.6	0.7
18141466−3147157	273.561110	−31.787708	11.308	10.026	J181414.66−314715.77	273.561100	−31.787716	11.394	10.169	3004763	273.561	−31.7877	4.0	0.8
18141530−3152108	273.563782	−31.869684	9.658	8.266	J181415.31−315210.94	273.563811	−31.869707	9.620	8.334	3005019	273.564	−31.8697	−83.1	0.9
18141536−3149119	273.564001	−31.819984	12.602	11.531	J181415.36−314911.98	273.564037	−31.819997	12.533	11.505	RGB.200142492	273.564	−31.8200	−106.6	0.2
18141536−3149119	273.564001	−31.819984	12.602	11.531	J181415.36−314911.98	273.564037	−31.819997	12.533	11.505	3004544	273.564	−31.8200	−106.8	0.7
18141603−3143218	273.566798	−31.722740	14.595	13.729	J181416.03−314321.89	273.566804	−31.722748	14.556	13.700	RGB.200143651	273.567	−31.7227	7.1	0.7
18141608−3152455	273.567005	−31.879316	12.428	11.329	J181416.08−315245.59	273.567009	−31.879332	12.368	11.347	3005423	273.567	−31.8793	−23.4	0.8
18141608−3152455	273.567005	−31.879316	12.428	11.329	...	...	...	...	...	RGB.200143543	273.567	−31.8794	−21.7	0.2
18141622−3151415	273.567619	−31.861542	11.889	10.676	J181416.22−315141.51	273.567619	−31.861531	11.821	10.582	3005073	273.568	−31.8615	−28.0	0.8
18141647−3152094	273.568632	−31.869301	11.711	10.602	J181416.47−315209.47	273.568642	−31.869299	11.620	10.472	3005285	273.569	−31.8693	−80.8	0.7
18141648−3147218	273.568680	−31.789413	11.582	10.410	J181416.48−314721.92	273.568686	−31.789422	11.564	10.456	3005164	273.569	−31.7894	−99.1	0.8
18141651−3142274	273.568810	−31.707615	11.843	10.775	J181416.51−314227.45	273.568832	−31.707626	11.840	10.857	3008336	273.569	−31.7076	117.5	0.6
18141664−3147496	273.569372	−31.797129	9.491	8.027	J181416.64−314749.66	273.569357	−31.797129	9.473	8.230	3005086	273.569	−31.7971	168.6	1.0
18141695−3147546	273.570629	−31.798519	12.048	10.882	J181416.95−314754.67	273.570633	−31.798521	11.989	10.873	3005130	273.571	−31.7985	136.0	0.4
18141700−3145594	273.570836	−31.766520	14.017	13.057	J181417.00−314559.46	273.570850	−31.766518	13.931	13.038	RGB.200145001	273.571	−31.7665	−88.2	1.6
18141701−3147325	273.570914	−31.792381	12.323	11.219	J181417.02−314732.58	273.570958	−31.792384	12.268	11.165	3005237	273.571	−31.7924	−117.1	0.7

Table 3—Continued

Star Name (2MASS)	RA (J2000)	DEC (J2000)	J (mag)	K_S (mag)	Star Name (VVV)	RA (J2000)	DEC (J2000)	J (mag)	K_S (mag)	Star Name (VLT)	RA (J2000)	DEC (J2000)	$RV_{helio.}$ (km s^{-1})	RV Error (km s^{-1})
18141796−3148492	273.574856	−31.813683	12.481	11.426	J181417.96−314849.12	273.574860	−31.813647	12.410	11.399	3005221	273.575	−31.8137	−104.5	0.8
18141799−3143289	273.574984	−31.724697	14.346	13.433	J181418.00−314328.97	273.575009	−31.724716	14.286	13.418	RGB.200146348	273.575	−31.7247	62.1	0.7
18141883−3150426	273.578464	−31.845194	14.387	13.645	J181418.82−315042.54	273.578457	−31.845152	14.341	13.511	RGB.200147285	273.578	−31.8452	38.7	0.2
18142006−3144453	273.583621	−31.745918	14.493	13.812	J181420.07−314445.31	273.583626	−31.745921	14.455	13.604	RGB.200148951	273.584	−31.7459	31.6	0.3
18142014−3148507	273.583920	−31.814087	13.030	12.020	...	...	...	...	...	RGB.200148963	273.584	−31.8141	−155.7	0.8
18142065−3151095	273.586065	−31.852648	11.018	9.767	J181420.65−315109.48	273.586061	−31.852635	10.945	9.637	3005992	273.586	−31.8526	16.9	0.8
18142099−3147557	273.587480	−31.798809	14.064	13.058	J181420.99−314755.64	273.587474	−31.798791	14.006	13.101	RGB.200149920	273.587	−31.7988	−0.1	0.3
18142153−3151580	273.589718	−31.866133	9.465	8.124	J181421.52−315158.04	273.589708	−31.866124	11.223	...	3006433	273.590	−31.8661	38.8	0.8
18142198−3151040	273.591602	−31.851118	14.736	13.850	J181421.98−315103.97	273.591607	−31.851105	14.674	13.830	RGB.200150923	273.592	−31.8511	60.3	0.3
18142225−3149008	273.592712	−31.816914	10.294	8.973	J181422.25−314900.81	273.592713	−31.816893	11.116	8.951	3006256	273.593	−31.8169	225.3	0.8
18142408−3150463	273.600374	−31.846203	11.879	10.692	J181424.09−315046.23	273.600379	−31.846175	11.884	10.779	3006845	273.600	−31.8462	138.9	0.7
18142413−3149313	273.600551	−31.825369	14.231	13.339	J181424.13−314931.26	273.600559	−31.825353	14.151	13.288	RGB.200153033	273.601	−31.8254	31.7	0.4
18142492−3147524	273.603835	−31.797895	12.765	11.673	J181424.91−314752.39	273.603827	−31.797887	12.695	11.629	3007177	273.604	−31.7979	−27.6	0.7
18142543−3145557	273.605968	−31.765493	13.290	12.384	...	...	...	...	...	RGB.200154159	273.606	−31.7656	−138.4	1.3
18142763−3144215	273.615136	−31.739311	13.629	12.647	J181427.63−314421.51	273.615138	−31.739309	13.560	12.652	RGB.200155802	273.615	−31.7393	19.7	0.2
18142775−3152133	273.615651	−31.870363	11.682	10.618	J181427.75−315213.26	273.615657	−31.870352	11.646	10.652	3008324	273.616	−31.8704	−14.2	0.6
18142861−3152397	273.619218	−31.877714	12.252	11.197	J181428.61−315239.76	273.619222	−31.877713	12.195	11.159	3008774	273.619	−31.8777	45.0	0.8
18142892−3147372	273.620519	−31.793684	14.628	13.828	J181428.92−314737.30	273.620530	−31.793696	14.548	13.722	RGB.200156566	273.621	−31.7937	116.4	0.3
18142962−3147549	273.623457	−31.798586	14.735	13.881	J181429.62−314754.88	273.623457	−31.798580	14.672	13.834	RGB.200156917	273.623	−31.7986	−254.5	0.5
18143030−3145260	273.626260	−31.757227	13.635	12.643	J181430.30−314525.98	273.626271	−31.757219	13.581	12.658	RGB.200157286	273.626	−31.7572	−20.5	0.3
...	...	...	...	...	J181419.20−315350.80	273.580011	−31.897446	9.801	8.494	3006703	273.580	−31.8974	−69.8	0.7
...	...	...	...	...	J181352.57−315609.75	273.469068	−31.936042	10.369	9.201	3003980	273.469	−31.9360	−145.7	0.7
...	...	...	...	...	J181336.83−315235.90	273.403470	−31.876639	11.098	9.907	3001048	273.403	−31.8766	78.7	0.8
...	...	...	...	...	J181311.95−315229.17	273.299832	−31.874770	11.722	10.755	3003280	273.300	−31.8747	34.7	0.6
...	...	...	...	...	J181334.07−314422.02	273.391985	−31.739451	11.962	10.958	3002369	273.392	−31.7394	−11.7	0.6
...	...	...	...	...	J181321.45−315520.91	273.339416	−31.922477	12.052	10.983	3003650	273.339	−31.9224	14.3	0.8
...	...	...	...	...	J181349.92−315446.66	273.458035	−31.912963	12.176	11.073	3002662	273.458	−31.9129	−15.9	0.7
...	...	...	...	...	J181320.79−315504.00	273.336646	−31.917780	12.203	11.204	3003509	273.337	−31.9177	−107.4	0.7
...	...	...	...	...	J181338.52−315854.31	273.410531	−31.981755	12.350	11.238	3006368	273.410	−31.9817	−4.7	0.7
...	...	...	...	...	J181337.94−320038.71	273.408111	−32.010756	12.437	11.374	3008865	273.408	−32.0107	89.2	0.7
...	...	...	...	...	J181400.19−314618.99	273.500813	−31.771944	12.412	11.493	3002578	273.501	−31.7719	−82.3	0.8
...	...	...	...	...	J181356.62−315055.39	273.485924	−31.848722	12.914	11.935	3001515	273.486	−31.8487	165.6	0.6
...	...	...	...	...	J181326.83−315143.33	273.361814	−31.862036	12.941	11.992	3001187	273.362	−31.8620	−151.1	0.7
...	...	...	...	...	J181352.75−314936.99	273.469831	−31.826944	12.947	11.998	3001008	273.470	−31.8269	−71.5	0.7
...	...	...	...	...	J181347.41−315206.02	273.447567	−31.868341	12.778	12.012	2000153	273.448	−31.8683	125.8	0.8
...	...	...	...	...	J181355.98−314741.60	273.483251	−31.794890	13.073	12.198	3001577	273.483	−31.7949	−94.0	0.8
...	...	...	...	...	J181333.14−315222.62	273.388113	−31.872951	13.873	13.010	3001049	273.388	−31.8729	−130.2	0.6
...	...	...	...	...	J181341.08−315142.31	273.421197	−31.861754	14.012	13.152	2000387	273.421	−31.8617	−89.7	0.7
...	...	...	...	...	J181334.47−314847.31	273.393649	−31.813143	14.126	13.217	2000394	273.394	−31.8131	73.1	0.8
...	...	...	...	...	J181338.15−315011.42	273.408992	−31.836506	14.082	13.355	1401512	273.409	−31.8365	99.8	0.8
...	...	...	...	...	J181330.05−315008.33	273.375208	−31.835649	14.209	13.356	2000453	273.375	−31.8356	−102.2	0.6
...	...	...	...	...	J181327.83−314802.63	273.365969	−31.800733	14.291	13.448	2000475	273.366	−31.8007	−21.2	0.8
...	...	...	...	...	J181335.82−314959.31	273.399282	−31.833143	14.372	13.599	2000489	273.399	−31.8331	93.6	0.7
...	...	...	...	...	J181257.19−315009.33	273.238307	−31.835927	14.507	13.658	RGB.100014399	273.238	−31.8359	19.5	0.1
...	...	...	...	...	J181324.86−315033.75	273.353589	−31.842708	14.494	13.659	3001094	273.354	−31.8427	156.8	0.7
...	...	...	...	...	J181336.79−313903.85	273.403297	−31.651072	14.594	13.738	RGB.200054310	273.403	−31.6511	−13.8	0.3
...	...	...	...	...	J181346.15−314846.20	273.442312	−31.812836	14.850	13.959	2000736	273.442	−31.8128	26.5	0.5
...	...	...	...	...	J181326.89−315615.28	273.362059	−31.937579	14.797	13.982	RGB.100076364	273.362	−31.9376	−18.4	0.3
...	...	...	...	...	J181345.19−315913.44	273.438315	−31.987067	14.823	14.086	RHB.100113086	273.438	−31.9871	−4.9	1.9
...	...	...	...	...	J181320.51−314528.50	273.335467	−31.757917	14.857	14.166	RHB.200015044	273.335	−31.7579	13.7	0.5

Table 3—Continued

Star Name (2MASS)	RA (J2000)	DEC (J2000)	J (mag)	K_S (mag)	Star Name (VVV)	RA (J2000)	DEC (J2000)	J (mag)	K_S (mag)	Star Name (VLT)	RA (J2000)	DEC (J2000)	$RV_{helio.}$ (km s^{-1})	RV Error (km s^{-1})
...	...	...	...	...	J181341.65−315915.47	273.423548	−31.987632	14.803	14.207	RHB.100106700	273.424	−31.9876	24.1	0.4
...	...	...	...	...	J181315.67−320010.06	273.315298	−32.002797	14.909	14.260	RHB.100051767	273.315	−32.0028	−10.2	0.4
...	...	...	...	...	...	...	...	...	...	RHB.100088307	273.385	−32.0261	10.1	0.5
...	...	...	...	...	...	...	...	...	...	RHB.100059569	273.330	−31.9922	40.2	0.4
...	...	...	...	...	...	...	...	...	...	3001297	273.445	−31.7733	−94.1	0.8
...	...	...	...	...	...	...	...	...	...	3001466	273.397	−31.7623	73.2	0.6
...	...	...	...	...	...	...	...	...	...	3001027	273.442	−31.7836	11.3	0.6
...	...	...	...	...	...	...	...	...	...	3003485	273.483	−31.7330	−115.1	0.8
...	...	...	...	...	...	...	...	...	...	2000222	273.448	−31.8070	2.4	0.7
...	...	...	...	...	...	...	...	...	...	2000234	273.450	−31.8107	15.7	0.8
...	...	...	...	...	...	...	...	...	...	3002309	273.483	−31.7632	−72.3	0.6
...	...	...	...	...	...	...	...	...	...	2000068	273.446	−31.8134	7.8	0.8
...	...	...	...	...	...	...	...	...	...	3001751	273.409	−31.8997	50.2	0.6
...	...	...	...	...	...	...	...	...	...	2000324	273.399	−31.8685	15.0	0.7
...	...	...	...	...	...	...	...	...	...	2000223	273.394	−31.8620	−230.8	0.9
...	...	...	...	...	...	...	...	...	...	2000162	273.381	−31.8058	11.2	0.7
...	...	...	...	...	...	...	...	...	...	3000941	273.405	−31.7797	−27.7	0.8
...	...	...	...	...	...	...	...	...	...	3002087	273.443	−31.7484	−142.0	0.7
...	...	...	...	...	...	...	...	...	...	2000312	273.450	−31.8124	109.7	3.2
...	...	...	...	...	...	...	...	...	...	3001231	273.445	−31.7769	63.2	0.7
...	...	...	...	...	...	...	...	...	...	1201122	273.426	−31.8251	−87.9	0.8
...	...	...	...	...	...	...	...	...	...	3003575	273.542	−31.8059	70.3	0.7
...	...	...	...	...	...	...	...	...	...	3001257	273.462	−31.8659	−70.7	0.7
...	...	...	...	...	...	...	...	...	...	3001331	273.454	−31.8761	−185.3	0.7
...	...	...	...	...	...	...	...	...	...	3006837	273.508	−31.9652	−12.6	0.7
...	...	...	...	...	...	...	...	...	...	3001310	273.433	−31.8842	−175.6	0.8
...	...	...	...	...	...	...	...	...	...	3003181	273.389	−31.9297	0.4	1.0
...	...	...	...	...	...	...	...	...	...	2000256	273.389	−31.8671	53.4	0.7
...	...	...	...	...	...	...	...	...	...	3001473	273.377	−31.8848	103.6	0.9
...	...	...	...	...	...	...	...	...	...	3001054	273.353	−31.8183	−186.5	0.8
...	...	...	...	...	...	...	...	...	...	3001565	273.336	−31.8038	102.0	1.0
...	...	...	...	...	...	...	...	...	...	3005240	273.266	−31.7622	93.0	0.6
...	...	...	...	...	...	...	...	...	...	3005295	273.426	−31.6869	−100.9	0.7
...	...	...	...	...	...	...	...	...	...	3000995	273.468	−31.8173	7.4	0.7
...	...	...	...	...	...	...	...	...	...	3007577	273.591	−31.9022	−26.9	0.8
...	...	...	...	...	...	...	...	...	...	3006280	273.398	−31.9802	−7.6	1.1
...	...	...	...	...	...	...	...	...	...	3002869	273.311	−31.8764	−248.1	0.8
...	...	...	...	...	...	...	...	...	...	3005488	273.262	−31.8911	67.8	0.6
...	...	...	...	...	...	...	...	...	...	3006229	273.256	−31.9037	−97.0	0.6
...	...	...	...	...	...	...	...	...	...	3001582	273.353	−31.7797	−94.1	0.9
...	...	...	...	...	...	...	...	...	...	2000596	273.405	−31.8679	−118.9	1.4

[a]Observed with both M2FS and FLAMES.

Note. — The first set of coordinates and photometry are on the 2MASS system, the second set are on the VVV system, and the third set of identifiers and coordinates are from the FLAMES image headers.

Table 4. M2FS RGB Cluster Member Model Atmosphere Parameters

Star Name (2MASS)	Star Name (VVV)	T_{eff} (K)	log(g) (cgs)	[Fe/H] (dex)	$\xi_{mic.}$ (km s^{-1})
18133083−3148103	J181330.83−314810.39	4075	0.75	−0.91	2.05
18133222−3147158	J181332.22−314715.86	4125	1.05	−0.96	1.70
18133324−3150194	J181333.24−315019.50	4225	1.45	−0.83	1.85
18133412−3148218	J181334.12−314821.82	4175	1.25	−0.85	1.65
18133417−3149571	J181334.17−314957.21	4325	1.15	−0.88	2.10
18133519−3149272	J181335.20−314927.26	4375	1.65	−0.90	2.00
18133584−3149447	···	4250	1.45	−0.94	2.10
18133610−3148112	J181336.10−314811.20	4250	1.20	−0.86	2.10
18133620−3149040	J181336.20−314904.09	4250	1.15	−0.94	2.00
18133678−3150244	J181336.78−315024.51	4225	1.45	−0.87	2.00
18133747−3149410	J181337.46−314941.16	4525	1.75	−0.80	1.90
18133789−3147295	J181337.89−314729.53	4100	1.00	−0.92	2.00
18133813−3145274	J181338.13−314527.31	4350	1.25	−0.75	2.10
18133819−3149224	J181338.19−314922.45	4150	1.25	−0.90	1.75
18134051−3150295	J181340.52−315029.57	4200	1.40	−0.86	1.85
18134089−3149095	J181340.89−314909.61	4100	1.15	−0.86	1.75
18134136−3150001	J181341.37−315000.19	4400	1.65	−0.88	1.85
18134151−3148556	J181341.50−314855.52	4225	1.25	−0.79	1.85
18134300−3150280	J181343.00−315028.01	4200	1.20	−0.87	1.95

Table 5. M2FS RGB Cluster Member Abundance Ratios and Uncertainties: Oxygen to Calcium

Star Name (2MASS)	Star Name (VVV)	[O/Fe] (dex)	Δ[O/Fe] (dex)	[Na/Fe] (dex)	Δ[Na/Fe] (dex)	[Mg/Fe] (dex)	Δ[Mg/Fe] (dex)	[Al/Fe] (dex)	Δ[Al/Fe] (dex)	[Si/Fe] (dex)	Δ[Si/Fe] (dex)	[Ca/Fe] (dex)	Δ[Ca/Fe] (dex)
18133083−3148103	J181330.83−314810.39	0.74	0.10	−0.03	0.05	0.43	0.06	0.42	0.08	0.39	0.11	0.07	0.05
18133222−3147158	J181332.22−314715.86	0.58	0.10	−0.10	0.05	0.54	0.05	0.40	0.07	0.28	0.10	0.30	0.07
18133324−3150194	J181333.24−315019.50	0.46	0.10	0.34	0.06	0.38	0.05	0.58	0.09	0.38	0.10	0.38	0.05
18133412−3148218	J181334.12−314821.82	0.02	0.10	0.40	0.06	0.34	0.06	0.58	0.10	0.32	0.09	0.23	0.06
18133417−3149571	J181334.17−314957.21	0.18	0.10	0.25	0.07	0.33	0.06	0.56	0.08	0.15	0.13	0.15	0.06
18133519−3149272	J181335.20−314927.26	0.83	0.10	0.09	0.05	0.36	0.06	0.55	0.07	0.37	0.10	0.25	0.06
18133584−3149447	···	···	···	0.22	0.08	0.31	0.05	0.41	0.08	0.46	0.14	0.21	0.07
18133610−3148112	J181336.10−314811.20	0.19	0.10	0.63	0.05	0.35	0.06	0.84	0.10	0.32	0.11	0.36	0.06
18133620−3149040	J181336.20−314904.09	···	···	−0.14	0.11	0.42	0.05	0.44	0.08	0.45	0.08	0.07	0.06
18133678−3150244	J181336.78−315024.51	···	···	0.30	0.09	0.35	0.06	0.47	0.08	0.42	0.09	0.22	0.06
18133747−3149410	J181337.46−314941.16	···	···	0.00	0.10	0.39	0.06	0.56	0.07	0.21	0.07	0.28	0.06
18133789−3147295	J181337.89−314729.53	···	···	−0.05	0.08	0.31	0.05	0.31	0.08	0.36	0.10	0.08	0.07
18133813−3145274	J181338.13−314527.31	···	···	0.36	0.06	0.52	0.05	0.91	0.14	0.22	0.12	0.42	0.06
18133819−3149224	J181338.19−314922.45	···	···	0.11	0.10	0.32	0.07	0.44	0.07	0.36	0.10	0.11	0.06
18134051−3150295	J181340.52−315029.57	···	···	0.14	0.07	0.40	0.05	0.58	0.08	0.38	0.09	0.16	0.07
18134089−3149095	J181340.89−314909.61	···	···	−0.01	0.10	0.53	0.05	0.46	0.07	0.48	0.07	0.16	0.06
18134136−3150001	J181341.37−315000.19	···	···	−0.13	0.06	0.59	0.05	0.46	0.08	0.44	0.10	0.21	0.06
18134151−3148556	J181341.50−314855.52	0.56	0.10	−0.02	0.06	0.35	0.05	0.46	0.08	0.27	0.07	0.17	0.06
18134300−3150280	J181343.00−315028.01	···	···	0.08	0.07	0.51	0.05	0.50	0.08	0.31	0.10	0.17	0.05

Table 6. M2FS RGB Cluster Member Abundance Ratios and Uncertainties: Chromium to Europium

Star Name (2MASS)	Star Name (VVV)	[Cr/Fe] (dex)	Δ[Cr/Fe] (dex)	[Fe I/H] (dex)	Δ[Fe I/H] (dex)	[Fe II/H] (dex)	Δ[Fe II/H] (dex)	[Ni/Fe] (dex)	Δ[Ni/Fe] (dex)	[La II/Fe] (dex)	Δ[La II/Fe] (dex)	[Eu II/Fe] (dex)	Δ[Eu II/Fe] (dex)
18133083−3148103	J181330.83−314810.39	−0.18	0.10	−0.94	0.10	−0.88	0.11	−0.08	0.08	0.18	0.11	0.37	0.11
18133222−3147158	J181332.22−314715.86	−0.12	0.07	−0.97	0.10	−0.95	0.12	−0.14	0.06	0.28	0.11	0.41	0.09
18133324−3150194	J181333.24−315019.50	0.09	0.11	−0.81	0.10	−0.84	0.13	−0.06	0.06	0.48	0.11	0.53	0.10
18133412−3148218	J181334.12−314821.82	−0.15	0.08	−0.85	0.10	−0.85	0.12	0.00	0.07	0.43	0.11	0.53	0.09
18133417−3149571	J181334.17−314957.21	−0.03	0.09	−0.88	0.10	−0.87	0.12	−0.14	0.06	0.29	0.11	0.43	0.12
18133519−3149272	J181335.20−314927.26	0.21	0.07	−0.88	0.10	−0.92	0.11	−0.06	0.06	0.52	0.12	0.55	0.09
18133584−3149447	···	0.01	0.07	−0.94	0.10	−0.94	0.12	−0.10	0.05	0.36	0.10	···	···
18133610−3148112	J181336.10−314811.20	0.30	0.09	−0.86	0.10	−0.85	0.13	−0.12	0.07	0.68	0.12	0.51	0.09
18133620−3149040	J181336.20−314904.09	−0.10	0.07	−0.94	0.10	−0.93	0.12	−0.10	0.09	0.27	0.11	0.47	0.09
18133678−3150244	J181336.78−315024.51	0.03	0.07	−0.87	0.10	−0.87	0.11	−0.04	0.06	0.52	0.11	0.47	0.09
18133747−3149410	J181337.46−314941.16	···	···	−0.77	0.10	−0.82	0.11	−0.20	0.05	0.62	0.12	0.88	0.09
18133789−3147295	J181337.89−314729.53	−0.27	0.07	−0.92	0.10	−0.91	0.12	−0.12	0.07	0.26	0.12	0.42	0.09
18133813−3145274	J181338.13−314527.31	···	···	−0.75	0.10	−0.75	0.12	−0.02	0.10	0.19	0.10	0.43	0.09
18133819−3149224	J181338.19−314922.45	−0.08	0.10	−0.90	0.10	−0.89	0.11	−0.08	0.10	0.27	0.10	0.52	0.09
18134051−3150295	J181340.52−315029.57	0.14	0.08	−0.83	0.10	−0.89	0.12	−0.05	0.05	0.53	0.10	···	···
18134089−3149095	J181340.89−314909.61	−0.06	0.10	−0.86	0.10	−0.85	0.12	−0.06	0.06	0.35	0.12	0.46	0.09
18134136−3150001	J181341.37−315000.19	0.17	0.10	−0.87	0.10	−0.89	0.12	−0.01	0.09	0.45	0.10	···	···
18134151−3148556	J181341.50−314855.52	0.09	0.07	−0.78	0.10	−0.79	0.11	−0.07	0.07	0.28	0.12	0.39	0.09
18134300−3150280	J181343.00−315028.01	0.26	0.08	−0.87	0.10	−0.86	0.13	−0.08	0.07	0.36	0.12	0.45	0.09

Table 7. FLAMES RGB and HB Calcium Triplet Metallicity Data for Cluster Members

Star Name (2MASS)	Star Name (VVV)	Star Name (VLT)	EW_{8542} (Å)	EW_{8662} (Å)	ΣEW (Å)	W′ (Å)	[Fe/H] (dex)	Δ[Fe/H] (dex)
18131138−3148128	J181311.39−314812.91	3002910	4.19	3.17	7.36	5.15	−0.70	0.01
18132157−3151036	J181321.57−315103.68	3001489	3.43	2.71	6.14	5.22	−0.63	0.27
18132381−3151202	J181323.81−315120.31	3001323	3.74	2.92	6.66	5.00	−0.82	0.08
18132416−3151095	···	3001259	3.58	2.60	6.17	5.31	−0.55	0.38
18132703−3150191	J181327.03−315019.17	3000849	3.30	2.52	5.82	4.92	−0.89	0.04
18132719−3155450	J181327.19−315545.14	3003469	3.81	2.89	6.70	4.58	−1.12	0.50
18132987−3147575	J181329.88−314757.53	2000503	3.11	2.42	5.53	4.82	−0.96	0.11
18132999−3150248	J181329.98−315024.90	2000789	2.93	2.14	5.07	4.65	−0.92	0.03
18133061−3150479	J181330.61−315048.09	2000151	3.48	2.69	6.17	4.90	−0.90	0.12
18133083−3148103	J181330.83−314810.39	2000042	3.83	2.94	6.77	4.89	−0.91	0.21
18133187−3150175	J181331.90−315017.56	2000707	3.09	2.44	5.53	5.03	−0.79	0.12
18133222−3147158	J181332.22−314715.86	3000888	3.88	2.91	6.79	5.22	−0.64	0.17
18133329−3146211	···	3001237	3.23	2.57	5.80	4.75	−1.01	0.22
18133354−3148257	J181333.54−314825.65	2000735	3.09	2.67	5.77	5.26	−0.70	0.22
18133365−3149030	J181333.65−314903.02	2000486	3.31	2.60	5.91	5.15	−0.70	0.20
18133419−3149168	J181334.17−314916.96	RHB.200046493	···	···	···	···	···	···
18133439−3147146	J181334.39−314714.64	3000816	2.99	2.40	5.39	4.90	−0.90	0.01
18133444−3149435	J181334.25−314943.33	2000412	3.15	2.34	5.50	5.21	−0.65	0.35
18133449−3151332	J181334.49−315133.27	2000606	3.12	2.73	5.85	5.20	−0.87	0.06
18133459−3147379	J181334.59−314737.98	2000135	3.61	2.65	6.26	4.96	−0.86	0.07
18133504−3148567	J181335.06−314856.77	RHB.200049021	···	···	···	···	···	···
18133550−3148442	J181335.50−314843.57	RHB.200050301	···	···	···	···	···	···
18133584−3149081	J181335.83−314908.37	2000784	3.11	2.56	5.67	5.15	−0.70	0.24
18133592−3146465	J181335.92−314646.53	3000968	3.83	2.84	6.67	5.18	−0.67	0.14
18133625−3153094	J181336.25−315309.54	3001304	3.07	2.55	5.61	4.95	−0.86	0.03
18133726−3146267	J181337.24−314626.87	3001104	3.05	2.52	5.57	5.08	−0.76	0.17
18133753−3151020	J181337.53−315102.16	1402137	···	···	···	···	···	···
18133789−3147295	J181337.89−314729.53	2000048	3.98	2.96	6.93	5.11	−0.73	0.02
18133813−3145274	J181338.13−314527.31	3001594	···	···	···	···	···	···
18133817−3149355	···	1101214	4.16	3.24	7.40	5.25	−0.60	0.13
18133818−3147243	J181338.19−314724.38	2000295	3.49	2.66	6.15	5.10	−0.74	0.11
18133820−3151145	J181338.20−315114.55	1402110	3.31	2.57	5.87	4.89	−0.91	0.08
18133827−3149413	···	1100865	4.04	3.06	7.10	5.03	−0.80	0.10
18133843−3150157	J181338.44−315015.87	1401475	3.08	2.47	5.55	4.90	−0.91	0.04
18133851−3151401	J181338.51−315140.18	2000595	3.27	2.50	5.77	5.11	−0.73	0.18
18133859−3149585	···	1401160	3.90	3.14	7.04	4.72	−1.03	0.43
18133863−3150077	J181338.63−315007.84	1401269	4.22	3.32	7.55	5.11	−0.74	0.08
18133865−3151050	J181338.66−315104.99	1401944	3.07	2.59	5.65	5.11	−0.70	0.23
18133867−3147435	J181338.67−314743.55	2000548	3.31	2.49	5.80	5.10	−0.74	0.17
18133884−3150488	···	1401759	3.30	2.48	5.78	4.76	−1.00	0.20
18133895−3148326	J181338.97−314832.34	1200710	2.71	2.27	4.98	4.62	−0.92	0.03
18133914−3150341	J181339.14−315034.26	1401485	3.08	2.24	5.32	4.84	−0.91	0.03
18133920−3147297	J181339.20−314729.71	2000575	3.01	2.32	5.33	4.73	−1.02	0.17
18133940−3150132	···	1401068	4.34	3.22	7.55	5.14	−0.70	0.04
18133967−3150152	···	1400994	4.32	3.20	7.52	5.33	−0.53	0.22
18133989−3148580	···	1200629	3.30	2.56	5.86	5.14	−0.71	0.20
18134008−3149023	···	1200659	3.37	2.63	6.00	5.29	−0.71	0.18
18134010−3151232	J181340.10−315123.24	2000364	3.17	2.55	5.72	4.82	−0.96	0.13
18134025−3149477	J181340.25−314947.76	1400288	4.17	3.18	7.35	5.18	−0.67	0.04
18134027−3147004	J181340.27−314700.40	3000839	4.16	3.12	7.27	5.34	−0.53	0.26

Table 7—Continued

Star Name (2MASS)	Star Name (VVV)	Star Name (VLT)	EW_{8542} (Å)	EW_{8662} (Å)	ΣEW (Å)	W′ (Å)	[Fe/H] (dex)	Δ[Fe/H] (dex)
18134028−3148398	J181340.27−314839.83	1201183	...	...	...	...	...	...
18134035−3151076	...	1401524	3.28	2.57	5.84	4.81	−0.97	0.16
18134042−3149401	J181340.41−314940.17	1100182	4.26	3.21	7.47	5.24	−0.62	0.10
18134095−3150365	J181340.95−315036.62	1400828	3.85	3.09	6.94	4.56	−1.13	0.56
18134095−3150478	J181340.92−315047.91	1401013	3.09	2.50	5.60	5.17	−0.89	0.03
18134124−3148156	...	2000628	2.97	2.46	5.43	4.53	−0.99	0.14
18134133−3148374	J181341.33−314837.50	1201513	3.37	2.60	5.98	4.96	−0.86	0.03
18134145−3148318	...	1201617	3.34	2.54	5.88	4.95	−0.87	0.03
18134202−3151202	J181342.02−315120.31	2000623	3.07	2.38	5.45	4.83	−0.95	0.09
18134207−3149041	J181342.07−314904.22	1201418	3.30	2.63	5.93	5.40	−0.71	0.19
18134218−3148191	J181342.17−314819.16	1201884	3.44	2.68	6.13	5.15	−0.70	0.18
18134302−3150431	J181343.02−315043.15	1400043	3.26	2.63	5.89	4.81	−0.97	0.17
18134306−3150091	J181343.06−315009.19	1300949	4.15	3.16	7.31	4.92	−0.89	0.25
18134315−3152167	J181343.15−315216.77	3000949	3.26	2.67	5.93	5.00	−0.82	0.03
18134318−3149121	...	1201631	3.35	2.60	5.96	4.85	−0.94	0.14
18134352−3148584	...	1201846	4.08	3.10	7.18	5.10	−0.74	0.04
18134370−3150080	J181343.70−315008.10	1300986	3.21	2.49	5.70	4.93	−0.88	0.02
18134393−3149397	J181343.92−314939.89	1300460	2.76	2.16	4.92	4.55	−1.14	0.28
18134405−3146148	J181344.05−314614.85	3001272	3.27	2.55	5.82	4.92	−0.89	0.05
18134412−3147150	J181344.12−314715.13	3000837	2.92	2.35	5.27	4.71	−0.96	0.07
18134457−3152197	J181344.56−315219.81	3001031	3.07	2.51	5.58	5.03	−0.80	0.11
18134493−3150073	J181344.93−315007.53	1301091	3.17	2.32	5.49	5.00	−0.81	0.12
18134502−3150190	J181345.01−315019.20	1301234	3.12	2.35	5.46	4.96	−0.85	0.05
18134511−3147546	J181345.11−314754.60	2000220	3.68	2.79	6.47	5.32	−0.54	0.35
18134563−3150339	J181345.63−315033.89	1301431	3.19	2.42	5.60	5.07	−0.76	0.17
18134635−3147366	J181346.35−314736.61	2000218	3.35	2.62	5.98	4.86	−0.93	0.13
18134635−3152231	J181346.37−315223.33	3001136	3.00	2.19	5.20	4.76	−0.83	0.13
18134651−3150219	J181346.51−315021.93	1301369	3.07	2.60	5.67	5.02	−0.81	0.09
18134689−3149595	J181346.89−314959.58	1301147	3.48	2.69	6.17	4.89	−0.91	0.13
18134725−3147570	J181347.25−314757.14	2000177	3.62	2.72	6.34	5.12	−0.72	0.12
18134754−3147217	J181347.54−314721.78	2000390	3.10	2.50	5.60	4.73	−1.02	0.21
18134793−3148059	...	2000408	3.46	2.60	6.06	5.20	−0.66	0.25
18134846−3149413	...	2000460	3.29	2.39	5.68	4.89	−0.91	0.06
18134865−3142176	J181348.65−314217.70	3004381	4.01	3.08	7.09	5.16	−0.69	0.05
18135069−3149440	J181350.69−314944.03	3000812	3.26	2.48	5.74	4.81	−0.97	0.14
18135122−3151068	J181351.21−315106.85	3001045	3.33	2.70	6.03	5.01	−0.82	0.03
18135154−3151406	J181351.53−315140.65	3001219	3.49	2.73	6.22	5.02	−0.81	0.01
18135174−3151173	J181351.74−315117.26	3001138	3.26	2.50	5.76	5.11	−0.70	0.22
18135186−3151302	J181351.86−315130.29	3001200	2.67	2.38	5.05	4.56	−0.80	0.18
18135512−3150484	J181355.13−315048.42	3001330	3.38	2.64	6.02	5.02	−0.80	0.04
18135665−3148002	J181356.65−314800.24	3001570	3.55	2.84	6.39	5.36	−0.50	0.42
18135670−3147531	J181356.70−314753.20	3001607	3.82	2.95	6.77	5.31	−0.55	0.29
18135701−3150541	J181357.02−315054.14	3001557	3.25	2.64	5.89	5.25	−0.80	0.07
18140259−3142225	J181402.58−314222.48	3005733	3.42	2.66	6.09	4.75	−0.96	0.19
18142065−3147172	J181420.65−314717.18	3006184	3.50	2.56	6.06	4.67	−1.07	0.33
18142246−3153087	J181422.46−315308.76	3007155	3.29	2.64	5.93	4.65	−1.08	0.33
...	J181256.24−314948.95	3006051	3.60	2.83	6.43	4.89	−0.91	0.17
...	J181332.65−314955.58	2000534	3.06	2.36	5.43	4.76	−1.01	0.16
...	J181333.51−314952.71	2000495	3.17	2.45	5.62	4.90	−0.90	0.04
...	J181333.61−314753.37	2000318	3.33	2.57	5.90	4.94	−0.87	0.04

Table 7—Continued

Star Name (2MASS)	Star Name (VVV)	Star Name (VLT)	EW_{8542} (Å)	EW_{8662} (Å)	ΣEW (Å)	W′ (Å)	[Fe/H] (dex)	Δ[Fe/H] (dex)
···	J181336.52−314921.39	2000779	2.82	2.35	5.17	4.60	−1.11	0.28
···	J181338.61−314809.34	2000842	2.82	2.25	5.06	4.65	−0.83	0.14
···	J181340.05−315100.27	1401526	2.96	2.41	5.37	4.81	−0.96	0.09
···	J181342.97−314909.73	1201600	2.79	2.07	4.86	4.47	−1.19	0.33
···	J181344.55−315013.55	1301128	3.18	2.50	5.67	4.89	−0.91	0.05
···	J181346.54−314909.97	2000440	3.26	2.51	5.77	4.97	−0.85	0.01

Table 8. Literature References

Population	Reference
HP-1	Barbuy et al. (2006)
HP-1	Barbuy et al. (2016)
NGC 6266	Yong et al. (2014)
NGC 6273	Johnson et al. (2015a)
NGC 6273	Johnson et al. (2017a)
NGC 6287	Lee & Carney (2002)
NGC 6293	Lee & Carney (2002)
NGC 6342	Johnson et al. (2016)
NGC 6342	Origlia et al. (2005a)
NGC 6352	Feltzing et al. (2009)
NGC 6362	Massari et al. (2017)
NGC 6366	Johnson et al. (2016)
NGC 6388	Carretta et al. (2007a)
NGC 6440	Muñoz et al. (2017)
NGC 6440	Origlia et al. (2008)
NGC 6441	Gratton et al. (2006)
NGC 6441	Gratton et al. (2007)
NGC 6441	Origlia et al. (2008)
NGC 6522	Barbuy et al. (2014)
NGC 6522	Ness et al. (2014)
NGC 6528	Carretta et al. (2001)
NGC 6528	Origlia et al. (2005a)
NGC 6539	Origlia et al. (2005b)
NGC 6541	Lee & Carney (2002)
NGC 6553	Alves-Brito et al. (2006)
NGC 6553	Johnson et al. (2014)
NGC 6553	Tang et al. (2017)
NGC 6558	Barbuy et al. (2007)
NGC 6624	Valenti et al. (2011)
NGC 6626	Villanova et al. (2017)
NGC 6681	O'Malley et al. (2017)

Table 8—Continued

Population	Reference
NGC 6723	Gratton et al. (2015)
NGC 6723	Rojas-Arriagada et al. (2016)
Terzan 1	Valenti et al. (2015)
Terzan 4	Origlia & Rich (2004)
UKS1	Origlia et al. (2005b)
Bulge Field	Alves-Brito et al. (2010)
Bulge Field	Gonzalez et al. (2011)
Bulge Field	Johnson et al. (2012)
Bulge Field	Bensby et al. (2013)
Bulge Field	García Pérez et al. (2013)
Bulge Field	Howes et al. (2014)
Bulge Field	Johnson et al. (2014)
Bulge Field	Howes et al. (2015)
Bulge Field	Van der Swaelmen et al. (2016)